GROUNDWATER HYDRAULICS

SURFACE WATER - GROUNDWATER INTERACTIONS

TABEA BROECKER[1], JONAS SCHAPER[2], FATIMA EL-ATHMAN[3], MIKAEL GILLEFALK[4], SABINE HILT[5] & REINHARD HINKELMANN[6]

[1,3,6] Technische Universität Berlin, Berlin, Germany,
tabea.broecker@uwi.tu-berlin.de, f.el-athman@tu-berlin.de, reinhard.hinkelmann.wahyd.tu-berlin.de
[2,4,5] Leibniz-Institute of Freshwater Ecology and Inland Fisheries, Berlin, Germany,
schaper@igb-berlin.de, gillefalk@igb-berlin.de, hilt@igb-berlin.de

ABSTRACT

Almost all types of surface water are interrelated with the groundwater. Therefore, the knowledge of interactions between ground- and surface water is very important for understanding processes within the whole water cycle. This paper presents surface water-groundwater interactions from different perspectives and with various emphases including investigations of flow processes, the impact on the ecosystem functioning, the local biota and chemical turnover rates. The application and extension of an integral single-domain model for flow and transport processes in the groundwater - surface water interaction space is the objective of one research project. Most numerical investigations consider ground- and surface water as separate environmental compartments or couple of the corresponding models. For the integral model concept, the three-dimensional Navier-Stokes equations are extended by the consideration of porosities using the open source CFD software OpenFOAM. In a further project, the retention of chemical compounds in hyporheic reactors of urban freshwater systems is examined. Biogeochemical factors that affect retention and dynamics of micropollutants as a function of flow characteristics in hyporheic zones are determined with the help of laboratory experiments and field approaches. A simple one-dimensional transport and reaction model will be extended for the quantitative prediction of trace compounds such as organic micropollutant dynamics in sediments. Furthermore, various effects of bank filtration are investigated in two projects. Passing the soil layers, different purification processes and chemical reactions are taking place resulting in a modified water quality and changed properties. The reductive metabolism of iodinated X-ray contrast media as important organic pollutants in urban surface water as well as changes in groundwater seepage including effects on lake ecosystems are examined. This contribution gives an overview on different research activities with special emphasis on the integral model concept for the surface water-groundwater interaction space.

Keywords: Hyporheic exchange; Computational Fluid Dynamics (CFD); OpenFOAM, fluid mechanics; bank filtration.

1 INTRODUCTION

The Urban Water Interfaces Research Training Group (UWI), funded by the German Research Foundation, aims to achieve a broad process understanding in urban water systems, focusing on various natural and technical interfaces (Gessner et al., 2014). Engineers as well as natural scientists collaborate closely in different interdisciplinary topics. Surface water – groundwater interactions is one of the so-called common topics. Within this group, interactions between groundwater and surface water from lakes as well as from lotic systems are considered. These interfaces are characterized by diverse microbial communities and highly active biota leading to steep biogeochemical gradients (Birgand et al., 2007; Greskowiak et al., 2006). The temporal and spatial variability of surface water and groundwater exchange driven by steep hydrodynamic gradients and biogeochemical cycling are considered by experimental measurements as well as by modelling these processes. The very complex exchange processes require interdisciplinary approaches, exchanging knowledge, expertise and technology from different backgrounds. Within this group, engineers as well as natural scientists collaborate for an advanced understanding of surface water-groundwater interactions with emphases on different researches. Figure 1 shows an overview of the four research topics, which are focused on the hyporheic zone as well as on bank filtration.

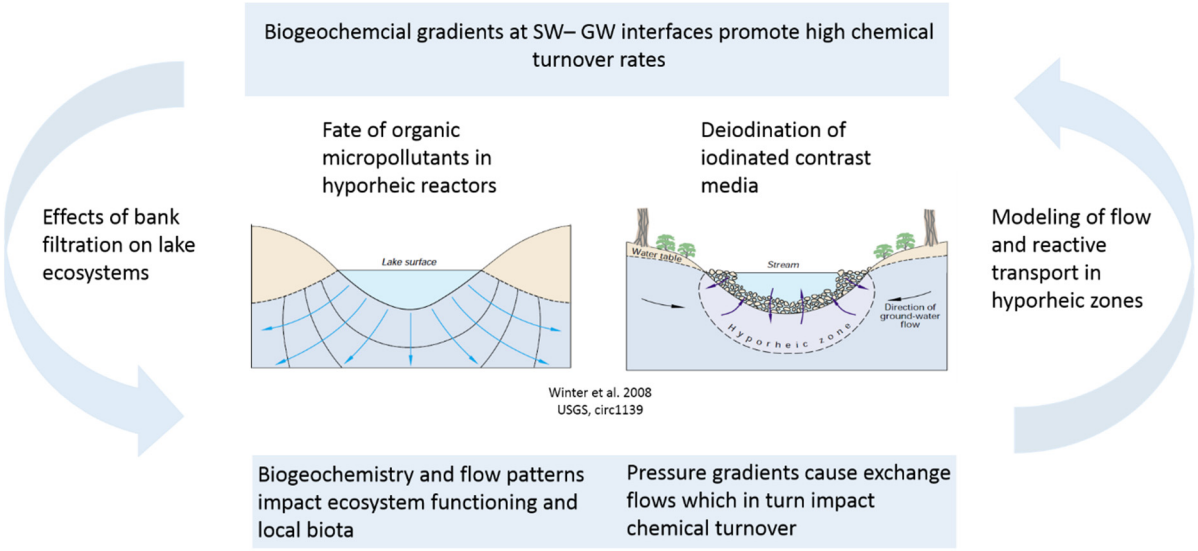

Figure 1. Research topics of UWI for surface water-groundwater interactions

1.1 Hyporheic Zone

The hyporheic zone is the transition zone between saturated river sediments and groundwater (Boano et al., 2014). This zone is considered to constitute a major sink for trace organic compounds from wastewater treatment plant in lotic systems and thus plays a pivotal role in urban water cycles, with regards to both, ecosystem functioning as well as drinking water protection (Li et al., 2015; Lewandowski et al., 2011; Hester & Gooseff, 2010). The stability of trace organic compounds in saturated sediments is generally thought to be dependent on biogeochemical conditions like the redox potential (e.g., Heberer et al., 2008), availability of labile organic carbon or the distribution of reactive surfaces (Borch et al., 2010). The biogeochemical processes are significantly controlled by the fluxes, the flow paths and the residence time within the hyporheic zone, which can be calculated with the help of different model types. For the quantitative prediction of trace compounds a simple, one-dimensional model is sufficient. Spatially explicit results investigating hyporheic exchange processes can be achieved with numerical models and were applied on different scales. However, most numerical investigations consider groundwater and surface water as separate environmental compartments or couple of groundwater and surface water model. The objective of one UWI research is to apply and extend an integral model in the groundwater-surface water interaction space for investigating flow and transport processes. The modelling results can be used for another UWI research, investigating the retention of chemical compounds in hyporheic reactors of urban freshwater systems. A quantitative as well as qualitative understanding of the behavior of many trace organic compounds as a function of the interactive effects of both transport characteristics and biogeochemical conditions, commonly encountered in hyporheic zones, is still lacking. Likewise, chemical mechanisms that govern the numerous transformation and translocation processes of trace organic compounds in the subsurface are unclear. The lack of mechanistic understanding also results in a lack of predictive tools. Hitherto comprehensive models describing the dynamics of trace organic compounds in hyporheic zones as a function of both biogeochemical and hydrological conditions have not been developed. The primary goals of one research are thus to: (i) further our conceptual understanding of the factors that control the overall efficiency of hyporheic zones with respect to trace organic compounds removal and ii) to determine first order attenuation rates for a variety of trace organic compounds under different environmental conditions.

1.2 Bank Filtration

Two further research topics within this group are focused on bank filtration, which is one of the oldest techniques used for drinking water production and purification. Close to the bank of a river or lake, the groundwater level is lowered by water abstraction causing an infiltration of the surface water through the bank. Although bank filtration has been used for more than 100 years, especially purification efficiency and infiltration capacities were investigated so far, whereas significant knowledge gaps concerning the effects on the ecosystem of rivers and lakes still exist. Based on the present knowledge, various hypotheses are tested in order to examine whether bank filtration affects macrophytes in lakes and lake water quality in one research project.

Besides physical effects like filtration and sorption, microbiological degradation occurs for flow time of several weeks or months. Pathogens, but also different organic micropollutants can be partially removed or transformed by these processes. The degradability of many substances is dependent on the prevailing redox conditions which are changing along the flow length. In the first section, molecular oxygen is still available and allows for aerobic respiration. This section is followed by anoxic and anaerobic conditions with nitrate, manganese, iron and sulfate reduction. (Baumgarten, 2013; Jekel & Czekalla, 2017)

Iodinated X-ray contrast media are found at much higher concentrations than any other pharmaceutical compound in wastewater and surface water (Umweltbundesamt, 2014). Under aerobic conditions, an almost complete transformation of the contrast medium Iopromide has been observed, however, without any deiodination of the molecule (removal of iodine) (Wiese et al., 2011). A release of iodide has been found under anoxic/anaerobic conditions (Stieber et al., 2008). The deiodination is assessed by the decrease of the sum parameter adsorbable organic bound iodine (AOI) which measures unchanged or partially deiodinated molecules as well as molecules with only altered side chains.

One research project of UWI concentrates on the deiodination of ICM in bank filtration of urban waters to achieve a better understanding of the already observed deiodination and to contribute to the further understanding of the decrease of anthropogenic trace substances in the aquatic environment. While the AOI decrease of contaminated water at the production side, e.g., by nanofiltration (Drews et al., 2003) or ozonation (Putschew et al., 2007) has been studied extensively, the deiodination in natural environments is still widely unknown.

2 INTEGRAL MODELLING APPROACH FOR FLOW AND TRANSPORT IN GROUNDWATER-SURFACE WATER INTERACTION SPACE

It is a research project that is presented more detailed, which applies and extends an integral modelling approach for the hyporheic zone. The concept behind as well as first results are presented in the following sections.

2.1 Governing equations and numerical model

The three-dimensional Navier-Stokes equations are extended by the consideration of the porosity Φ and an additional drag term D. For all calculations, the free, open source computer fluid dynamics (CFD) software “OpenFOAM” (Open Field Operation and Manipulation) is applied. The two-phase flow solver “interFoam”, which is usually applied for surface water simulations, serves as starting point for the integral solver and solves the three-dimensional Navier-Stokes equations. Values, that are represented by $[\,]^f$ are averaged only over the void region, which means that the solid fraction is not considered. For the integral solver, the equations are defined after Oxtoby et al. (2013):

Mass conservation equation

$$\phi \nabla \cdot \left[\vec{U}\right]^f = 0 \qquad [1]$$

Momentum conservation equation

$$\phi \left(\frac{\partial \left[\rho\right]^f \left[\vec{U}\right]^f}{\partial t} + \cdot \left[\vec{U}\right]^f \nabla \left(\left[\rho\right]^f \left[\vec{U}\right]^f \right) \right) = - \phi \nabla \left[p\right]^f + \phi \left[\mu\right]^f \nabla^2 \left[\vec{U}\right]^f + \phi \left[\rho\right]^f \vec{g} + D \qquad [2]$$

with the following parameters

$$\rho = \alpha \rho_w + \rho_a (1 - \alpha) \qquad [3]$$

$$\mu = \alpha \mu_w + \mu_a (1 - \alpha) \qquad [4]$$

and the porous drag term D

$$D = - \left(150 \frac{1 - \phi}{d_p \phi} \left[\mu\right]^f + 1.75 \left[\rho\right]^f \left[\vec{U}\right]^f \right) \frac{1 - \phi}{d_p} \left[\vec{U}\right]^f - 0.34 \frac{1 - \phi}{\phi} \frac{\partial \left[\vec{U}\right]^f}{\partial t} \qquad [5]$$

For the drag term pressure loss, due to the friction of fluid with the porous medium (Ergun, 1952), is considered through the first term in first line. The second term in second line acts to increase the effective mass of the fluid due to flow recirculation caused by porous medium with an effective added mass coefficient after van Gent (1995).

Volume of Fluid equation

$$\phi \frac{\partial [\alpha]^f}{\partial t} + \phi \nabla \cdot ([\alpha]^f [\vec{U}]^f) = 0 \quad [6]$$

U is the velocity, t is time, ρ is the density with the subscripts a and w for air and water, α is a volume fraction which varies between 0 (for air) and 1 (for water), p is pressure, μ is the dynamic viscosity with the subscripts a and w is the density and turb for turbulent and g is the gravitational acceleration.

First of all, an advection-diffusion equation was implemented into the interFoam solver (see Equation 7) to examine the transport of a passive tracer with a concentration C. The user can define the physical diffusivity D_{phys} as well as the turbulent Schmidt number Sc_{turb}, which defines the turbulent diffusivity coefficient D_{turb} (Equation 8).

Transport equation

$$\frac{\partial C}{\partial t} + \nabla (C \vec{U}) + \nabla (D_{phys} + D_{turb}) \nabla C = 0 \quad [7]$$

$$D_{turb} = \frac{\mu_{turb} / \rho}{Sc_{turb}} \quad [8]$$

2.2 Validation and results

First simulations relating to this research consider the upper boundary of the hyporheic zone focusing on flow and transport processes around varying ripple morphologies and flow conditions using the interFoam solver with the implemented transport equation. The pressure distribution, related to the exact flow paths as well as the pressure gradient that is connected to the volumetric exchange flux in the hyporheic zone were significantly affected by the ripple geometries and the present flow rates. Moreover, the simulations showed the relevance of transport processes in surface waters for the spreading and retention of substances at the interface, probably influencing biogeochemical reactions within the hyporheic zone. The results of this research were submitted to Limnologica, Ecology and Management of Inland Waters (see Broecker et al., 2016). More information can be achieved by adding the sediment at the lower boundary with the help of the integral solver.

For the integral simulations, an algorithm by Oxtoby et al. (2013) simulating two-fluid flows in porous media with arbitrary heterogeneous porosity fields is tested. In a further step, a tracer transport equation will be implemented to this solver.

As first test, the seepage through a homogeneous earth dam with height of 22 m and constant water level of 17 m on the right side of the dam was simulated until steady state was achieved. The foundation is impermeable. The dam has a porosity of 0.25 and a median grain size radius of 1.59 cm which corresponds to a gravel material. Consequently, the influence of the drag term is relatively small. After 100 s, steady state was achieved. The simulated water table is compared between an analytical solution by Kozeny (see Lattermann 2010) and an improvement of this solution by Casagrande (1937). Close agreement is obtained between the numerical and the analytical results (see Figure 2). At the entrance of the water into the dam and at the outlet, a very good agreement can be observed between the numerical simulation and the solution after Casagrande (1937). Inside the dam, the water table is slightly higher in the numerical simulation.

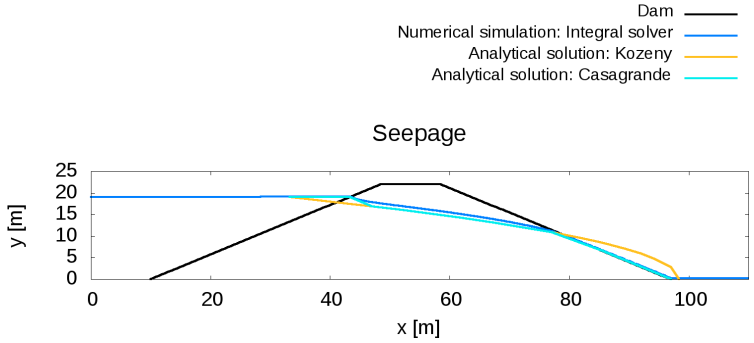

Figure 1. Comparison of seepages through a homogeneous dam with an impervious foundation for a numerical simulation using the integral solver and two analytical solutions

For a second test case, a rectangular dam (again with an impermeable foundation) is considered with the same soil properties as for the previous simulation. The dam has a height of 24 m and a width of 16 m. For this test case, the seepage calculated with the integral solver is compared with: an analytical one-dimensional solution (after Kobus and Keim, 2001), an analytical two-dimensional solution (after Di Nucci, 2015) and two further numerical solutions (Westbrook, 1985 and Aitchison, 1972). Figure 3 (left) shows the seepages for each approach. The lowest seepage is calculated for the analytical one-dimensional solution. With a look at the velocity vectors inside the dam calculated with the integral solver (Figure 3, right) it is obvious, that a one-dimensional solution is not sufficient for this case. In contrast to the analytical one-dimensional solution, the analytical two-dimensional solution shows very similar results compared to the seepage calculated with the integral solver. The numerical solutions by Westbrook 1985 and Aitchison 1972 show slightly lower seepages, but are still in a similar range.

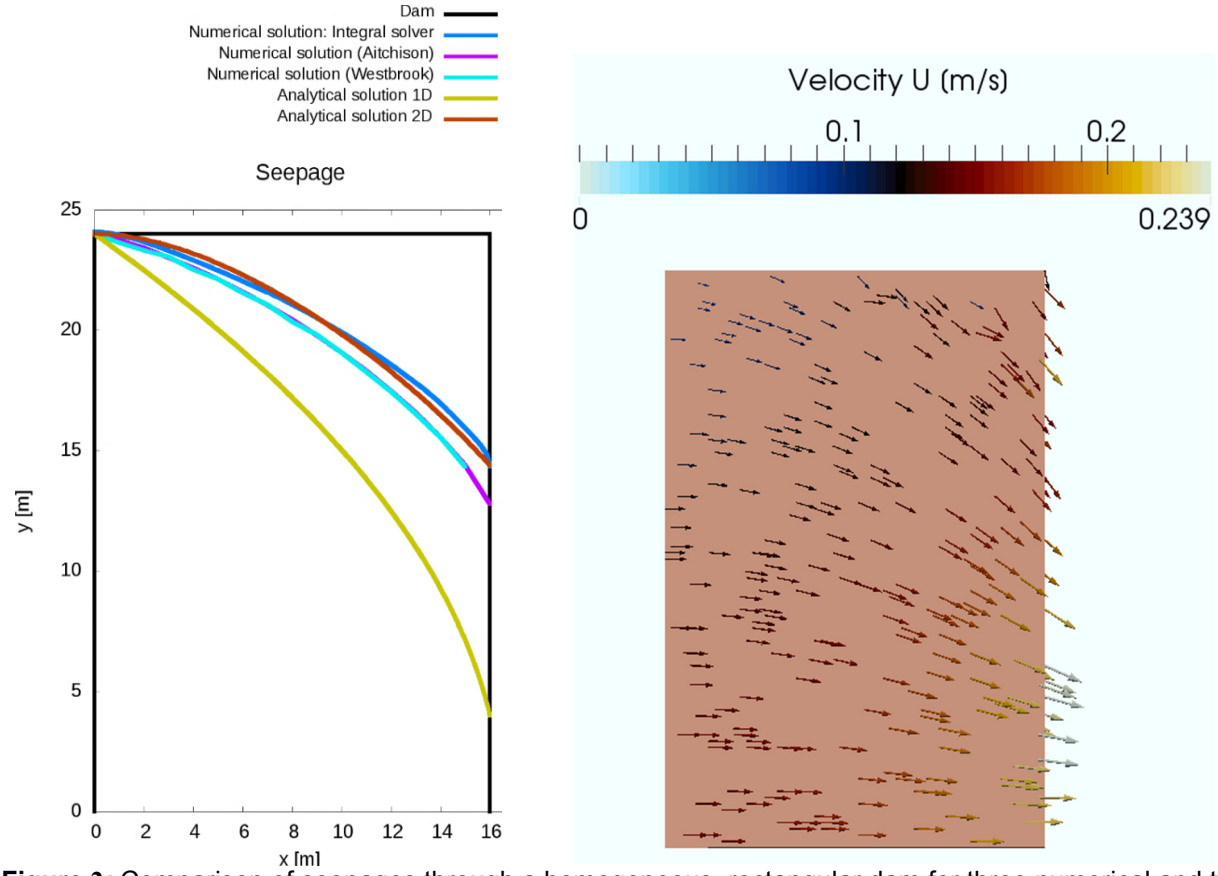

Figure 2*:* Comparison of seepages through a homogeneous, rectangular dam for three numerical and two analytical solutions (left) as well as velocity vectors inside the dam for the integral solver (right)

The integral solver is further examined concerning the applied drag term using the test case with the rectangular dam. In a first test, the drag term is completely deleted. Inside the dam the water level decreases and at the left side of the drag, disproportionately high turbulences can be observed even after 300 s simulation time due to the absence of a drag.

The test cases showed that the integral solver shows good results for groundwater-surface water interactions as long as the median grain size diameter of the soil is not too small. In the next step, smaller grain sizes will be applied and an advection-diffusion equation for the investigation of a passive tracer will be implemented. The model will be validated with the help of a flume experiment by Fox et al. (2014). After a successful validation, the presented study for varying ripple morphologies and flow conditions can be examined again considering surface water and groundwater at the same time in one model. Moreover, field measurements from partners within this group will be used for further simulations. In this context, modeled flow paths and residence times can be used to explain the retention of chemical compounds within the hyporheic zone for a further research project working on groundwater-surface water interactions (see section 3).

3 RETENTION OF CHEMICAL COMPOUNDS IN HYPORHEIC REACTORS OF URBAN FRESHWATER SYSTEMS

Next to flow and transport dynamics within the hyporheic zone, biogeochmical aspects are investigated in a further project. In this project it is hypothesized that the overall behavior of trace organic compounds in river sediments and the overall effectiveness of the hyporheic zone in removing trace organic compounds is, to a large extent, controlled by transport limitations. Hydraulic conditions in hyporheic zones do not only influence

the availability of terminal electron acceptors and electron donors and the spatial distribution of reactive surfaces. They also determine flow velocities and flow path lengths and hence reaction times and bioavailability on the pore scale. We further hypothesize that under similar flow characteristics, differences in attenuation rates between various trace of organic compounds will reflect their relative stability under different biogeochemical conditions and hence may provide mechanistic insights into their attenuation processes.

In order to derive relevant and transferable results, experiments were predominantly conducted in situ, which is in wastewater treatment plant influenced lotic systems. Hydrological methods such as temperature depth profiles (Anderson, 2005; Gordon et al., 2012), heat pulse sensors (Lewandowski et al., 2011) and seepage meters (Solder et al., 2015) were used to characterize hyporheic flow with respect to both direction and magnitude. A novel approach to determine flow velocities and hydrodynamic dispersion coefficients employing time series of pore water electrical conductivity is currently developed and tested in the field. In conjunction with flow measurements, samples of interstitial water are taken using both active and passive pore water sampling techniques. Porewater peepers, for instance, were deployed to obtain time integrated concentration profiles of trace organic compounds and various biogeochemical parameters in the hyporheic zone of a wastewater treatment plant effluent of urban river in Berlin, Germany. At the same site, a novel Mini Point Sampler was successfully used to obtain porewater time series over the course of 32 h. A 1D - transport and reaction model was subsequently used to calculate first order attenuation rate constants from the measured concentration profiles and flow characteristics. The findings of this project will be compared with those of the integral solver explained in section 2.

Preliminary results show that, under losing conditions, the hyporheic zone of an urban lowland river can indeed be considered a sink for wastewater treatment plant that is derived from trace of organic compounds. The overall magnitude of calculated first order attenuation rate constants reflects the general compound susceptibilities to biodegradation and sorption. The influence of biogeochemical conditions on trace organic compounds stability in the hyporheic zone was found to be compound specific. For most trace organic compounds studied, biogeochemical conditions such as the redox potential and the availability of respective reactive surfaces only had a minor influence on attenuation rates. These results indicate that, at the field site investigated, the effectiveness of the hyporheic zone is primarily controlled by hyporheic exchange and transport characteristics rather than by biogeochemical parameters.

While the majority of field experiments so far have been conducted in urban lowland rivers in central Europe, current efforts targets montane streams under more arid conditions. Using similar methods over climatic, geomorphological and geological gradients will not only broaden our mechanistic understanding of trace organic compound dynamics in hyporheic zones. It will also improve our predictive capabilities and offer river management and engineering guidelines, which in turn will be useful to meet the water quality challenges of urban areas.

4 DEIODINATION OF IODINATED CONTRAST MEDIA DURING BANK FILTRATION

While the first two presented projects dealt with the interface of groundwater and lotic systems, the following project is related to the interface between groundwater and lakes with the focus on degradation processes of iodinated contrast media.

4.1 Biological deiodination

For environmentally relevant chlorinated and brominated substances, a reductive dehalogenation by corrinoid containing enzymes of dehalorespiring microorganisms has been shown in various studies. As part of this UWI project, genus *Dehalococcoides mccartyi* strain CBDB1 was cultivated in culture bottles under anaerobic conditions with the iodinated substances Iopromide, Diatrizoate as well as 2,3,5- and 2,4,6-Triiodobenzoic acid (TIBA) as electron acceptors. In addition to the iodinated compounds, positive controls additionally included hexachlorobenzene which can be completely dechlorinated by strain CBDB1. A CBDB1 culture previously cultivated with hexachlorobenzene was used as inoculum and titanium (III) citrate was added for reducing conditions. During a period of several weeks, the concentrations of the added iodinated compounds, iodide and the sum parameter AOI as well as the cell density were measured. In additional tests, the enzyme activity of CBDB1 with iodinated substances was photometrically determined by the extinction decrease of methyl viologen which served as artificial electron donor and redox indicator changing color from blue in its reduced state to colorless in its oxidized state.

The degradation tests in culture bottles showed a deiodination of Iopromide of up to 95% but no cell growth in the absence of the additional electron acceptor hexachlorobenzene. Abiotic controls without microorganisms showed a similar deiodination degree, implying that the deiodination is not traced to microbiological activity. The activity tests with different iodinated substances in the presence of CBDB1 cells indicated a high electron transfer resulting in a deiodination (correlation was proven in preliminary tests). The specific activity is defined here as the amount of product (iodide) formed per second and protein mass and was calculated from the initial extinction decrease of the assays (Table 1). Control assays with heat-inactivated enzymes (5 min at 100 °C) did not show any activity.

Table 1: Enzyme activity and specific enzyme activity for Dehalococcoides mccartyi strain CBDB1 with different iodinated substances (300 µM)

Compound	activity [pmol iodide / s]	spec. activity [nmol iodide / (mg protein × s)]
Iopromide	0.20	0.50
Diatrizoate	0.20	0.50
2,3,5- TIBA	2.45	6.02
2,4,6-TIBA	1.84	4.51
Iopromide	0.20	0.50

4.2 Abiotic deiodination in the presence of corrinoids

Abiotic activity tests were conducted with commercially available corrinoids cyanocobalamin (synthetic form of vitamin B_{12}) and dicyanocobinamide. For dicyanocobinamide, the photometric measurement showed a significant extinction decrease for all three tested iodinated substances (Figure 4a). A decrease of the extinction was also shown in the presence of cyanocobalamin with Iopromide and 2,3,5-TIBA but not with 2,4,6-TIBA (Figure 4b).

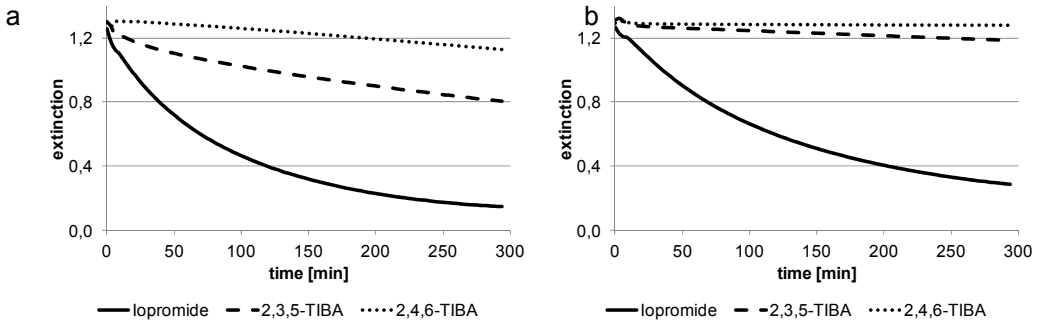

Figure 3: Extinction decrease (578 nm) by oxidation of reduced methyl viologen in the presence of 100 µM Iopromide, 2,3,5- or 2,4,6-TIBA and dicyanocobinamide (a) respectively cyanocobalamin (b). Blank values (extinction decrease in the absence of corrinoids) are subtracted from the graphs

In contrast to the biotic enzyme tests, the catalytic activity of the tested corrinoids is much higher for Iopromide than for the two Triiodobenzoic acids. The results found here will be discussed with those explained in section 5.

5 BANK FILTRATION: POTENTIAL EFFECTS ON SURFACE WATER QUALITY

There are many studies made on bank filtration, but almost all of them focus on water abstraction capacity and/or purification efficiency (e.g. Othman et al., 2015; Pholkern et al., 2015; Romero et al., 2014; Hoffman & Gunkel, 2011). However, there might also be effects of bank filtration on surface water quality and one of the research projects within UWI focuses on this question. This new research field is being opened using mainly three different approaches: 1) critical literature review of potential effects, 2) modeling of shallow lakes using the ecosystem model PCLake, and 3) field investigations and laboratory work.

5.1 Review of potential effects

Bank filtration may affect physical, chemical and biological parameters and processes and these might in turn affect one another, resulting in consequences for the surface water quality. Among the physical parameters water level, retention time, flow velocity and water temperature are subjected to be affected. Taking water temperature as an example, as the groundwater is hindered to enter the surface water by water abstraction wells, its cooling effect in summer and its warming effect in winter will disappear, an impact that potentially will change the conditions for water-living organisms and their interactions (e.g. Imholt et al., 2010; Boisneau et al., 2008; Boscarino et al., 2007; Wehrly et al., 2007; Harper & Peckarsky, 2006; Alvarez and Nicieza, 2005). Among the chemical parameters nutrients, toxic substances, dissolved organic and inorganic carbon (DOC and DIC) might be changed by bank filtration. Taking dissolved inorganic carbon as an example, groundwater often has higher concentrations than surface waters (Cole et al., 1994). When this source of DIC is removed, especially macrophytes solely relying on free CO_2 as their carbon source might disappear (Körner, 2001). This has been shown in cases not directly related to bank filtration, but under other circumstances (e.g. Maberly et al., 2015). The review assesses how the impact on physical and chemical parameters in turn might change the biodiversity, the macrophyte abundance and harmful blooms in surface waters. All in all, a comprehensive assessment of the potential effects on surface water quality by bank filtration is in progress.

5.2 Modeling of effects on shallow lakes

The shallow-lake model PCLake (Janse, 2005) provides the possibility of simulating whole-lake effects of bank filtration. Compared to what is possible in a field or a lab setting, the opportunity arises to examine the effects on more parameters and under more various conditions. PCLake is constantly being developed and

adapted to extend its original applications with for the example is shown in the study of deep lakes by Sachse et al. (2014). Early trials show promising prospects for the model to provide relevant results that will give insight to potential effects of bank filtration on (shallow) lakes.

5.3 Field investigations and laboratory work

Field investigations are being conducted in Lake Müggelsee, which is located in eastern Berlin and is fed by water from the Spree River. Around the lake bank filtration has been conducted since more than 100 years and at the moment approximately 50 million m^3 water per year is being abstracted in the area around the lake (BWB, 2015), the water being a mixture of groundwater and bank filtrated lake water.

Early results from a minor field campaign indicate that higher rates of bank filtration increases the sediment organic content in Lake Müggelsee, a result that is in accordance with studies performed in Lake Tegel, Berlin (Hoffmann & Gunkel, 2011). The results from Lake Müggelsee still need to be confirmed by conducting a more comprehensive field campaign. Next to this, field experiments aimed at investigating the effect of different levels of CO_2 on the water plant *Fontinalis antipyretica* will be conducted. While this has been done in a laboratory setting (Maberly, 1985a; Maberly, 1985b), it has not been performed in a field setting.

6 CONCLUSIONS

Interactions of groundwater and surface water are complex. They are related to the quantitative exchange of water, but also to chemical and ecological aspects. The UWI thematic group groundwater-surface water interactions addresses various knowledge gaps from different scientific disciplines, facing parts of all mentioned aspects. Within this group, engineers as well as natural scientists work on different projects, but at the same time knowledge as well as technologies are exchanged. Two projects are related to the hyporheic zone, while further two projects consider bank filtration. Overall, we expect to achieve a new quality of process understanding.

One project investigates flow and transport processes within the hyporheic zone with an integral numerical model. First of all, the upper boundary of the hyporheic zone was examined injecting a pulse of a passive tracer with various streambed morphologies. It was shown that the streambed morphology significantly influences where and for how long a tracer reaches the hyporheic interface. In a next step, the integral solver was applied and tested for two cases that account for groundwater as well as for surface water. For the validation of the integral solver, analytical as well as numerical results were compared. A good agreement was observed for big medium grain sizes of the soil. In a next step, smaller grain sizes will be investigated and an advection-diffusion equation will be implemented in the integral solver. The solver will then be validated with the help of a flume experiment and data from another project within UWI, which includes field experiments. The field experiments are conducted to elucidate next to flow and transport processes also biogeochemical processes. Moreover, the project aims to improve measurement techniques for the hyporheic zone. Control factors for the efficiency of trace organic compound removal in the hyporheic zone are investigated, using next to field experiments also a 1D – transport-reaction model. Present results from a wastewater treatment plant effluent urban river in Berlin show that biogeochemical conditions had only a minor influence on attenuation rates. Consequently, the effectiveness is predominantly affected by flow and transport characteristics at the investigated field site. Actual analysis targets montane streams under more arid conditions.

Next to the hyporheic zone, the interaction of lake and groundwater is examined in two further projects. One project concerns the degradation process of iodinated contrast media during bank filtration. Iodinated X-ray contrast media are known for their persistence in the aquatic environment. The results to date indicate a deiodination of these compounds during anoxic/anaerobic bank filtration quantifiable by the sum parameter AOI. The microbiological deiodination of iodinated contrast media with Dehalococcoides mccartyi strain CBDB1 could not be demonstrated by cell growth. However, an enzymatic activity with CBDB1 cells was shown for two contrast agents and two other iodinated aromatics. High deiodination rates, especially for Iopromide, were also achieved by using synthetic dicyanocobinamide as catalyst. Further microbiological experiments are planned with other dehalogenating bacteria strains. Abiotic batch tests will be conducted under nature related conditions in the presence of manganese(II), iron(II), iron(II) sulfide or sodium. One other project is also examining effects of bank filtration, but with a different focus, namely the effects on surface water quality. Since it is a new research field, much work has been done to think of potential effects and to come up with hypotheses to test using the ecosystem model PCLake as well as field investigations. Early results indicate that there are noticable effects, for example by increased sediment organic matter content in the littoral zone of lakes.

ACKNOWLEDGMENTS

The funding provided by the German Research Foundation (DFG) within the Research Training Group Urban Water Interfaces' is gratefully acknowledged.

REFERENCES

Anderson, M.P. (2005). Heat as a Ground Water Tracer. *Ground Water*, 43(6), 951–968. doi:10.1111/j.1745-6584.2005.00052.x

Aitchison, J. (1972). Numerical Treatment of a Singularity in a Free Boundary Problem. *Proceedings of the Royal Society of London*, *Series A*, 330(1583), 573–580.

Alvarez, D. & Nicieza, A.G. (2005). Compensatory Response 'Defends' Energy Levels but not Growth Trajectories in Brown Trout, Salmo Trutta L. *Proceedings of the Royal Society B: Biological Sciences* 272(1563), 601–607.

Baumgarten, B. (2013). Entfernung von Sulfamethoxazol in der Bodenpassage, PhD Dissertation. University of Berlin.

Berliner Wasserbetriebe (2015). *Data on Pumping Rates,* Berlin Water Works (Berliner Wasserbetriebe).

Birgand, F., Skaggs, R.W., Chescheir, G.M. & Gilliam, J.W. (2007). Nitrogen Removal in Streams of Agricultural Catchments- A Literature Review. *Environmental Science and Technology*, 37(5), 381-487.

Boano, F., Harvey, J.W., Marion, A., Packman, A.I., Revelli, R., Ridolfi, L. & Wörman, A. (2014). Hyporheic Flow and Transport Processes: Mechanisms, Models and Biogeochemical Implications. *Reviews of Geophysics*, 52(4), 603-679.

Boisneau, C., Moatar, F., Bodin, M. & Boisneau, Ph. (2008). Does Global Warming Impact on Migration Patterns and Recruitment of Allis Shad (Alosa Alosa L.) Young of the Year in the Loire River, France. *Hydrobiologia,* 602(1), 179–186.

Borch, T., Kretzschmar, R., Kappler, A., Cappellen, P. V., Ginder-Vogel, M., Voegelin, A. & Campbell, K. (2009). Biogeochemical Redox Processes and Their Impact on Contaminant Dynamics. *Environmental Science & Technology*, 44(1), 15-23.

Boscarino, B.T., Rudstam, L.G. & Mata, S. (2007). The Effects of Temperature and Predator-Prey Interactions on the Migration Behavior and Vertical Distribution of Mysis Relicta. *Limnology and Oceanography* 52(4), 1599–1613.

Broecker, T., Elsesser, W., Teuber, K., Özgen, I., Nützmann, G. & Hinkelmann, R. (2016). High Resolution Simulation of Free-Surface Flow and Tracer Transport Over Streambeds with Ripples. Manuscript Submitted for Publication.

Casagrande, A. (1937). Seepage Through Dams. *Journal of The New England Water Works Association*, 51(2), 131-170.

Cole, J.J., Caraco, N.F., Kling, G.W. & Kratz, T.K. (1994). Carbon Dioxide Supersaturation in the Surface Waters of Lakes. *Science*, 265(5178), 1568-1570. Doi:10.1126/Science.265.5178.1568

Di Nucci, C. (2015). A Free Boundary Problem for Fluid Flow Through Porous Media. *Fluid Dynamics*, Arxiv:1507.05547.

Drews, A., Klahm, T., Renk B., Saygili M., Baumgarten G. & Kraume M. (2003). Nanofiltration of CIP Waters from Iodine X-Ray Contrast Media Production: Process Design and Modelling. *Desalination*, 159 (2), 119–129.

Ergun, S. (1952). Fluid Flow Through Packed Columns. *Chemical Engineering Progress*, 48(2), 89-94.

Fox, A., Boano, F. & Arnon, S. (2014). Impact of Losing and Gaining Streamflow Conditions on Hyporheic Exchange Fluxes Induced by Dune-Shaped Bed Forms. *Water Resources Research*, 50, 1895–1907.

Gessner, M. O., Hinkelmann, R., Nützmann, G., Jekel, M., Singer, G., Lewandowski, J., Nehls, T. & Barjenbruch, M. (2014). Urban Water Interfaces. *Journal of Hydrology*, 514, 226-232.

Gordon, R P., Lautz, L.K., Briggs, M.A. & Mckenzie, J.M. (2012). Automated Calculation of Vertical Pore-Water Flux from Field Temperature Time Series Using the VFLUX Method and Computer Program. *Journal of Hydrology*, 420, 142-158.

Greskowiak, J., Prommer, H., Massmann, G. & Nützmann, G. (2006). Modelling Seasonal Redox Dynamics and the Corresponding Fate of the Pharmaceutical Residue Phenazone During Artificial Recharge of Groundwater. *Environmental Science and Technology*, 40(21), 6615-6621.

Harper, M.P. & Peckarsky, B.L. (2006). Emergence Cues of a Mayfly in a High-Altitude Stream Ecosystem: Potential Response to Climate Change. *Ecological Applications*, 16, 612–621.

Heberer, T., Massmann, G., Fanck, B., Taute, T. & Dünnbier, U. (2008). Behaviour and Redox Sensitivity of Antimicrobial Residues During Bank Filtration. *Chemosphere*, 73(4), 451-460.

Hester, E.T. & Gooseff, M. N. (2010). Moving Beyond the Banks: Hyporheic Restoration Is Fundamental to Restoring Ecological Services and Functions of Streams. *Environmental Science & Technology*, 44(5), 1521-1525.

Hoffmann, A. & Gunkel, G. (2011). Bank Filtration in The Sandy Littoral Zone of Lake Tegel (Berlin): Structure and Dynamics of The Biological Active Filter Zone and Clogging Processes. *Limnologica - Ecology and Management of Inland Waters*, 41, 10–19. Doi:10.1016/J.Limno.2009.12.003

Imholt, C., Gibbins, C.N., Malcolm, I.A. & Soulsby, C. (2010). Influence of Riparian Cover on Stream Temperatures and The Growth of The Mayfly Baetis Rhodani in An Upland Stream. *Aquatic Ecology*, 44(4), 669–678.

Janse, J. (2005). Model Studies on The Eutrophication of Shallow Lakes and Ditches, Doctoral Dissertation. Wageningen University, ISBN 90-8504-214-3

Jekel, M. & Czekalla, C. (2017). *Wasseraufbereitung - Grundlagen Und Verfahren*. Munich: DIV Gmbh. DVGW Lehr- Und Handbuch Wasserversorgung (2nd Ed.), Band 6.

Kobus, H. & Keim, B. (2001). *Grundwasser In*. Blackwell Wissenschaftsverlag, Taschenbuch Der Wasserwirtschaft, 8, 277-313.

Körner, S. (2001). Development of Submerged Macrophytes in Shallow Lake Müggelsee (Berlin, Germany) Before and After Its Switch to The Phytoplankton-Dominated State. *Archiv Für Hydrobiologie*, 152(3) , 395-409.

Lattermann, E. (2010). *Wasserbau-Praxis: Mit Berechnungsbeispielen*. Bauwerk-Basis-Bibliothek, 128-131 ppLi, Z., Sobek, A. & Radke, M. (2016). Fate of Pharmaceuticals and Their Transformation Products in Four Small European Rivers Receiving Treated Wastewater. *Environmental Science & Technology*, 50 (11), 5614–5621.

Lewandowski, J., Angermann, L., Nützmann, G. & Fleckenstein, J. H. (2011). A Heat Pulse Technique for The Determination of Small-Scale Flow Directions and Flow Velocities in The Streambed of Sand-Bed Streams. *Hydrological Processes*, 25(20), 3244-3255.

Lewandowski, J., Putschew, A., Schwesig, D., Neumann, C. & Radke, M. (2011). Fate of Organic Micropollutants in the Hyporheic Zone of a Eutrophic Lowland Stream: Results of a Preliminary Field Study. *Science of Total Environment*, 409(10), 1824-1835.

Maberly, S.C. (1985a). Photosynthesis by Fontinalis Antipyretica. I. Interaction Between Photon Irradiance, Concentration of Carbon Dioxide and Temperature, *New Phytologist*, 100(2), 127–140. Doi:10.1111/J.1469-8137.1985.Tb02765.X

Maberly, S.C. (1985b). Photosynthesis by Fontinalis Aantipyretica. II. Assessment of Environmental Factors Limiting Photosynthesis and Production, *New Phytologist*, 100(2), 141–155. Doi:10.1111/J.1469-8137.1985.Tb02766.X

Maberly, S.C., Berthelot, S.A., Stott, A.W. & Gontero, B. (2015). Adaptation by Macrophytes to Inorganic Carbon Down a River with Naturally Variable Concentrations of CO2. *Journal of Plant Physiology*, 172, 120–127. Doi:10.1016/J.Jplph.2014.07.025

Othman, S.Z., Adlan, M.N. & Selamat, M.R. (2015). A Study on the Potential of Riverbank Filtration for the Removal of Color, Iron, Turbidity and E. Coli in Sungai Perak, Kota Lama Kiri, Kuala Kangsar, Perak, Malaysia. *Jurnal Teknologi*, 74(11), 83-91.

Oxtoby, O., Heyns, J. & Suliman, R. (2013). A Finite-Volume Solver for Two-Fluid Flow in Heterogeneous Porous Media Based on Openfoam. *Open Source CFD International Conference*, Doi: 10.13140/2.1.3075.8400.

Pholkern, K., Srisuk, K., Grischek, T., Soares, M., Schäfer, S., Archwichai, L., Saraphirom, P., Pavelic, P. & Wirojanagud, W. (2015). Riverbed Clogging Experiments at Potential River Bank Filtration Sites Along the Ping River, Chiang Mai, Thailand. *Environmental Earth Sciences*, 73, 7699–7709. Doi:10.1007/S12665-015-4160-X

Putschew, A., Miehe, U., Tellez, A. & Jekel, M. (2007). Ozonation and Reductive Deiodination of Iopromide to Reduce the Environmental Burden of Iodinated X-Ray Contrast Media. *Water Science & Technology*, 56 (11), 159–165.

Romero, L.G., Mondardo, R.I., Sens, M.L. & Grischek, T. (2014). Removal of Cyanobacteria and Cyanotoxins During Lake Bank Filtration at Lagoa Do Peri, Brazil. *Clean Technologies and Environmental Policy*, 16(6), 1133–1143. Doi:10.1007/S10098-014-0715-X

Stieber, M., Putschew, A. & Jekel, M. (2008). Reductive Dehalogenation of Iopromide by Zero-Valent Iron. *Water Science & Technology*, 57 (12), 1969–1975.

Solder, J.E., Gilmore, T.E., Genereux, D.P. & Solomon, D.K. (2015). A Tube Seepage Meter for In Situ Measurement of Seepage Rate and Groundwater Sampling. *Groundwater*, 54(4), 588-595.

Umweltbundesamt (2014). Arzneimittel In Der Umwelt – Vermeiden, Reduzieren, Überwachen. Retrieved November 12, 2015, From Https://www.Umweltbundesamt.De/Sites/Default/Files/Medien/378/Publikationen/01.08.2014_Hintergrundpapier_Arzneimittel_Final_.Pdf

Van Gent, M.R.A. (1995). Wave Interaction with Permeable Coastal Structures. Doctoral Thesis. Delft University Press.

Wehrly, K.E., Wang, L. & Mitro, M. (2007). Field-Based Estimates of Thermal Tolerance Limits for Trout: Incorporating Exposure Time and Temperature Fluctuation. *Transactions of The American Fisheries Society*, 136(2), 365–374.

Westbrook, D.R. (1985). Analysis of Inequality and Residual Flow Procedures and an Iterative Scheme for Free Surface Seepage. *International Journal for Numerical Methods in Engineering*, 21(10), 1791–1802.

Wiese, B., Massmann, G., Jekel, M., Heberer, T., Dünnbier, U., Orlikowski, D. & Grützmacher, G. (2011). Removal Kinetics of Organic Compounds and Sum Parameters Under Field Conditions for Managed Aquifer Recharge. *Water Research*, 45(16), 4939–4950.

EVALUATION OF DIFFERENTIAL EVOLUTION AND PARTICLE SWARM OPTIMIZATION ALGORITHMS ON SOLVING THE CONSTRUCTION SITE DEWATERING PROBLEMS

MUSTAFA TAMER AYVAZ[1]

[1] Department of Civil Engineering, Pamukkale University, Denizli, Turkey,
tayvaz@pamukkale.edu.tr

ABSTRACT

The objective of this study is to evaluate the performance of the differential evolution (DE) and the particle swarm optimization (PSO) approaches for solving the construction site dewatering optimization problems. In the proposed approaches, the same analytical groundwater flow model was considered in the simulation part. The objective of both DE and PSO based optimization approaches is to determine the locations and the pumping rates of the dewatering wells by minimizing the total groundwater withdrawal rate as the objective function. The constraints related with the drawdown and well locations were considered by means of the penalty function approach during the search process. The performance of the proposed approaches were evaluated on a hypothetical construction excavation site in detail for different well numbers. Identified results indicated that both DE and PSO based optimization approaches can effectively determine the optimum dewatering system for the given construction site.

Keywords: Construction dewatering; simulation-optimization; groundwater modeling.

1 INTRODUCTION

With development of the community, the requirement to the large construction projects increases. These projects usually require deep foundation excavations such that some problems in terms of safe working conditions and slope stability may occur in the case of the bottom of the excavation is below the groundwater table. Therefore, high groundwater table elevations need to be lowered in the site before starting the excavation works. One of the most widely used approach for this purpose is to use of the construction dewatering systems. The main purpose of these systems is to take the water out of the excavation site. Regarding this problem, there are various dewatering approaches which are usually site-specific, meaning that the geology, groundwater conditions, and the type of the excavation influence the selection of the dewatering approach (Nemati, 2007). Among the proposed approaches, dewatering through pumping wells is one of the best options since they can be used in large areas and high excavation depths (Nemati, 2007). However, since drilling and operation of these wells are costly, it is required to determine the best dewatering system in terms of the engineering point of view. For this purpose, the following questions can be asked before starting to design a dewatering system: *How many pumping wells should be used for lowering the groundwater table below a certain level? Where these pumping wells should be located over the site? What amount of groundwater should be pumped from each pumping well?* These questions are usually answered by the site engineers based on their previous experiences. However, such a configuration may not be optimal in terms of the safe working conditions, slope stability problems and drilling-dewatering costs. Therefore, determination of the optimum dewatering system is considered as an optimization problem in this study.

The current literature includes several studies regarding the construction dewatering optimization problems (Ayvaz, 2017; Jiang et al., 2013; Ayvaz et al., 2011; Zhou et al., 2010; Demirbaş et al., 2008; Altan-Sakarya and Önder, 2003; Tokgöz et al., 2002; Önder and Değirmenci, 2000). These studies considered different simulation and optimization approaches and almost all of them solved the problem for the fixed dewatering well locations. Although it is a simple and useful solution approach, practically, locations of the pumping wells are still unknown just as their numbers and pumping rates. Therefore, simultaneous determination of the numbers, locations, and pumping rates of the dewatering system becomes an important problem for optimally designing the construction dewatering system.

The main objective of this study is to evaluate the performance of two different optimization approaches which are the differential evolution (DE) and particle swarm optimization (PSO) for solving the construction site dewatering problems. In both approaches, the problem is solved by considering the same analytical groundwater simulation model to calculate the hydraulic head or drawdown values at the given monitoring locations. The objective of the DE and PSO are to minimize the total groundwater withdrawal by considering locations and pumping rates of the dewatering wells as the decision variables. During the solution of the problem, two managerial constraints need to be satisfied by the model. Since both DE and PSO are the unconstrained optimization approaches, these two constraints are included to the optimization process by

means of the penalty function approach. The performance of the proposed approaches are compared on a hypothetical construction excavation site for different number of wells and the identified results are evaluated in detail.

2 SIMULATION MODEL

Simulation model is one of the most important components of the proposed optimization approaches since it transforms the pumping information of the dewatering system into the hydraulic head or drawdown values at the monitoring locations. As indicated previously, an analytical groundwater simulation model is used to simulate the drawdown values at any location for the given dewatering system. Figure 1 shows the hydrogeological cross-section view of an ideal, homogeneous, isotropic, unconfined aquifer with uniform thickness and horizontal base. As can be seen, aquifer system includes a pumping well and a piezometer whose length fully penetrate the entire aquifer thickness. In the case of steady-state groundwater pumping from this well with a constant pumping rate of Q $[L^3T^{-1}]$, hydraulic head value at piezometer P1 can be calculated as follows (Kresic, 2007):

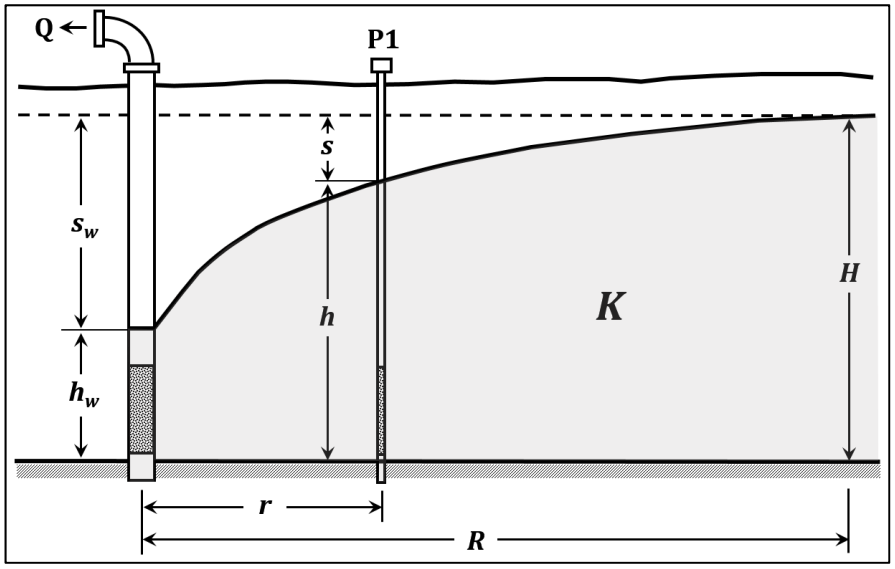

Figure 1. Hydrogeologic cross-section of an unconfined aquifer with a fully penetrating pumping well and a piezometer.

$$h = \sqrt{H^2 - \frac{Q}{\pi K}\ln\left(\frac{R}{r}\right)} \qquad [1]$$

where h is the hydraulic head value at piezometer location after pumping $[L]$, H is the hydraulic head value before pumping $[L]$, K is the hydraulic conductivity of the aquifer $[LT^{-1}]$, R is the radius of well influence $[L]$, r is the measured radial distance from piezometer to well $[L]$. After calculation of hydraulic head using Eq. [1], the drawdown value (s $[L]$) at P1 can be calculated as follows:

$$s = H - h \qquad [2]$$

It can be seen that the drawdown value is calculated by taking the difference between the initial hydraulic head and the hydraulic head after pumping. Note that the value of s in Eq. [2] is the result of a single pumping event. For more pumping wells, the drawdown of s at any point can be calculated by taking the algebraic sum of drawdowns caused by each independent well operation. This principle of the flow superposition allows a simple application of the governing equations describing the flow toward a single well in an unconfined aquifer (Kresic, 2007; Usul, 2007). A detailed explanation of this flow superposition principle is shown in Figure 2. As can be seen, the total drawdown is calculated by taking the algebraic sum of the two individual drawdown events ($s = s_1 + s_2$). This flow superposition principle allows the calculation of the final drawdown values at any point due to the groundwater pumping from any location of the aquifer system.

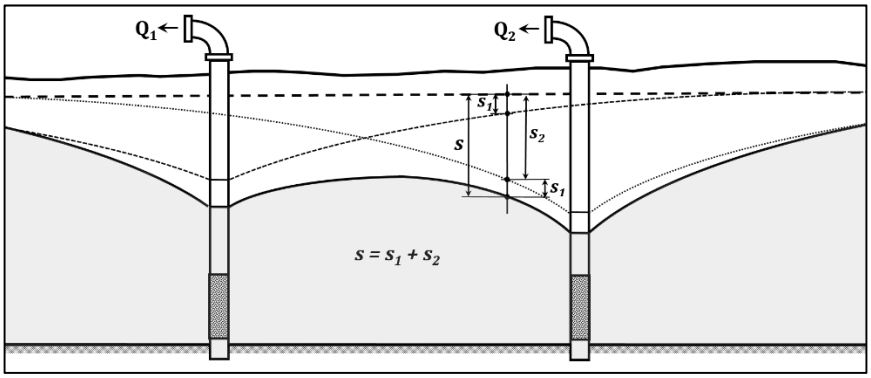

Figure 2. Superposition of flows toward two pumping wells.

3 OPTIMIZATION MODEL

As indicated previously, optimum construction dewatering system design problem was solved by using both DE and PSO based solution approaches. In the following, after giving the basic computational schemes of the DE and PSO, how these algorithms were applied to the construction dewatering system optimization problem is explained in detail.

3.1 Differential Evolution (DE) Optimization Algorithm

DE, first proposed by Storn and Price (1997), is a population-based evolutionary optimization algorithm. Basically, it has similar computational scheme with the genetic algorithms (GA) where the given solutions are evolved by using the mutation, crossover, and selection operators. The key difference between DE and GA is that all the individual solutions in DE are subjected to evolution whereas the same task is performed based on a probability in GA. After this evolution process, all the evolved solutions are directly transferred to next generations if their corresponding fitness values are improved. The basic computational steps of DE can be given as follows (Gökçe and Ayvaz, 2014):

- Randomly initialize all agents $\tilde{\boldsymbol{x}}$ (e.g. candidate solutions) in the population (NI being the number of individuals in the population).
- Repeat the following until a termination criterion is met:
  - For each agent $\tilde{\boldsymbol{x}}$ in the population do:
    - Randomly select three distinct solutions a, b and c from the population
    - Pick a random index $R \in \{1,2,3,\cdots,n\}$ (n being the dimension of the problem).
    - Compute the agent's potentially new position $\tilde{\boldsymbol{y}} = [\tilde{y}_1, \tilde{y}_2, \tilde{y}_3, \cdots, \tilde{y}_n]$ as follows:
      - For each k, pick a uniformly distributed random number, $r_k = U(0,1)$
      - If $r_k < CR$ (CR is the crossover rate) or $k = R$, then set $\tilde{y}_k = a_k + F(b_k - c_k)$ ($F \in [0,2]$ is the differential weight) otherwise, set $\tilde{y}_k = \tilde{x}_k$.
  - If $f(\tilde{\boldsymbol{y}}) < f(\tilde{\boldsymbol{x}})$, replace the agent in the population with the improved candidate solution, that is, replace $\tilde{\boldsymbol{x}}$ with $\tilde{\boldsymbol{y}}$ in the population
- Pick the agent from the population that has the highest fitness or lowest cost and return it as best found candidate solution.

3.2 Particle Swarm Optimization (PSO) Algorithm

PSO, first proposed by Kennedy and Eberhart (1995), is a population based heuristic optimization algorithm which is based on the social behavior of the animals like bird flocking or fish schooling. In PSO, the population is called as the swarm and each individual solution in the swarm is called as the particle. During the solution, each particle in the swarm explores the search space to seek the optimum solution by using their current positions and velocities. These positions and velocities are generated randomly from the possible search space in the beginning of the optimization process. Then, velocity of each particle is updated based on their individual experiences and experiences of the other particles in the swarm. Finally, the position of each particle is updated by using the updated velocities and this process is repeated until the convergence criterion is met. This solution sequence guarantees that each particle in the swarm move towards the optimum solution based on their own experiences (local search) and the experiences of the other particles in the swarm (global search). The computational scheme of the PSO can be given as follows (1995):

- Randomly initialize all positions $\tilde{\boldsymbol{x}}$ and velocity vectors $\tilde{\boldsymbol{v}}$ for each particle in the swarm (NP being the number of particles in the swarm) such that $\tilde{\boldsymbol{x}} \in \mathrm{rand}(\tilde{\boldsymbol{x}}_{\min}, \tilde{\boldsymbol{x}}_{\max})$ and $\tilde{\boldsymbol{v}} = 0$
- $\tilde{\boldsymbol{p}} = \tilde{\boldsymbol{x}}$ and $\tilde{\boldsymbol{g}} = \arg \underbrace{\min}_{\tilde{x}} \left(f(\tilde{\boldsymbol{x}})\right)$
- Repeat the following until a termination criterion is met:
  - For each particle:

- Generate uniform random numbers
- Update velocities of each particle: $\tilde{\boldsymbol{v}}^{k+1} = \omega\tilde{\boldsymbol{v}}^{k} + c_1\,\mathrm{rand}(0,1)(\tilde{\boldsymbol{p}} - \tilde{\boldsymbol{x}}^{k}) + c_2\,\mathrm{rand}(0,1)(\tilde{\boldsymbol{g}} - \tilde{\boldsymbol{x}}^{k})$
- Update positions of each particle: $\tilde{\boldsymbol{x}}^{k+1} = \tilde{\boldsymbol{x}}^{k} + \tilde{\boldsymbol{v}}^{k+1}$
- Calculate $f(\tilde{\boldsymbol{x}}^{k+1})$
- Update local best: $\tilde{\boldsymbol{p}} = \tilde{\boldsymbol{x}}$ if $f(\tilde{\boldsymbol{x}}) < f(\tilde{\boldsymbol{p}})$
- Update global best: $\tilde{\boldsymbol{g}} = \tilde{\boldsymbol{x}}$ if $f(\tilde{\boldsymbol{x}}) < f(\tilde{\boldsymbol{g}})$

4 PROBLEM FORMULATION

As indicated in the previous sections, the objective of the DE and PSO based optimization approaches are to determine the numbers, locations, and pumping rates of the wells which will be used in the construction dewatering system. Since the cost of the dewatering system is directly related with the pumping rates, the objective function of the optimization model is used as the minimization of the total groundwater withdrawal rate which is supplied from all the pumping wells. The problem was solved for different number of wells and the identification results were evaluated together. Regarding this solution scheme, the problem of construction dewatering optimization can be mathematically formulated as follows:

Let n_w be the number of pumping wells to be used in the dewatering system; $Q(x_i, y_i)$ be the pumping rate of the well located at (x_i, y_i) where $i = 1,2,3,\cdots,n_w$; n_p be the number of piezometers where the groundwater table elevations are controlled; and s_j is the calculated drawdown value at j^{th} piezometer where $j = 1,2,3,\cdots,n_p$. Depending on these definitions, the objective function and the constraints of the optimization model is defined as follows:

$$z = \min\left\{\sum_{i=1}^{n_w}[Q(x_i, y_i) + \lambda_1 P(x_i, y_i)] + \lambda_2 \sum_{j=1}^{n_p} P(s_j)\right\} \quad [3]$$

subjected to

$$Q_{min} \le Q(x_i, y_i) \le Q_{max} \quad [4]$$

$$x_{min} \le x_i \le x_{max} \quad [5]$$

$$y_{min} \le y_i \le y_{max} \quad [6]$$

$$P(x_i, y_i) = \begin{cases} 0 & \text{if the location } (x_i, y_i) \text{ is a suitable region} \\ 1 & \text{otherwise} \end{cases} \quad [7]$$

$$P(s_j) = \begin{cases} 0 & \text{if } s_j \ge \delta \\ |s_j - \delta| & \text{otherwise} \end{cases} \quad [8]$$

where $P(x_i, y_i)$ is the penalty function regarding the well location suitability, $P(s_j)$ is the penalty function regarding the allowable drawdown of δ, λ_1 and λ_2 are the penalty coefficients which are used to adjust the magnitude of the penalty terms, Q_{min} and Q_{max} are the minimum and maximum pumping rates, x_{min}, y_{min}, x_{max}, and y_{max} are the minimum and maximum limit values of the well locations in x and y directions, respectively. The decision variables of the optimization model are x_i, y_i, and $Q(x_i, y_i)$ for all $i = 1,2,3,\cdots,n_w$.

5 NUMERICAL APPLICATION

In this section, the applicability of the proposed DE and PSO based solution approaches were evaluated by solving a hypothetical construction site dewatering problem. The plan view of the site and the surrounding buildings can be seen in Figure 3. Note that this is a shopping mall construction site, and thus, it has a deep foundation with a depth of $20\,m$.

Hydrogeological studies around the site indicated that the aquifer system was unconfined and the groundwater table was $5\,m$ below the ground surface. The hydraulic conductivity value, radius of well influence, and aquifer thickness before pumping were determined as $K = 0.00002\,m/s$, $R = 250\,m$, and $H = 60\,m$, respectively. In order to measure the variation of the groundwater table elevations, this site was surrounded by 9 piezometers with each of them fully penetrated the entire aquifer thickness. In order to maintain safe working conditions and prevent the slope stability problems, groundwater table elevations must be lowered to $5\,m$ below the bottom of the excavation site ($\delta = 20$ m). For this purpose, the contractor planned to drill new pumping wells which were equipped with the submersible pumps with a maximum pumping rate of $40\,l/s$. Since these wells will be active throughout the construction period, it is required to

minimize their numbers and pumping rates for obtaining the best solution in terms of the final dewatering cost. Therefore, the objective here is to determine the numbers, locations, and pumping rates of these submersible pumps by minimizing Eq. [3] subjected to the constraints in Eq. [4]-[8]. Note that DE solution of this example problem was already performed by Ayvaz (2017) by using the following parameters: $NI = 20$, $F = 0.80$, $CR = 0.90$, and the maximum generation numbers of 10,000. In these parameters, NI corresponds to the number of individuals in the population, F is the scaling factor which corresponds to the mutation operator in GA, and CR is the crossover rate which is used to produce new offspring from the parents. Note that although $NI = 20$ may be sufficient to solve a complex optimization problem in DE, the same situation may not be observed in PSO. Therefore, $NP = 200$ is used in the PSO solution depending on the recommendations in literature and the previous experiences. Note that since 10,000 DE generations with $NI = 20$ corresponds to 200,000 simulation model runs, the same limit value is also considered in PSO by assuming the maximum generation number of 1,000. Depending on the recommendations of Hu and Eberhart (2001), the other solution parameters of PSO are used as $\omega = (0.5 + \mathrm{rand}(0,1))/2$ and $c_1 = c_2 = 2$. Selection the value of these parameters are very important in PSO. While the value of ω controls the impact of previous historical values on their current ones, c_1 and c_2 are used to determine the contribution of particle's own experiences and the experiences of the other particles in the swarm. By using these parameters in PSO, the construction site dewatering problem was solved for different number of pumping wells. In order to maintain the consistency in DE and PSO solutions, the following parameter bounds were used just as given in Ayvaz (2017): $x_{min} = 0$, $y_{min} = 0$, $x_{max} = 500$, $y_{max} = 300$, $Q_{max} = 40\ l/s$, $Q_{max} = 40\ l/s$, $\lambda_1 = 100$, $\lambda_2 = 100$. Table 1 compares the identification results for $n_w = 1$ to 5 pumping wells in the system. As can be seen from Table 1, for $n_w = 1$, both DE and PSO resulted with the same objective function values of 9973.78 and this value has a penalty of 9933.78 for both models. Similar situation is also observed for $n_w = 2$ such that both model takes about the penalty value of 3459. These results indicated that the dewatering optimization problem cannot be solved by using 1 or 2 pumping wells due to the locations and drawdown constraints if the upper bound of the pumping rates are fixed to $Q_{max} = 40\ l/s$. For $n_w = 3$ to 5, it is observed no penalty value in both DE and PSO based optimization models which indicates that the dewatering optimization problem can be solved without any constraint violations in terms of Eqs. [7] and [8]. When the objective function values are compared, it can be seen that their final values decrease with inclusion of the new pumping wells in both models. However, these improvements are not significant in both DE and PSO solutions. For each solution, the identified well locations for both DE and PSO based optimization approaches are compared in Figure 4.

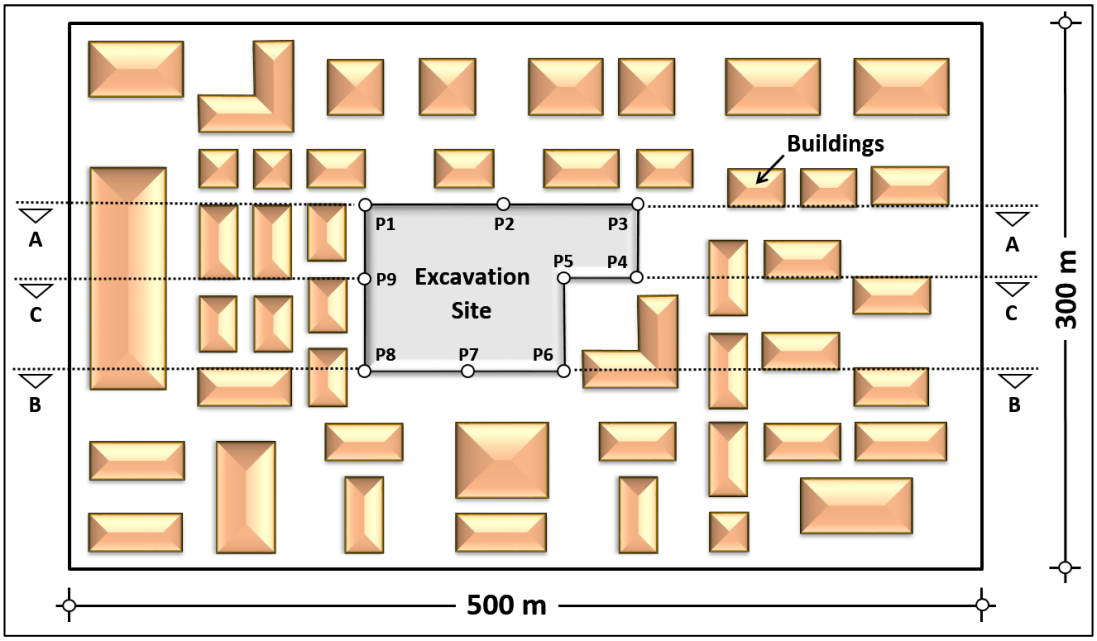

Figure 3. Example construction site dewatering problem.

Table 1. Comparison of the identification results for $n_w = 1$ to 5 in both DE and PSO.

	n_w	z	Total Penalty Value	Identified Pumping Rates (l/s)				
				$Q(x_1, y_1)$	$Q(x_2, y_2)$	$Q(x_3, y_3)$	$Q(x_4, y_4)$	$Q(x_5, y_5)$
DE	1	9973.78	9933.78	40.00	-	-	-	-
	2	3538.91	3458.91	40.00	40.00	-	-	-
	3	118.18	-	40.00	38.38	39.80	-	-
	4	113.09	-	37.05	24.63	11.40	40.00	-
	5	108.78	-	40.00	5.89	21.59	13.94	27.36
PSO	1	9973.78	9933.78	40.00	-	-	-	-
	2	3539.03	3459.03	40.00	40.00	-	-	-
	3	118.30	-	40.00	38.30	40.00	-	-
	4	111.78	-	22.88	33.35	15.55	40.00	-
	5	111.34	-	18.19	21.32	30.49	13.22	28.12

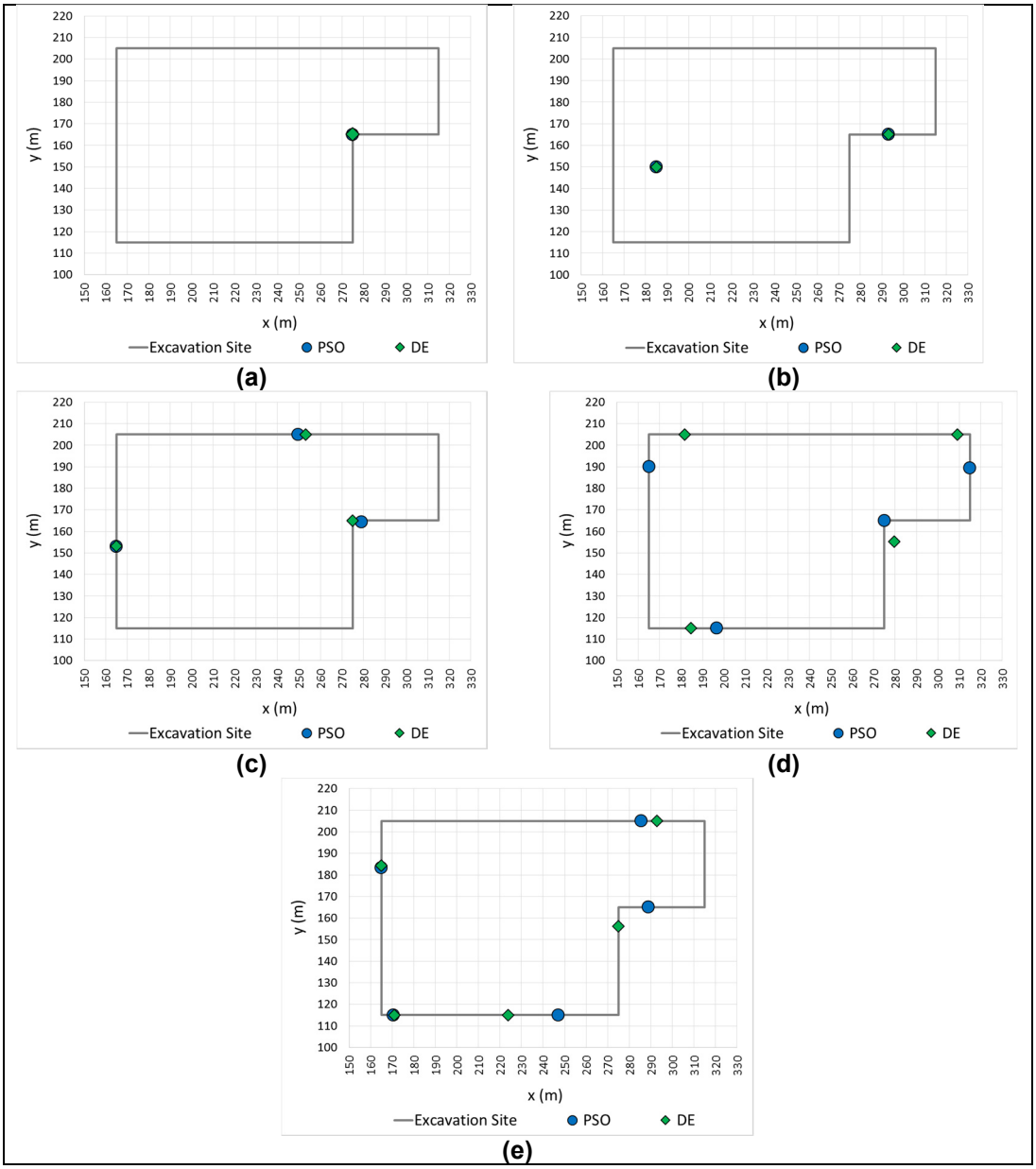

Figure 4. Identified well locations for the PSO and DE based optimization models for (a): $n_w = 1$; (b): $n_w = 2$; (c): $n_w = 3$; (d): $n_w = 4$; (e): $n_w = 5$.

As can be seen from Figure 4, for both models, all the wells are located around the border line of the excavation site which is an expected behavior. While the same or very close locations are identified for $n_w = 1$ to 3, there are some differences in the identified locations for $n_w = 4$ and 5. However, these differences are not too much. For these results, the measured drawdown values at piezometer locations are compared in Table 2. As can be seen, the drawdown constraint given in Eq. [8] is not satisfied for $n_w = 1$ and 2. Although all the piezometers satisfy the given drawdown constraint for $n_w = 3$ for both DE and PSO, it obtains big drawdowns especially in P2, P5, and P9. Since the cost of pumping is directly related with the magnitude of drawdowns, use of this solution may not be feasible in terms of the operation cost of the dewatering system. Note that these big drawdown values can be significantly reduced by including additional pumping well in $n_w = 4$ especially for the DE solution. Finally, in $n_w = 5$, all the drawdown values become more uniform except for the piezometer P5 in DE although it is obtained as acceptable in PSO. After evaluating the model results in terms of the final pumping rates and measured drawdown values, the solution of $n_w = 4$ for DE may be selected as the feasible solution in terms of the engineering point of view. However, by considering well drilling, dewatering equipment, and operation costs, a detailed analysis should be conducted which is the beyond of the scope of this study. For $n_w = 4$, variations of the identified well locations for each generation and the final locations of the pumping wells are compared in Figure 5 and 6 (small icons represent the variations of the well locations through different generations and big icons represent the final locations). As can be seen, although the wells are located over the buildings and/or excavation site in early generations, the final locations are all obtained in the feasible regions due to the use of the constraint in Eq. [7].

Table 2. Comparison of the measured drawdown values at piezometer locations for $n_w = 1$ to 5.

Piezometers	Number of Wells (n_w)									
	1		2		3		4		5	
	DE	PSO	DE	PSO	DE	PSO	DE	PSO	DE	PSO
P1	4.49	4.49	12.65	12.64	20.00	20.00	25.66	20.70	20.00	20.00
P2	9.31	9.31	14.59	14.58	32.19	33.60	20.75	20.00	20.00	20.00
P3	9.31	9.31	14.24	14.23	20.00	20.00	20.00	20.26	20.00	20.01
P4	11.47	11.47	20.00	20.00	21.47	22.07	20.00	21.68	20.31	20.00
P5	23.53	23.53	20.06	20.05	38.46	34.85	26.65	34.24	28.70	23.53
P6	9.88	9.88	14.86	14.86	20.00	20.00	20.00	20.00	20.00	20.00
P7	7.09	7.09	15.73	15.73	20.13	20.00	20.12	23.39	20.00	20.00
P8	4.31	4.31	15.35	15.37	20.00	20.00	20.35	20.00	20.00	20.00
P9	4.79	4.79	20.00	20.00	32.02	31.77	20.00	20.02	20.00	20.32

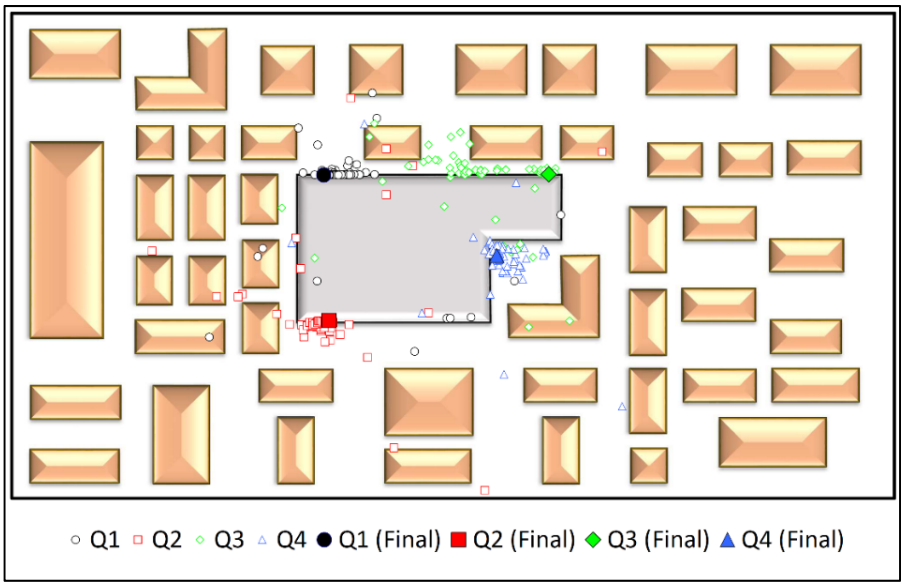

Figure 5. Locations of the identified final well locations for DE.

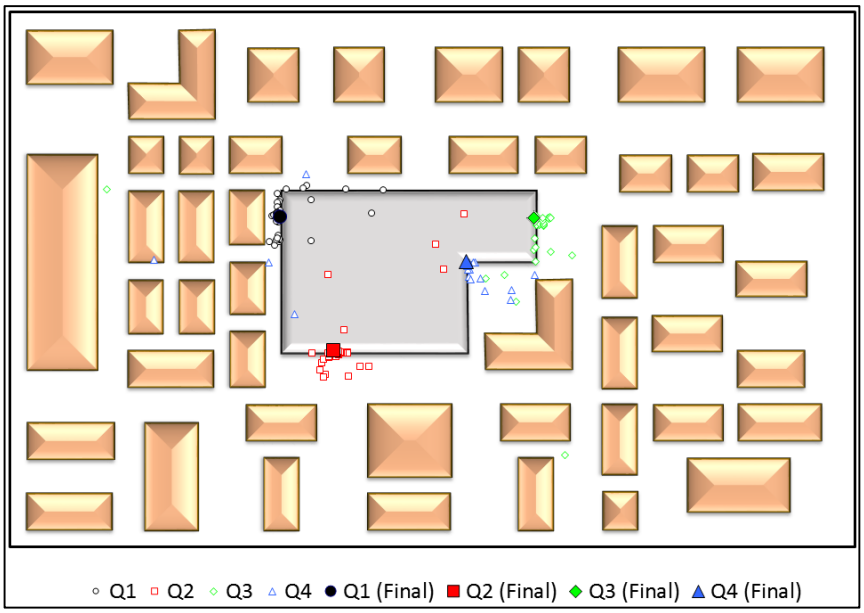

Figure 6. Locations of the identified final well locations for PSO.

For these dewatering configurations, the calculated groundwater table elevations are compared in Figure 7 for the cross-sections of A-A, B-B, and C-C given in Figure 3. As can be seen, minimum drawdown condition is satisfied in all the piezometers for both DE and PSO solutions.

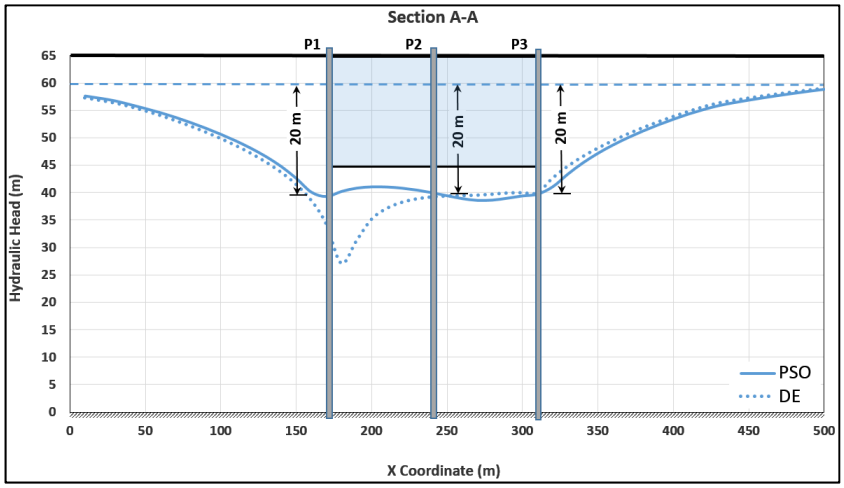

Figure 7. Groundwater table elevations through cross-section A-A.

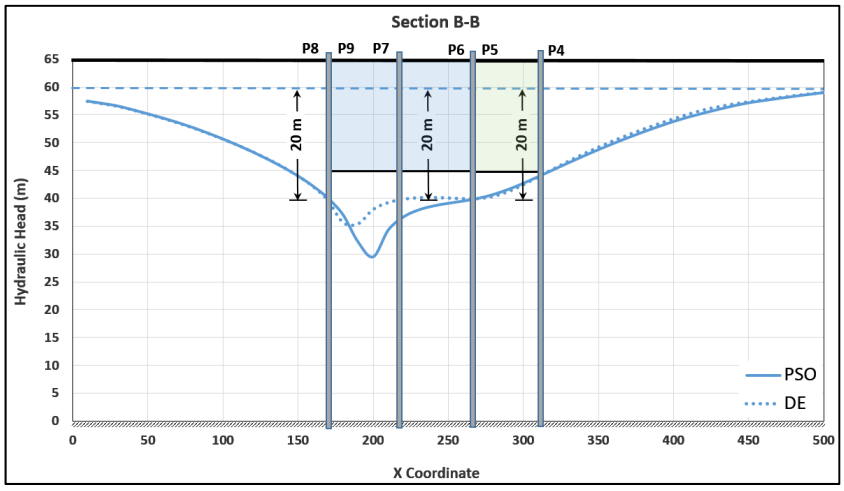

Figure 8. Groundwater table elevations through cross-section B-B.

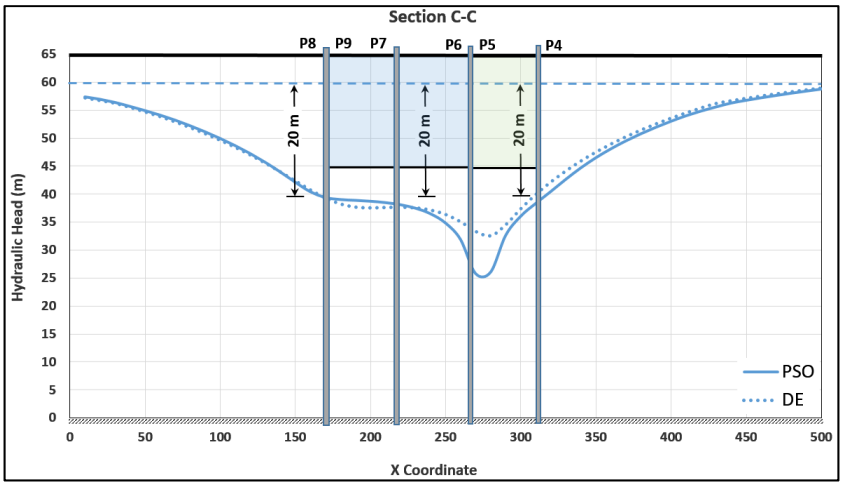

Figure 9. Groundwater table elevations through cross-section B-B.

6 CONCLUSIONS

In this study, performance of DE and PSO optimization approaches were evaluated by considering the same analytical groundwater flow model to solve the excavation site dewatering problems. The objective of the both approaches is to determine the locations and the pumping rates of the dewatering wells by minimizing the total groundwater withdrawal as the objective function. The best number of wells was determined by solving the problem for different number of dewatering wells implicitly. After obtaining the results for each solution, the identified results were compared in terms of both objective function and drawdown values in the piezometer locations. Comparison of these solutions indicates that both DE and PSO cannot determine a feasible solution for the configurations with 1 and 2 dewatering wells. For the other obtained configurations, although both approaches resulted with feasible solutions, the accuracy of the DE results is slightly better than PSO for the solutions with 3 and 5 dewatering wells. After evaluating the model results for both solutions, the configuration with 4 dewatering wells is selected as the best alternative solution. However, this decision should be supported with a detailed decision-making analysis by considering different physical and managerial criteria. Note that since the proposed model uses an analytical groundwater flow model in the simulation part, it requires to satisfy the steady-state flow and the idealized hydrogeological conditions. However, these limitations can be handled by integrating a more sophisticated numerical groundwater flow model, such as MODFLOW in the simulation part.

REFERENCES

Altan-Sakarya, A.B. & Onder, H. (2003). Insaat Kazı Sahasının Optimum Drenajı I. *Ulusal Su Mühendisligi Sempozyumu, Gümüldür, Izmir. Devlet Su Isleri Yayinlari, Turkey*, 169-180.

Ayvaz, M.T. (2017). Optimal Dewatering of an Excavation Site by using a Linked Simulation-Optimization Approach, IWA Regional Symposium on Water, Wastewater and Environment, March 22-24, 2017, Izmir, Turkey.

Ayvaz, M.T., Gürarslan, G., Eryiğit, M., Genç, Ö. & Eken, M. (2011). Simülasyon-optimizasyon modelleri kullanılarak inşaat kazı alanlarındaki yeraltı su seviyesinin düşürülmesi, İMO Denizli Teknik Bülteni, Sayı 67, Denizli. (In Turkish)

Demirbaş, K., Altan-Sakarya, A.B. & Önder H. (2008). Combined simulation-optimization of an excavation site for dewatering purpose. 8th International Congress on Advances in Civil Engineering, Sep 15-17, 2008, Gazimagusa, Cyprus.

Gökçe, S. & Ayvaz, M.T. (2014). A simulation-optimization model for optimal estimation of the numbers, locations and chlorine ınjection rates of the booster stations in water distribution networks. 11th International Conference on Hydroinformatics (HIC2014), Aug 17-21, 2014, New York, USA.

Hu, X. & Eberhart, R.C. (2001, April). Tracking Dynamic Systems with PSO: Where's the Cheese. *Proceedings of the workshop on particle swarm optimization* , 80-83.

Jiang, S., Kong, X., Ye, H. & Zhou, N. (2013). Groundwater Dewatering Optimization in the Shengli No. 1 Open-Pit Coalmine, Inner Mongolia, China. *Environmental earth sciences*, 69(1), 187-196.

Kayhan, A.H., Ceylan, H., Ayvaz, M.T. & Gurarslan, G. (2010). PSOLVER: A New Hybrid Particle Swarm Optimization Algorithm for Solving Continuous Optimization Problems. *Expert Systems with Applications*, 37(10), 6798-6808.

Kennedy, J. & Eberhart, R. (1995). Particle Swarm Optimization (PSO). *Proc. IEEE International Conference on Neural Networks, Perth, Australia*, 1942-1948.

Kresic, N. (2007). *Hydrogeology and Groundwater Modeling (Second Edition)*. CRC Press, NY, USA.

Nemati, K.M. (2007). Construction Dewatering and Ground Freezing, Temporary Structures Lecture Notes, University of Washington, USA.
Önder, H. & Değirmenci, M. (2000). Optimal dewatering system of an excavation. 4th International Congress on Advances in Civil Engineering, Nov 1-3, 2000, Gazimagusa, Cyprus.
Storn, R. & Price, K. (1997). Differential Evolution–A Simple and Efficient Heuristic for Global Optimization over Continuous Spaces. *Journal of global optimization*, 11(4), 341-359.
Tokgoz, M., Yilmaz, K.K. & Yazicigil, H. (2002). Optimal Aquifer Dewatering Schemes for Excavation of Collector Line. *Journal of water resources planning and management*, 128(4), 248-261.
Usul, N. (2007). Engineering Hydrology, METU Press, Ankara, Turkey.
Zhou, N., Vermeer, P.A., Lou, R., Tang, Y. & Jiang, S. (2010). Numerical Simulation of Deep Foundation Pit Dewatering and Optimization of Controlling Land Subsidence. *Engineering Geology*, 114(3), 251-260.

NEW EQUATIONS OF PARTIAL PENETRATION WELL

SUNJOTO SUNY(1)

Universitas Gadjah Mada, Yogyakarta, Indonesia,
sunysunyoto@gmail.com; sunysunyoto@ugm.ac.id

ABSTRACT

Partial penetration well is a well which its depth or tip of its casing does not reach an impermeable stratum beneath the aquifer. Basic pumping system equations of Dupuit-Thiem formulas is based on Darcy's Law for confined and unconfined aquifer as well as for full penetration well with fully perforated casing. In the practical implementation, this condition rarely occurs especially for thick aquifer; therefore, many researchers developed a correction for those formulas from full penetration to be partial penetration wells. Despite the correction, those formulas still have difficulty to compute the design of pumping system due to its need for hydraulic gradient data which can only be defined by two real time data of piezometric head before and after pumping related to horizontal distance of both points. This value is not a constant for different discharge of pumping. This study developed 16 equations for the confined and unconfined aquifer based on Forchheimer's formula. There are 6 configurations of confined aquifer which all of those equations are valid for computation of pumping as well as of recharging. For the unconfined aquifer, there are 10 configurations which contain 4 equations valid for computation of pumping as well as of recharging, 3 equations are valid only for computation of pumping of partly perforated casing and the 3 remaining equations are valid only for computation of recharging of fully perforated casing. All of those above equations are in steady state flow condition and it can be harmonized easily to be unsteady state flow condition by following Sunjoto's equation. With these proposed equations, the design of well systems can be computed easily, as to a relationship between coefficient of permeability, shape factor, discharge of pumping and drawdown or built-up.

Keywords: Full penetration well; partial penetration well; pumping; recharging; correction factor.

1 INTRODUCTION

1.1 Darcy's law

Darcy (1856) developed in his book '*Les fontains publiques de la ville de Dijon'*, an equation which it became basic equation of groundwater flow especially for theoretic solution was:

In scalar expression:

$$V = Ki \quad or \quad V = K\frac{dh}{dl} \tag{1}$$

In vector expression:

$$V = K\nabla H \tag{2}$$

Discharge:

$$q = KiA \tag{3}$$

1.2 Dupuit-Thiem's formula

Based on Darcy's Law (1856), Dupuit (1863) developed a formula of groundwater flow for unconfined aquifer and then it was completed by Thiem (1906) on confined aquifer, and it became more comprehensive, finally both equations were called Dupuit-Thiem equations which were determined as basic groundwater engineering computation for steady state radial flow, and the general equations were:

1.2.1 Unconfined aquifer

$$Q = \frac{\pi K(h_1^2 - h_2^2)}{ln\left(\frac{r_1}{r_2}\right)} \tag{4}$$

1.2.2 Confined aquifer.

$$Q = \frac{2\pi KD(h_1 - h_2)}{ln\left(\frac{r_1}{r_2}\right)} \quad [5]$$

where,

Q: discharge of pumping; *K*: coefficient of permeability; *D*: thickness of confined aquifer; r_1 & r_2: distance from well to observation well 1 and 2 respectively; h_1 & h_2: head of water in observation well 1 and 2 respectively.

Equation Eq. [4] or Eq. [5] need two real time data which it should be found only by pumping test, there are difference between h_1 and h_2 related to horizontal distance of the both observation wells with the radius r_1 and r_2.

1.3 Forchheimer's formula

Forchheimer (1930) developed a steady state radial flow condition to determine coefficient of permeability (*K*) of bore holes test with watertight casing, as:

$$Q_o = FKh \quad [6]$$

The formula is a relationship between discharge outflow from well to the ground (Q_o) is equal to shape factor (*F*) multiplied by coefficient of permeability (*K*), multiplied by hydraulic head or built-up (*h*), where this equation can be executed without pumping test data. In this equation, he also proposed a new parameter, which was 'shape factor'.

1.4 Sunjoto's formula

Based on Forchheimer (1930), Sunjoto (1988) developed an equation to compute built up of recharging well on the unsteady state condition which was derived mathematically by integration solution, as:

$$h = \frac{Q}{FK}\left\{1 - exp\left(\frac{-FKt}{\pi r_w^2}\right)\right\} \quad [7]$$

where:

Q: recharge or discharge (L^3/T); *F*: shape factor of well (L); *K*: coefficient of permeability (L/T); *h*: built-up (L); *t*: duration of flow (T); r_w: radius of well (L).

The equation, Eq. [7] is an unsteady state condition and when radius of well $r_w=1$ and duration of flow $T=\infty$, the equation will become $Q=FKh$ or equal to Forchheimer (1930) of equation Eq. [6] which is a steady state condition.

2 EXISTING CORRECTION

The basic concept of existing corrections formula development of partial penetration well was the computation result using full penetration well parameters multiplied by correction factor; though some researchers also introduced new parameters of partial penetration well. All of this formula are based on the Darcy's Law and most of them used Dupuit-Thiem equations.

For the purpose to better understand the comparison between each formula, to the extent that it is possible, the parameters in this paper are changed to the same legend without decreasing its substance, for example, all thickness of confined aquifer is *D*, radius of well is r_w etc., as on the original formula are differed from each other.

2.1 Unconfined aquifer

Formulas of partial penetration well in unconfined aquifer are wells with configuration that watertight casing in upper side and perforated casing in lower side with pervious and impervious base of well as shown in Figure 1.

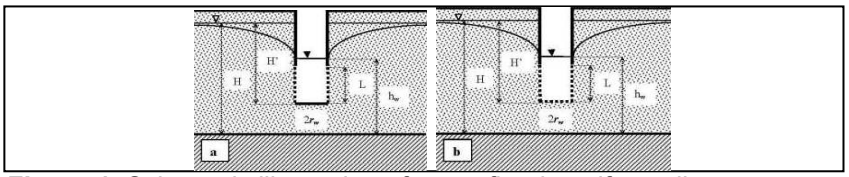

Figure 1. Schematic illustration of unconfined aquifer well parameters.

2.1.1 Forchheimer

Forcheimer in Bogomolov et.al. (1955) developed formulas for partly perforated casing, which are:

- Pervious well base (Fig.1b.):

$$Q_p = 2\pi K \frac{H^2 - h_w^2}{ln\left(\frac{R_i}{r_w}\right)} \times \left(\sqrt{\frac{L + 0.50 r_w}{h_w}} \times \sqrt[4]{\frac{2h_w - L}{h_w}} \right) \quad [8]$$

- Impervious well base (Fig.1a.):

$$Q_p = 2\pi K \frac{H^2 - h_w^2}{ln\left(\frac{R_i}{r_w}\right)} \left(\sqrt{\frac{L}{h_w}} \times \sqrt[4]{\frac{2h_w - L}{h_w}} \right) \quad [9]$$

2.1.2 Porchet

Porchet (1931) developed a formula for partly perforated casing and impervious well base (Fig.1a.) as:

$$Q_p = \pi K \frac{\left(H' + \frac{L}{2}\right)^2 - \left(h_w + \frac{L}{2}\right)^2}{ln\left(\frac{R_i}{r_w}\right)} \quad [10]$$

2.1.3 Castany

Inspired by Bogomolov et.al. (1955) of equations Eq. [18] & Eq. [19], Castany (1967) developed a similar formula for partly perforated casing formula and for:

- Pervious well base (Fig.1b.) was:

$$Q_p = 2\pi K \frac{H^2 - h_w^2}{ln\left(\frac{R_i}{r_w}\right)} \times \left(\sqrt{\frac{L + 0.50 r_w}{h_{wp}}} \times \sqrt[4]{\frac{2h_{wp} - L}{h_{wp}}} \right) \quad [11]$$

- Impervious well base (Fig.1a.) was:

$$Q_p = 2\pi K \frac{H^2 - h_w^2}{ln\left(\frac{R_i}{r_w}\right)} \times \left(\sqrt{\frac{L}{h_{wp}}} \times \sqrt[4]{\frac{2h_{wp} - L}{h_{wp}}} \right) \quad [12]$$

2.1.4 Todd

In his book '*Groundwater Hydrology-Second Edition'*, Todd (1980) improved the previous formula for partly perforated casing and pervious well base (Fig.1b.) as follows:

$$Q_p = \frac{2\pi K L\left(h_w - h_{wp}\right)}{\left(1 - \frac{L}{h_w}\right) ln \frac{\left(1 - \frac{L}{h_w}\right) L}{r_w}} \quad [13]$$

2.2 Confined aquifer

Formulas of partial penetration well in confined aquifer are well with configuration that perforated casing placed below the impermeable layer with pervious and impervious well base as shown in Figure 2.

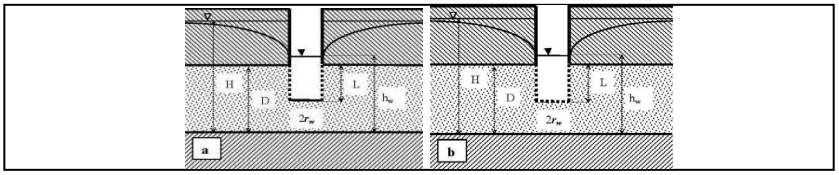

Figure 2. Schematic illustration of confined aquifer well parameters.

2.2.1 Samsioe

Samsioe (1931) considered a bundle of line sink and from this starting point and he derived the approximate formula as follows:

$$Q_p = \frac{2\pi KL(H-h_w)}{ln\left\{\frac{r_w}{2L}\left(\frac{4D}{R_i}\right)^{L/D}\left(\frac{D-0.72L}{D+0.72L}\right)^{0.40}\right\}} \quad [14]$$

2.2.2 Muskat

Muskat (1932) applying method of images, developed approximate formula:

$$Q_p = \frac{2\pi KD(H-h_w)}{\frac{1}{2L/D}\times\left\{2ln\frac{4D}{r_w}ln\frac{\Gamma(0.875L/D)\Gamma(0.125L/D)}{\Gamma(1-0.875L/D)\Gamma(1-0.125L/D)}\right\}-ln\frac{4D}{R_i}} \quad [15]$$

2.2.3 Kozeny

Based on Muskat's (1932) formula and number of calculated example, Kozeny (1933) has proposed a formula for impervious well base (Figure 2a.), as:

$$Q_p = \frac{2\pi KD(H-h_w)}{ln\left(\frac{R_i}{r_w}\right)}\frac{L}{D}\times\left(1+7\sqrt{\frac{r_w}{2L}}\times cos\frac{\pi L}{2D}\right) \quad [16]$$

2.2.4 Li, Bock, Benton

According to Li et.al. (1954), the formula for impervious well base (Fig.2a.) was:

$$Q_p = \frac{2\pi KD(H-h_w)}{ln\left(\frac{R_i}{r_w}\right)+\left\{\left(\frac{D}{L}\right)^n-1\right\}ln\left(\frac{D}{r_w}\right)} \quad [17]$$

and,

$$n = \frac{3}{4}\left(\frac{D}{100r_w}\right)^{0.05} \quad [17a]$$

This formula valid for:

$$800 \geq \frac{D}{r_w} \geq 25 \;;\; r_w \geq D-L \;;\; 1 \geq \frac{L}{D} \geq 0.10 \quad [17b]$$

2.2.5 Bogomolov & Silin-Bektchourine

Inspired by Forchheimer of equation Eq. [8] and Eq. [9], Bogomolov et.al. (1955) developed a formula for:

- Pervious well base (Fig.2b.) which was:

$$Q_p = 2\pi KD\frac{(H-h_w)}{ln\left(\frac{R_i}{r_w}\right)}\times\left(\sqrt{\frac{L+0{,}50r_w}{D}}\times\sqrt[4]{\frac{2D-L}{D}}\right) \quad [18]$$

- Impervious well base (Fig.2a.) which was:

$$Q_p = 2\pi KD\frac{(H-h_w)}{ln\left(\frac{R_i}{r_w}\right)}\times\left(\sqrt{\frac{L}{D}}\times\sqrt[4]{\frac{2D-L}{D}}\right) \quad [19]$$

2.2.6 Todd

Todd (1980) developed a formula with partly perforated casing and pervious well base, which is valid for *L/D>0.20* (Fig.2b.) as:

$$Q_p = \frac{2\pi KL\left(h_w - h_{wp}\right)}{\left(1-\frac{L}{D}\right) ln \frac{\left(1-\frac{L}{D}\right)L}{r_w}} \quad [20]$$

where:

Q_p: discharge of partial penetration well (m^3/s); K: coefficient of permeability (m/s); D: thickness of aquifer (m); L: length of perforated casing (m); H: initial depth of groundwater (m); H': depth between groundwater level to tip of well for full penetration well (m); h_w: depth of water at well for full penetration well (m); h_{wp}: depth of water at well for partial penetration well (m); h_{2m}: piezometric head at 2meters from well axis for full penetration well (m); r_w: radius of well (m); and R_i: radius of influence for full penetration well (m).

Besides full penetration well parameters, Castany (1967) introduced a parameter of partial penetration well h_{wp} or depth of water at well for partial penetration well and Todd (1980) proposed a parameter s_p or drawdown of partial penetration well, which is $s_p=(H-h_{wp})$, where it was found from pumping in equal discharge between full and partial penetration well.

2.2.7 Hantush

According to Hantush (1962), when an aquifer is pumped by partial penetration well the assumption that the well receives from horizontal flow is no longer valid and leading to an extra loss of head. He developed a formula of partial penetration well in confined aquifer and the drawdown was:

$$s(r,t) = \frac{Q}{4\pi T}\{W_u + f_s\} \quad [21]$$

and,

$$f_s = \frac{2D}{\pi(b-d)} \sum_{n=1}^{\infty} \left(\frac{1}{n}\right) W\left(u_s \frac{n\pi r}{D}\right) \left\{sin\left(\frac{n\pi b}{D}\right) - sin\left(\frac{n\pi d}{D}\right)\right\} \left(cos\frac{n\pi z}{D}\right) \quad [21a]$$

where:

Q: discharge (m^3/s); T: transmissivity (m^2/s); $s(r,t)$: drawdown (m); $W(u, n\pi r/D)$: Hantush well function; b: penetration depth of pump (m); b': piezometer head (m); d: non-screened part (m); d': piezometer head (m); and z=(b'+d')/2 (m).

Besides the above correction formulas, most researchers examining the topic used formulas developed based on Dupuit-Thiem equation. Nonetheless, they still have difficulty to compute a design of well system due to the existence of parameters of hydraulic gradients which can only be figured out by pumping test first.

3 ANALYSIS

3.1 Shape factor

Besides his new formula, Forchheimer (1930) introduced a parameter which was called shape factor. Shape factor (F) multiplied by hydraulic head (h) (Eq. [6]) are representation of gradient hydraulic (i) multiplied by area of flow (A) in Darcy's Law (1856) (Eq. [3]). The shape factor value depends on radius and perforated length of casing and condition of base of well and soil layers existence.

Figure 3. shows a configuration of confined and unconfined aquifer without an information of impermeable layer existence. Dahler (1936) derived the formula based on the concept that flow line is hyperbolic form, equipotential was ellipse form and the value of shape factor (F) of well with perforated casing on confined aquifer Fig.3a. was:

$$F = \frac{2\pi L}{ln\left\{\frac{L}{r_w} + \sqrt{\left(\frac{L}{r_w}\right)^2 + 1}\right\}} \quad [22]$$

and for unconfined aquifer Fig.3c. was:

$$F = \frac{2\pi L}{ln\left\{\frac{L}{2r_w} + \sqrt{\left(\frac{L}{2r_w}\right)^2 + 1}\right\}} \quad [23]$$

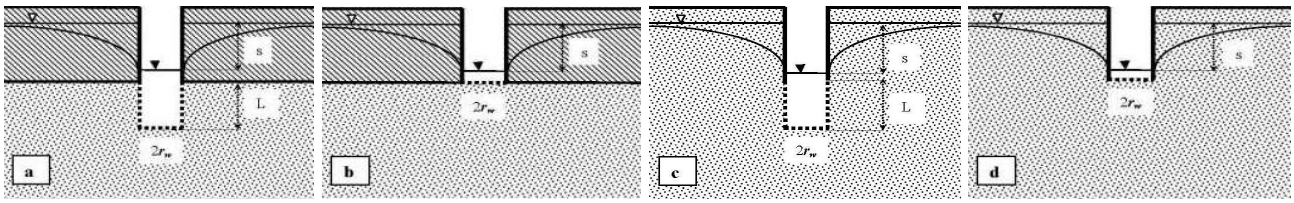

Figure 3. Schematic of illustrating well parameters of confined and unconfined aquifer without an information of impermeable stratum existence.

When the value of *L=0,* the well Fig.3a. becomes Fig.3b. and the well Fig.3c. becomes Fig.3d., therefore, the shape factor will be equal respectively. However, when *L=0*, the value of shape factors of Eq. [22] and Eq. [23] are 'indefinite'. The shortage of those formulas validity caused by the assumption that the well base is pervious while the formula derivation based on impervious base of well.

To solve the problem on practical implementation, Dahler (1936) determined that the both equations only valid for $L/r_w>10$. However, Sunjoto (2002) proved that equation Eq. [22] is valid for $L/r_w>0.96$ and equation Eq. [23] is valid for $L/r_w>2.71$.

Forchheimer in Bogomolov et.al. (1955), Bogomolov et.al. (1955) and Castany (1967) attempted to differ the formula of a well with pervious base and impervious base. They decided for the well with pervious base that the transformation value from area of well base to length of perforated casing was $0.50r_w$, see equations Eq. [8], Eq. [11] and Eq. [18], but Sunjoto (2002) proved that transformation value was $r_w ln2$. Based on this value, equation Eq. [22] of Fig.3a. can be improved to:

$$F = \frac{2\pi L + 2\pi r_w ln2}{ln\left\{\frac{L+2r_w}{r_w} + \sqrt{\left(\frac{L}{r_w}\right)^2 + 1}\right\}} \qquad [24]$$

and equation Eq. (23) of Fig.3c. to:

$$F = \frac{2\pi L + 2\pi r_w ln2}{ln\left\{\frac{L+2r_w}{2r_w} + \sqrt{\left(\frac{L}{2r_w}\right)^2 + 1}\right\}} \qquad [25]$$

When $L=0$, $r_w=1$ or $L/r_w=0$ and these values are substituted to equation Eq. [24], the shape factor of Fig.3a. will be equal to $F=3.964r_w$. This value is almost equal to analytic value of equation Eq. [26] which was derived mathematically, that is $F=4r_w$.

Forhheimer (1930), Dachler (1936) and Aravin (1965) with different ways, derived analytically the shape factor formula of Fig.3b. and it should exactly be equal to:

$$F = 4r_w \qquad [26]$$

However, on the field test to find coefficient of permeability, Forcheimer (1930) implemented the shape factor value of confined aquifer equation Eq. [26] for condition of unconfined well Fig.3d.

Five years later, on their laboratory test, Harza (1935) using sand tank obtained $F=4.8r_w$ to $5.6r_w$ for shape factor of well Fig.3d. Then, Taylor (1948) by flow net obtained $F=5.7r_w$, and Hvorslev (1951), by using electric analog apparatus, concluded the compromised value of those shape factors (Fig.3d) became:

$$F = 5.50r_w \qquad [27]$$

Moreover, Sunjoto (2002) proved that when *L=0,* of equation Eq. [25], well Fig.3c. will change to be Fig.3d. When *L=0,* $r_w=1$ or $L/r_w=0$, the value of shape factor (*F*) will be equal to $6.283r_w$, and based on this reason it was concluded theoretically that the shape factor of well Fig.(3d) is:

$$F = 2\pi r_w \qquad [28]$$

This value of equation Eq. [28] improved Eq. [27] since it was derived analytically so it has better validity and reliability than above laboratory test which had differ result.

3.2 Correction factor

The basic idea of the proposed equations is a modification of shape factor (*F*) by a correction factor (Ω). Correction factor is comparison of space between tip of well and impermeable stratum beneath of aquifer (λ) to value of transformation of well base area to be length of perforated casing. Then, based on Forchheimer equation Eq. [6], discharge of partial penetration well can be developed using corrected shape factor.

With transformation approval of Sunjoto (2002) from horizontal circle area with radius r_w as a well base to be a vertical cylinder as a casing is $r_w ln2$, and λ is a space under tip of well, the correction factor becomes:

$$\Omega = \frac{\lambda}{r_w ln2} \qquad [29]$$

When value of $\Omega=0$, the flow is a full penetration well, and when $1>\Omega>0$ it is a partly partial penetration well, then when $\Omega \geq 1$ the flow of water under the tip of well has no obstacle anymore and this condition is called a partial penetration well.

where:

Ω: correction factor; λ: gab between tip of well to impermeable stratum (L); and r_w: radius of well (L).

3.3 Drawdown versus built-up

Drawdown is an occurrence of decreasing of groundwater table near a well and surroundings caused by pumping (*s*) and on the contrary when it increases caused by recharging it is called built-up (*h*). For the equal condition of discharge, shape factor, coefficient of permeability and duration of pumping or recharging the drawdown and built-up will be equal value but with inverse direction or $s = -h$, and for the next analysis for Fig.4. to Fig.7. and for the equations Eq. [30] to Eq. [47] the legend of built up is equal to drawdown, that is *s* and the equation will be (Sunjoto, 2014):

For the unsteady state condition:

$$Q = \frac{FKs}{\left\{1 - exp\left(\frac{-FKt}{\pi r_w^2}\right)\right\}} \qquad [30]$$

For the steady state condition:

$$Q = FKs \qquad [31]$$

where:

Q: recharge or discharge (L^3/T); *F*: shape factor of well (L); *K*: coefficient of permeability (L/T); *s*: drawdown or built-up (L); *t*: duration of flow (T); and r_w: radius of well (L).

4 RESULT OF STUDY

Base on Forchheimer (1930) equation Eq. [6] then using shape factor (*F*) and take into consideration the correction factor of equation Eq. [29] for the appropriate position of impermeable stratum beneath of the aquifer, equations of each condition can be developed. All of the proposed equations derived analytically based on the previous equations which the validity had been proved on the laboratory test.

4.1 Confined aquifer

For the confined aquifer, all of equations Eq. [32] to Eq. [3]) are valid for 'pumping as well as recharging', when the perforated casing is always below the groundwater surface on steady state condition pumping ($H-s>L+\lambda$) and before recharging ($H>L+\lambda$). The configurations of pumping are presented as Fig.4a. to Fig.4f. and for recharging are presented as the figure Fig.5a. to Fig.5f., but built-up *s* has equal value with upward direction. The symbol *s* is parameter of drawdown as well as built-up because of pumping and recharging.

For 'pumping as well as recharging' on the confined aquifer, there are six configurations with the parameters which can be seen in Fig.4. and Fig.5., and based on shape factor (Sunjoto, 2002) the equations become:

4.1.1 Full penetration well with fully perforated casing (Fig.4a & 5a), where $L=D$ & $\lambda=0$:

$$Q_{pr} = \frac{2\pi DKs}{ln\left\{\frac{D+2r_w}{r_w} + \sqrt{\left(\frac{D}{r_w}\right)^2 + 1}\right\}} \qquad [32]$$

4.1.2 Partial penetration well without casing and pervious well base (Fig.4b & 5b), where λ=*D* & *L=0*:

$$Q_{pr} = 4\,\Omega r_w K s \qquad [33]$$

4.1.3 Full penetration well with partly perforated casing (Fig.4c & 5c), where *L<D* & λ*=0*:

$$Q_{pr} = \frac{2\pi LKs}{ln\left\{\frac{L+2r_w}{r_w} + \sqrt{\left(\frac{L}{r_w}\right)^2 + 1}\right\}} \qquad [34]$$

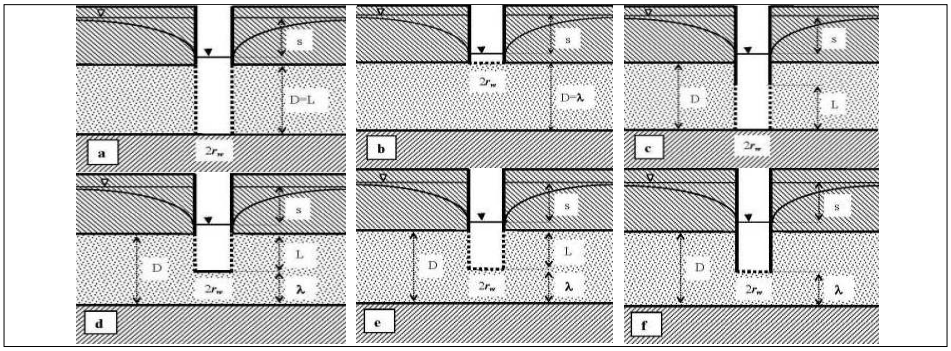

Figure 4. Schematic of illustrating confined aquifer well parameters for pumping.

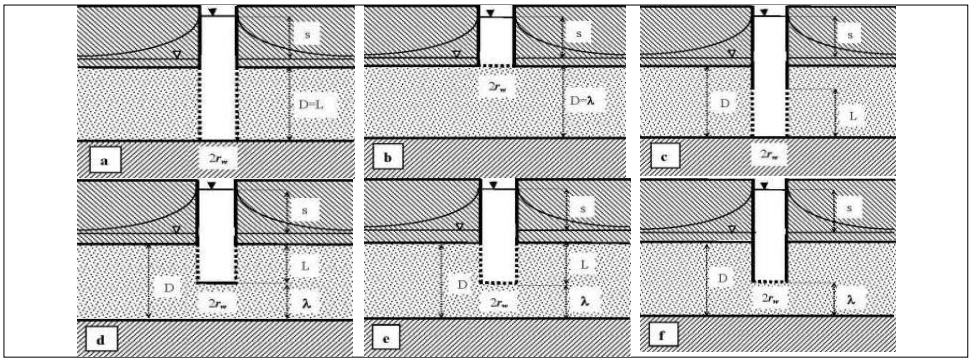

Figure 5. Schematic of illustrating confined aquifer well parameters for recharging.

4.1.4 Partial penetration well with fully perforated casing and impervious well base (Fig.4d & 5d), where λ+*L=D*:

$$Q_{pr} = \frac{2\pi LKs}{ln\left\{\frac{L+2r_w}{r_w} + \sqrt{\left(\frac{L}{r_w}\right)^2 + 1}\right\}} \qquad [35]$$

4.1.5 Partial penetration well with fully perforated casing and pervious well base (Fig.4e & 5e), where λ+*L=D*:

$$Q_{pr} = \frac{2\pi Ks(L + \Omega r_w ln2)}{ln\left\{\frac{L+2r_w}{r_w} + \sqrt{\left(\frac{L}{r_w}\right)^2 + 1}\right\}} \qquad [36]$$

4.1.6 Partial penetration well without perforated casing with pervious well base (Fig.4f & 5f), where λ<*D*:

$$Q_{pr} = 4\Omega r_w K s \qquad [37]$$

4.2 Unconfined aquifer

For the unconfined aquifer, there are two conditions, *firstly* is for full or partial penetration well with partly perforated casing which are valid for pumping as well as recharging (Fig.6.), *secondly* is full or partial penetration well with fully perforated casing which are only valid for pumping only and for recharging only (Fig.7).

4.2.1 Pumping as well as recharging for partly perforated casing

Well with watertight casing in upper side and perforated casing in lower side which all of the equations are valid for pumping on the steady state condition ($H-s>L+\lambda$) as well as recharging ($H>L+\lambda$) with the parameters which can be seen in Fig.6, and for pumping as well as recharging, the equation is as follows:

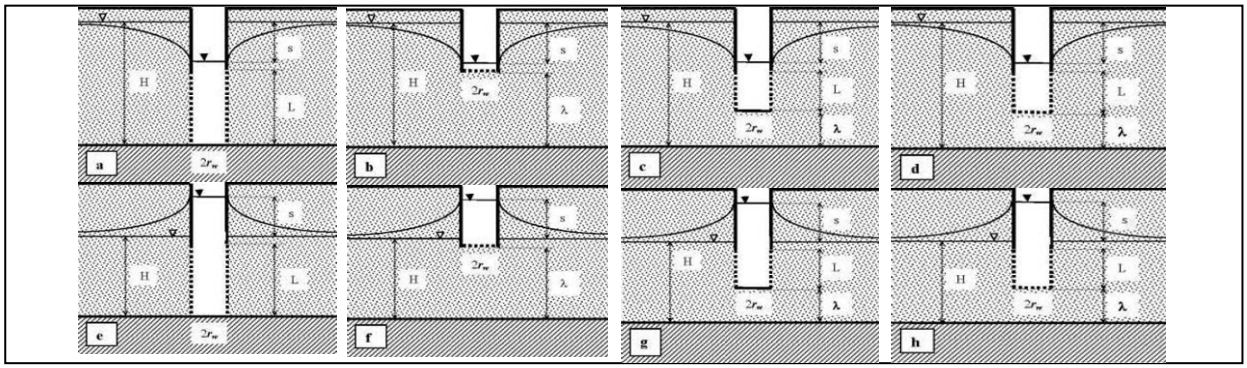

Figure 6. Schematic of illustrating unconfined aquifer well parameters for pumping as well as recharging.

- Full penetration well with partly perforated casing (Fig.6a & 6e), where $\lambda=0$:

$$Q_{pr} = \frac{2\pi LKs}{ln\left\{\frac{L+2r_w}{2r_w} + \sqrt{\left(\frac{L}{2r_w}\right)^2 + 1}\right\}} \quad [38]$$

- Partial penetration well without perforated casing and pervious well base (Fig.6b & 6f), where $\lambda\neq0$ & $L=0$:

$$Q_{pr} = 2\Omega\pi r_w Ks \quad [39]$$

- Partial penetration well with partly perforated casing and impervious well base (Fig.6c & 6g), where $\lambda\neq0$ & $L\neq0$:

$$Q_{pr} = \frac{2\pi LKs}{ln\left\{\frac{L+2r_w}{2r_w} + \sqrt{\left(\frac{L}{2r_w}\right)^2 + 1}\right\}} \quad [40]$$

- Partial penetration well partly perforated casing and pervious well base (Fig.6d & 6h), where $\lambda\neq0$ & $L\neq0$:

$$Q_{pr} = \frac{2\pi Ks(L + \Omega r_w ln2)}{ln\left\{\frac{L+2r_w}{2r_w} + \sqrt{\left(\frac{L}{2r_w}\right)^2 + 1}\right\}} \quad [41]$$

4.2.2 Pumping and recharging for fully perforated casing

For full or partial penetration well with fully perforated casing, the length of casing that water can flow into or out from the casing will differ between pumping and recharging. On the pumping it will decrease and become shorter and on the recharging it will increase and become longer.

The configuration of figures Fig.7a., Fig.7b., Fig.7c. is valid for pumping and Fig.7d., Fig.7e., Fig.7f. is valid for recharging and the development of equation of these configurations using previous shape factors (Sunjoto, 2002) become:

Equations for pumping

- Partial penetration well with fully perforated casing and pervious well base (Fig.7a.) where $\lambda \neq 0$:

$$Q_p = \frac{2\pi Ks\{(H'-s) + \Omega r_w ln2\}}{ln\left\{\frac{(H'-s)+2r_w}{2r_w} + \sqrt{\left(\frac{(H'-s)}{2r_w}\right)^2 + 1}\right\}} \quad [42]$$

- Partial penetration well with fully perforated casing and impervious well base (Fig.7b.) where $\lambda \neq 0$:

$$Q_p = \frac{2\pi Ks(H'-s)}{ln\left\{\frac{(H'-s)+2r_w}{2r_w} + \sqrt{\left(\frac{(H'-s)}{2r_w}\right)^2 + 1}\right\}} \quad [43]$$

- Full penetration well fully perforated casing (Fig.7c.) where $\lambda = 0$:

$$Q_p = \frac{2\pi Ks(H'-s)}{ln\left\{\frac{(H'-s)+2r_w}{2r_w} + \sqrt{\left(\frac{(H'-s)}{2r_w}\right)^2 + 1}\right\}} \quad [44]$$

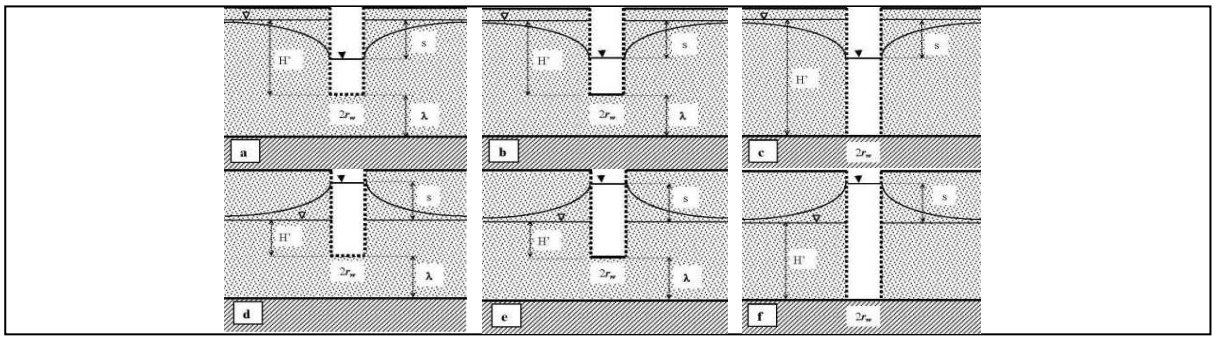

Figure 7. Schematic of illustrating unconfined aquifer well parameters, for pumping and for recharging.

Equations for recharging

- Partial penetration well fully perforated casing and pervious well base (Fig.7d.) where $\lambda \neq 0$:

$$Q_r = \frac{2\pi Ks\{(H'+s) + \Omega r_w ln2\}}{ln\left\{\frac{(H'+s)+2r_w}{2r_w} + \sqrt{\left(\frac{(H'+s)}{2r_w}\right)^2 + 1}\right\}} \quad [45]$$

- Partial penetration well with fully perforated casing and impervious well base (Fig.7e.) where $\lambda \neq 0$:

$$Q_r = \frac{2\pi Ks(H'+s)}{ln\left\{\frac{(H'+s)+2r_w}{2r_w} + \sqrt{\left(\frac{(H'+s)}{2r_w}\right)^2 + 1}\right\}} \quad [46]$$

- Full penetration well with fully perforated casing (Fig.7f.) where $\lambda = 0$:

$$Q_r = \frac{2\pi Ks(H'+s)}{ln\left\{\frac{(H'+s)+2r_w}{2r_w} + \sqrt{\left(\frac{(H'+s)}{2r_w}\right)^2 + 1}\right\}} \quad [47]$$

where (for Fig.4. to Fig.7. and Eq. [32]. to Eq. [47].):

Q_{pr}: discharge of pumping and recharging (L^3/T); Q_p: discharge of pumping (L^3/T); Q_r: discharge of recharging (L^3/T); K: coefficient of permeability (L/T); D: thickness of aquifer (L); H: initial groundwater depth (L); H': gap between initial groundwater level to tip of well (L); r_w: radius of well (L); s: drawdown or built-up (L); L: length of perforated casing (L); λ: gap between tip of well to the impervious layer (L); and Ω: correction factor (when $\Omega \geq 1$ on equation put Ω=1).

4.3 Condition

All of the proposed equations, Eq. [32] to Eq. [47] based on equation Eq. [31] are in steady state flow, and for unsteady state condition it must be harmonized based on equation Eq. [30].

5 CONCLUSIONS

- The proposed equations are relationship between discharge (Q), coefficient of permeability (K), drawdown or built-up (s) and shape factor (F) and are easily computed for design;
- When $\Omega = 0$, the condition is full penetration well, when $1 > \Omega > 0$, it is a partly partial penetration well and when $\Omega \geq 1$, the condition is a complete partial penetration well and put the value of correction factor on the equations is 'equal to one' ($\Omega = 1$);
- When the wells Fig.4., Fig.5., Fig.6. and Fig.7. have no information of stratum layer position beneath aquifer like Fig.3., therefore the condition of all equations, Eq. [32] to Eq. [47] are complete partial penetration wells, and put the value of correction factor on the equations is 'equal to one' ($\Omega = 1$).

REFERENCES

Aravin, V.I. & Numerov, S.N. (1965). *Theory of Fluid Flow in Undeformable Porous Media*. Translated from Russian, Israel Program for Scientific Translations, Jerusalem.

Bogomolov, G.V. & Silin-Bektchourine, A.I. (1955). *Hydrogéoloie Specialisée*, Moscow. Traduction par: Jayet, E., Castany, G., *Annales du Sevice d'Information Géologique, no. 37, 1959, Publié avec l'aide du* CNRS.

Castany, G. (1967). *Traité Pratique des Eaux Souterraines, Deuxième Édition*. Dunod, Paris.

Dachler, R. (1936). *Grundwasserstromung.* Julius Springer, Wien.

Darcy, H. (1856). *Histoire des Fontaines Publiques de la Ville de Dijon*. Dalmont, Paris.

Dupuit, J. (1863). *Éstudes Thèoriques et Pratiques sur le Mouvement des Eaux dans les Canaux Dècouverts et à Travers les Terrains Permèables.* (Second Edition), Dunod, Paris.

Forchheimer, P. (1930). *Hydraulik, 3rd*, B.G. Teubner, Leipzig.

Hantush, M.S. (1962). Aquifer Tests on Partially Penetrating Wells. *Amer. Soc. Civil. Engr. Trans*., 127(1), 284-308.

Harza, L.F. (1935). Uplift and Seepage under Dams on Sand. *Amer. Soc. Civil. Engr. Trans*., 100(1), 1352-1385.

Hvorslev, M.J. (1951). *Time Lag and Soil Permeability in Ground Water Observation*, Bulletin 36, Waterways Experiment Station, Vicksburg, Mississippi, 3-55.

Kozeny, J. (1933). Theorie und Berechnung der Brunnen. *Wasserkraft und Wasserwirtschaft,* 28, 88-92.

Li, W.H., Bock P. & Benton G. (1954). A New Formula for Flow into Partially Penetrating Wells in Aquifers. *Trans. Amer. Geophysical Union*, 35(5), 806-811.

Muskat, M. (1932). Potential Distribution in Large Cylindrical Discs with Partially Penetrating Electrodes. *Physics,* 2(5), 329-366.

Porchet, M. (1931). Hydrodinamique des Puits. *Ann. Du Genie Rural Fasc*., 6.

Samsioe, A.F. (1931). Einfluss von Rohrbrunnen auf die Bewegung des Grundwassers. *Zeitschrift für Angewandte Mathematik und Mechanik*, 11(2), 124-135.

Sunjoto, S. (1988). *Optimasi Sumur Resapan Sebagai Salah Satu Pencegahan Intrusi Air Laut,* In *Proc. Seminar PAU-IT-UGM*, Yogyakarta.

Sunjoto, S. (2002). Recharge Wells as Drainage System to Increase Groundwater Storage, In *Proc. on the 13rd IAHR-APD Congress, Advance in Hydraulics Water Eng*., Singapore, 1, 511-514.

Sunjoto, S. (2014). Drawdown Minimizing to Restrain Sea Water Intrusion in Urban Coastal Area, *SEATUC Symposium, Ibnu Sina Institute for Fundamental Science Studies*, UTM, Johor Bahru.

Taylor, D.W. (1948). *Fundamental of Soil Mechanics*, Wiley, New York.

Thiem, G. (1906). *Hydrologische Methoden*. J.M. Gebhart, Leipzig, 56.

Todd, D.K. (1980). *Groundwater Hydrology*. Second Edition, John Wiley and Sons, 151.

Proceedings of the 37th IAHR World Congress
August 13 – 18, 2017, Kuala Lumpur, Malaysia

QUANTIFICATION OF IRRIGATION EFFECT ON THE GROUDWATER RECHARGE IN CROP FIELDS OF THE SUBTROPICAL ISLAND, JAPAN

KOZUE YUGE[1], MITSUMASA ANAN[2] & KOSUKE HAMADA[3]

[1,2] Faculty of Agriculture, Saga University, Saga, Japan,
yuge@cc.saga-u.ac.jp; anan@cc.saga-u.ac.jp
[3] Graduate School of Bioresource and Bioenvironmental Sciences, Kyushu University, Fukuoka, Japan,
hama.suke1204@gmail.com

ABSTRACT

The aim of this study is quantifying irrigation effect on the groundwater recharge in crop fields of the subtropical island, Izena (N24° 55', E127° 56'), which is located in southwestern Japan. Izena Island is relatively plain and the soil of this island is classified as the special red-yellow clay soil (called Kunigami Maaji). This soil is acidic, and the hydraulic conductivity is high. The staple crop in this island is sugar cane and land use conditions can be categorized as the crop field, forest and artificial surface. In crop fields, a large amount of water is irrigated for not only supply water loss of evapotranspiration but also various purposes, for example, protection of salt breeze damage or leaching. Since main water resource for irrigation is dependent on groundwater in the study site and there is a serious risk of drought, subsurface dams have been constructed to supply the agricultural water and it is important to evaluate the groundwater movement to develop the subsurface dams, considering the land use condition and agricultural water use. The groundwater analysis was performed using MODFLOW in a subtropical island which is located in southwestern Japan. To simulate the groundwater flow, surface water balance in each land use condition was estimated in the study site. Boundary conditions were specified using elevation, surface water balance and sea water level. Scenario analysis was performed to evaluate the effect of irrigation water of crop fields on groundwater recharge under several assumed land use conditions. The results indicated that the irrigation water in crop fields contributed to the groundwater recharge and the water loss by the rainfall and the evapotranspiration in the crop field was less than the amount of that in the forest.

Keywords: Groundwater storage; multi-functionality of agriculture; land use condition; surface water balance; water demand.

1 INTRODUCTION

There are lots of subtropical islands in southwest Japan and various crops are produced taking advantage of warm climate. On the other hand, irrigation water demand has increased to produce various crops and water resources for agriculture are insufficient. In addition, since a large amount of water which is not only for supply water loss of evapotranspiration but also various purposes for example, protection of salt breeze damage or leaching, is irrigated in crop fields, there is a serious risk of drought in these islands. Agricultural water depends on the groundwater in most of these islands and subsurface dams have been constructed to supply the agricultural water (Kuronuma, 2015). In crop fields, the irrigation water and rainfall are consumed as the evapotranspiration and surface runoff. The surplus water infiltrates into the ground, and is stored in the permeable layer as the groundwater. It is important to evaluate the groundwater movement to develop the subsurface dams, considering the land use condition and agricultural water use.

The groundwater analysis, considering the land use condition, has been studied by many researchers. A simulation model to analyze the impacts induced by different irrigation management schemes on groundwater levels was established by Saleh et al. (1989). An integrated water management model for decision-making in irrigation water management to maintain the groundwater table was developed by Kumar and Singh (2003). Anan et al. (2007) quantified the effect of irrigation in rice paddy fields on groundwater recharge. These studies clarified the significant effects of irrigation on the groundwater; however, effect of crop fields in subtropical islands on the groundwater recharge has not been yet evaluated quantitatively.

The aim of this study is quantification of irrigation effect in crop fields of a subtropical island on the groundwater recharge. The groundwater analysis was performed using MODFLOW in a subtropical island which is located in southwestern Japan. To simulate the groundwater flow and quantify the groundwater storage, surface water balance in each land use condition was estimated in the study site. Boundary conditions were specified using elevation, surface water balance and sea water level. Scenario analyses were performed to evaluate the effect of irrigation water of crop fields on groundwater recharge under assumed several land use conditions.

2 STUDY SITE

A groundwater analysis was performed in Izena Island (N24°55´, E127°56´), which is located in Okinawa Prefecture (Figure 1). Climate of Okinawa Prefecture is subtropical and various crops are produced throughout the year taking advantage of warm climate as shown in Figure 2.

Figure 3 shows the elevation and land use condition in the study site. Using the geographic information system software (TNT lite), the land use conditions were specified with a resolution of 100m squares. As shown in this figure, the study site is relatively plain. The land uses are classified into three categories: crop field, forest, and artificial surface. The total area of the study site is about 1540 ha. The crop field and forest are about 52% and 29% of the total area, respectively. Sugar cane is the staple product and is cultivated in most of crop fields in the study site.

The soil of the study site is classified as the special red-yellow clay soil (Kunigami Maaji soil). The Kunigami Maaji soil is acidic, and the hydraulic conductivity of this soil is rather high. In the study site, the water resource for the agriculture is heavily dependent on groundwater. The drought occurs frequently because hydraulic conductivity is high and the soil water retentivity is relatively low and agricultural product has had large impact at the study site. In addition, irrigation water demand is increasing because of crop diversification as shown in Figure 2. To cope with the water resource problem, the development of the subsurface dam was conducted at the study site from 1999 to 2011.

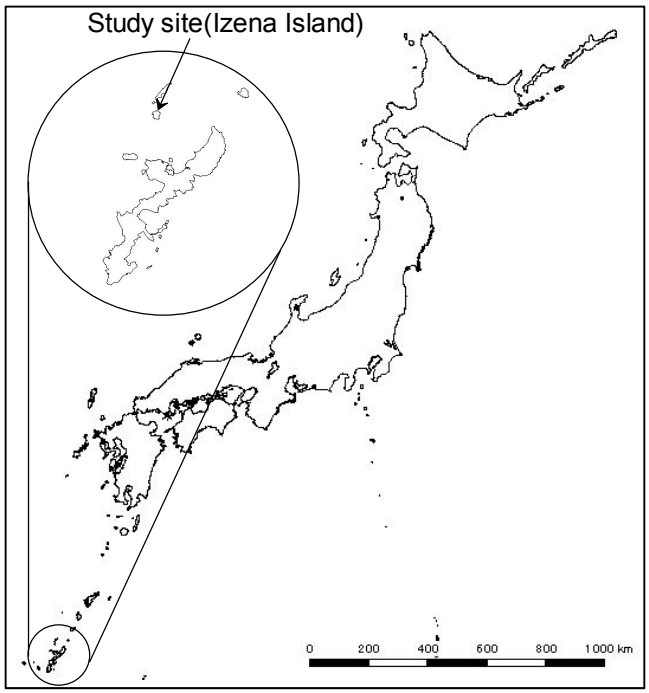

Figure 1. Location of study site.

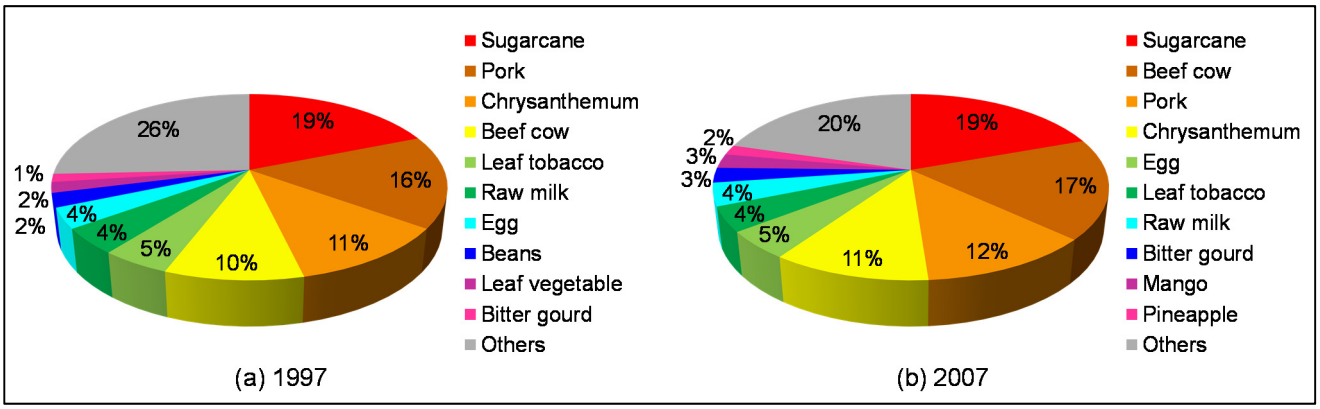

Figure 2. Gross agricultural production in Okinawa Prefecture in 1997 and 2007.

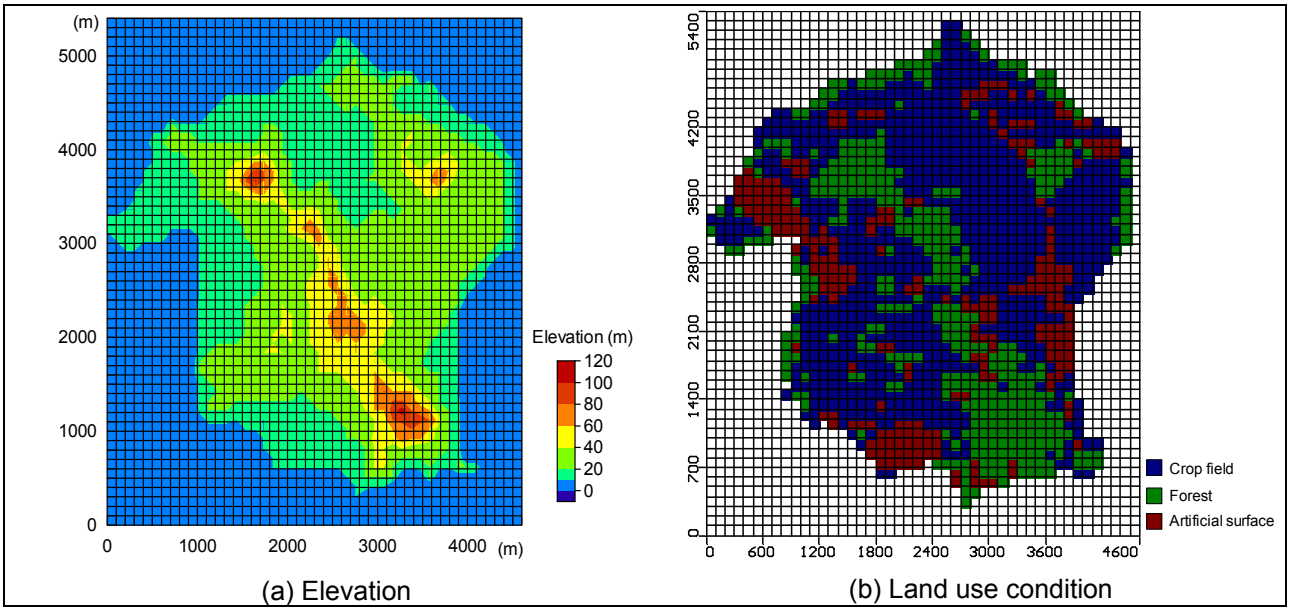

(a) Elevation (b) Land use condition

Figure 3. Elevation and land use condition in the study site.

3 MATERIALS AND METHODS

3.1 Governing equation

MODFLOW was used for groundwater analysis. MODFLOW is one of the most frequently used codes in groundwater hydrology (Anderson and Woessner, 1992). In this code, groundwater flow can be described with a following three-dimensional equation (McDonard and Harbaugh, 1988).

$$S\frac{\partial H}{\partial t}=\frac{\partial}{\partial x}\left(k_x h\frac{\partial H}{\partial x}\right)+\frac{\partial}{\partial y}\left(k_y h\frac{\partial H}{\partial y}\right)+\frac{\partial}{\partial z}\left(k_z h\frac{\partial H}{\partial z}\right)+Q+L \qquad [1]$$

where, S : effective porosity(-)
H : hydraulic head(m)
t : time(d)
k : hydraulic conductivity(m d^{-1})
h : sectional length of the groundwater flow(m)
Q : percolation of water from surface(m day^{-1})
L : outflow rate from the region(m day^{-1})

3.2 Initial and boundary conditions

The boundary condition was specified using the measured seawater level, which was given by the Japan Meteorological Agency. Figure 4 shows the schematic view of the specification of the initial conditions. Using the seawater level and elevation in Figure 3 of the study site, the initial heads at all nodes were specified with interpolation as shown in Figure 3.

Surface boundary condition can be specified using the water balance at the ground surface as follows:

$$\sum(R+A)-\sum(E+O+Q)=0 \qquad [2]$$

where, R : precipitation (m day^{-1}),
A : irrigation(m day^{-1})
E : evapotranspiration (m day^{-1})
O : runoff rate of rainfall (m day^{-1})

Evapotranspiration E in Eq. [2] was calculated as follows:

$$E = K_c ET_0 \qquad [3]$$

where, K_c : crop coefficient
ET_0 :is the reference evapotranspiration (m day^{-1})

ET_0 was estimated by the FAO Penman-Monteith method as follows:

$$ET_0 = \frac{0.408\Delta\left(R_n - G\right) + \gamma \frac{900}{T_a + 273} u_2 \left(e_s - e_a\right)}{\Delta + \gamma\left(1 + 0.34u_2\right)} \quad [4]$$

where, R_n : net radiation at the crop surface(MJ m^{-2} day^{-1})
G : ground heat flux(MJ m^{-2} day^{-1})
T_a : air temperature(°C)
u_2 : wind velocity(m s^{-1})
e_s : saturation vapor pressure (kPa)
e_a : actual vapor pressure (kPa)
γ : psychrometric constant (kPa °C $^{-1}$)
Δ : slope of vapor pressure curve(kPa °C $^{-1}$).

Runoff rate of rainfall, O, can be calculated by the following equation:

$$O = aR \quad [5]$$

where, a : runoff coefficient

Figure 5 shows the simulation model introduced by coupling the groundwater analysis and the land use information. For specifying the surface boundary conditions at all nodes, data on the land use condition (Figure 3) stored in the GIS database were transferred into the groundwater model using MODFROW.

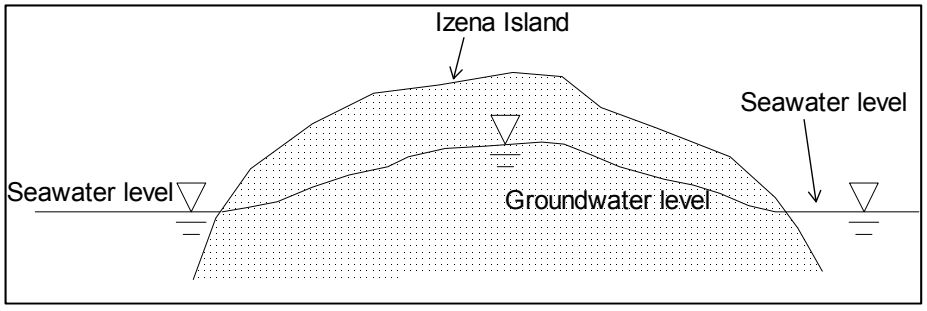

Figure 4. Schematic view of the specification of the initial conditions.

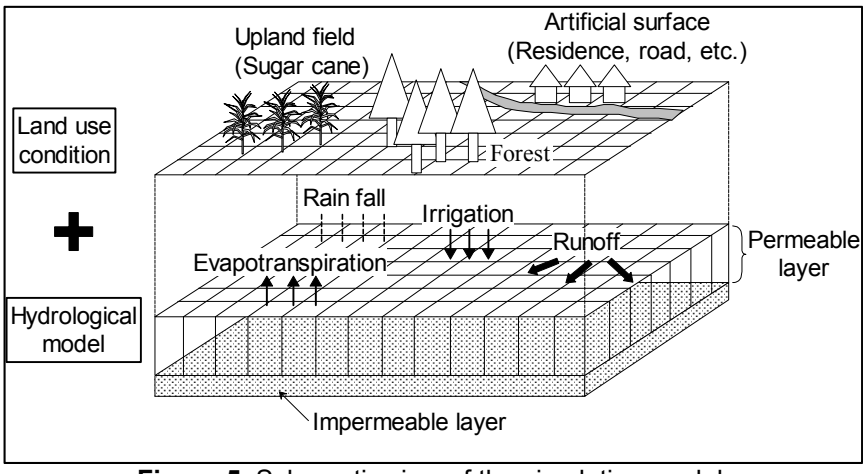

Figure 5. Schematic view of the simulation model.

4 SCENARIO ANALYSIS

The groundwater level was simulated in the area of 5400m times 4600m. The MODFLOW mesh for the study site had 54 columns and 46 rows. Each mesh size was 100 m square. The finite difference method was used to solve the governing equation in MODFLOW. The calculation was pursued with the SOR (Successive over-relaxation) method. The initial conditions were set using data in 1 Jan. 2003, and boundary conditions were specified by daily data from 1 Jan. to 31 Dec.

In the calculation, as the land use conditions was categorized as the crop field, forest, and artificial surface, the parameters in Eq. [2] should be estimated, considering the land use condition.

The amount of the irrigation water in the crop fields was given, assuming that all crop fields are used for cultivating the sugar cane from the present land use condition. The amount of irrigation water can be specified, considering the growth stages of the sugar cane, as shown in Table 1. Irrigation in the crop field was conducted until late in September, and irrigation interval was 7-8 days. Irrigation at the forest and the artificial surface were specified as 0.

The parameters for estimating the evapotranspiration E by Eq. [2] were estimated using the method suggested by Allen et al. (1998) with the meteorological data of the weather station. To estimate the evapotranspiration, considering the sugar cane growth stage, K_c of the crop field was given as shown in Figure 6 (Allen et al., 1998). The growth stages of the sugar cane were estimated using the cultivation guideline of the sugar cane (Okinawa Prefecture, 1999). K_c of the forest and artificial surface were set as 1.5 and 0.0 throughout the year, respectively.

The values of runoff coefficient in the crop field, the forest, and the artificial surface were assumed as 0.45, 0.5, and 0.9, respectively (Yoshikawa, 1966).

To evaluate the effect of the crop field irrigation on the groundwater storage, the groundwater level was simulated under three scenarios shown in Table 2. The groundwater movement was evaluated under the present land use condition (Scenario 1). The groundwater analysis was conducted, assuming that all forests are converted into crop fields and the land use condition was classified as the crop field and artificial surface (Scenario 2). In Scenario 3, land use condition was assumed as two categories (crop field and artificial surface) and runoff coefficient in the crop field was set as 0. This condition represented that facilities for water harvesting were constructed in crop fields.

Table 1. Irrigation schedule of the sugar cane.

Growth stages	Irrigation amount (mm)
Seeding	30-35
Germinating	15-20
Tillering	20-25
Mid-season	35-40

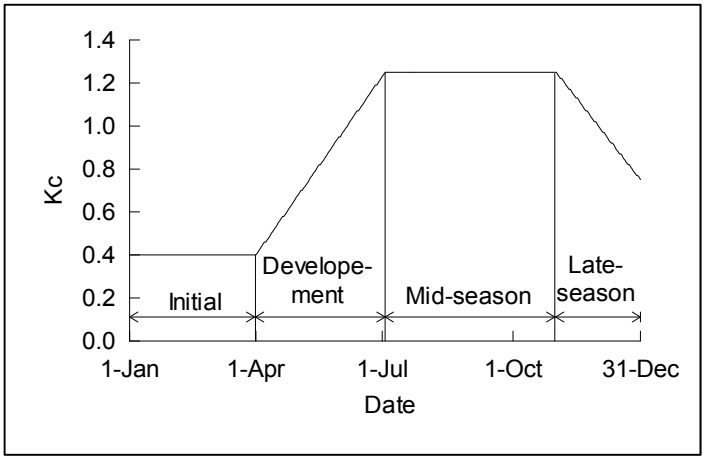

Figure 6. Growth stages and crop coefficient of the sugar cane.

Table 2. Scenarios for groundwater analysis.

Scenario No.	Land use condition	Runoff coefficient
1	Present condition (Crop field, Forest, Artificial surface)	Crop field: 0.45 Forest: 0.5 Artificial surface: 0.9
2	Forests were converted into crop fields (Crop field, Artificial surface)	Crop field: 0.45 Artificial surface: 0.9
3	Forests were converted into crop fields (Crop field, Artificial surface)	Crop field: 0.0 Artificial surface: 0.9

5 RESULTS AND DISCUSSIONS

Figure 7 shows daily changes of evapotranspiration in the crop field and forest. As shown in this figure, evapotranspiration in forest was relative high throughout the year. In the crop field, evapotranspiration was relative low from January to April and increased gradually with crop growth.

Figure 8 shows total amount of groundwater retained in the permeable layer simulated under three scenarios shown in Table 2. Under the present land use condition (Scenario 1), the groundwater storage increased during the growth period of the sugar cane. However, after the end of the growth stages, the groundwater storage decreased gradually, and in December, the amount of the groundwater storage reached 0 m^3. The groundwater storage, calculated on the assumption that all forests are converted into crop fields (Scenario 2), was larger than the storage under Scenario 1 as shown in Figure 8. The result indicated that irrigation in crop fields recharge the groundwater and water losses by evapotranspiration and runoff in crop fields were low compared with forests. Groundwater storage simulated under Scenario 3 increased compared with Scenarios 1 and 2. This result indicated that facilities for water harvesting are effective to increase the groundwater storage.

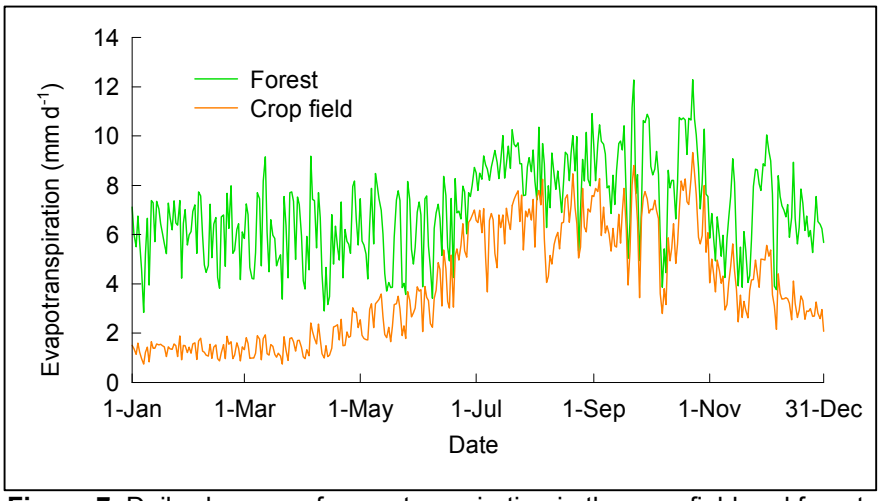

Figure 7. Daily changes of evapotranspiration in the crop field and forest.

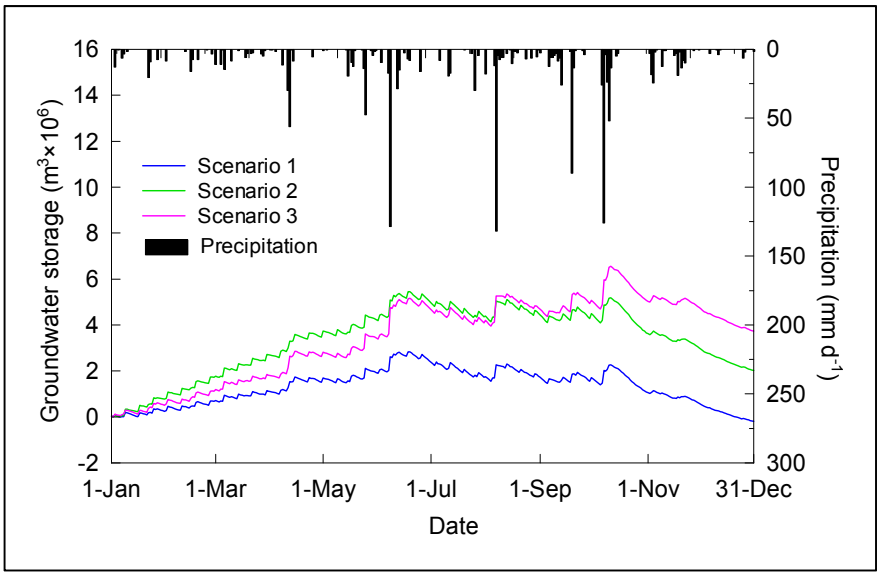

Figure 8. Daily changes of groundwater storage in three scenarios.

6 CONCLUSIONS

To evaluate the effect of the irrigation in crop fields on the groundwater recharge, the groundwater analysis was performed in Izena Island. A numerical model of groundwater flow using MODFLOW was introduced for quantifying the groundwater storage. To specify the initial groundwater level using the seawater level as the initial condition of the numerical model, the elevation data at the study site stored in GIS database were transferred into the model. Additionally, to set the surface boundary condition, data on the land use condition in the study site stored in the GIS database were transferred into the groundwater model. To quantify the effect of irrigation in the crop field on groundwater recharge, the groundwater flow was simulated

under three scenarios with various land use condition. The result of scenario analysis indicated that groundwater storage, when all forests are converted into the crop field, was larger than the groundwater storage under the present land use condition and the irrigation in crop fields recharge the groundwater and water losses by evapotranspiration and runoff in crop fields were low compared with forests. Groundwater storage simulated assuming that all forests are converted into the crop field and facilities for water harvesting were constructed in crop fields was the largest compared with other scenario. This result indicated that facilities for water harvesting are effective to enhance the infiltration of rainfall and reduce the water loss by runoff.

REFERENCES

Allen, R.G., Pereira, L.S., Raes, D. & Smith, M. (1998). Crop Evapotranspiration -Guidelines for Computing Crop Water Requirements. *FAO irrigation and drainage*, 56, 87-158

Anan, M., Yuge, K., Nakano, Y., Saptomo, S. & Haraguchi, T. (2007). Quantification of the Effect of Rice Paddy Area Changes on Recharging Groundwater. *Paddy and Water environment*, 5(1), 41-47.

Anderson, M.P. & Woessner, W.W. (1992). *Applied Groundwater Modeling Simulation of Flow and Advective Transport*. Academic Press, INC. 381.

Kumar, R. & Singh, J. (2003). Regional Water Management Modeling For Decision Support In Irrigated Agriculture. *Journal of irrigation and drainage engineering*, 129(6), 432-439.

Kuronuma, Y. (2015). The origin of underground dam and construction examples in islands. *Regional Studies*, 16, 81-102 (in Japanese)

McDonard, M.G. & Harbaugh, A.W. (1988). *A modular three-dimensional finite-difference ground water flow model*. Techniques of water-resources investigations of the U. S. Geological Survey, Book 6.

Okinawa Prefecture (1999). *Cultivation guideline of the sugar cane*. Okinawa Prefecture. (In Japanese)

Saleh, A.F.M., Steenhuis, T.S. & Walter, M.F. (1989). Groundwater Table Simulation Under Different Rice Irrigation Practices. *Journal of irrigation and drainage engineering*,115(4), 530-544.

GROUNDWATER HYDROGEOCHEMISTRY OF THE SHALLOW AQUIFER IN LOWER KELANTAN BASIN

ANUAR SEFIE[1], AHMAD ZAHARIN ARIS[2], TAHOORA SHEIKHY NARANY[3] MOHD KHAIRUL NIZAR SHAMSUDDIN[4], ISMAIL TAWNIE[5], AZRUL NORMI IDRIS[6], SYAIFUL BAHREN SAADUDIN[7] & ARSHAD OSMAN[8]

[1,4,5,6,7,8] Hydrogeology Research Centre, National Hydraulic Research Institute of Malaysia, Seri Kembangan, Malaysia, anuar@nahrim.gov.my; ismail@nahrim.gov.my; @nahrim.gov.my; nizar@nahrim.gov.my; azrul@nahrim.gov.my; bahren@nahrim.gov.my; arshad@nahrim.gov.my
[2] Faculty of Environmental Studies, Universiti Putra Malaysia, UPM Serdang, Malaysia, zaharin@upm.edu.my
[3] Technishe Universität Munchen, Münich, tahoora_sh@yahoo.com

ABSTRACT

Groundwater hydrogeochemical assessment of Lower Kelantan Basin has been carried out to determine the chemical constituents that controlled the groundwater quality. About 148 groundwater samples were collected from 37 wells and analysed for pH, electrical conductivity (EC), total dissolved solids (TDS), major cations (Ca^{2+}, Mg^{2+}, Na^{+}, K^{+}), anions (Cl^{-}, SO_4^{2-}, CO_3^{2-}, HCO_3^{-}, NO_3^{-}), Fe^{2+} and Mn^{2+}. Results revealed that groundwater is slightly acidic to alkaline. Four major hydrochemical facies Ca-HCO_3, Na-Cl, Na-HCO_3 and Ca-Cl were identified using a Piper trilinear diagram. The Ca-HCO_3 water type represents 57% of the groundwater samples suggest that the calcite solution has played an important role in controlling the groundwater chemistry in the study area. Na-Cl water type generally close to the coastal area and indicates a strong influence of ancient seawater and Na-HCO_3 water type show strong indicator of cation exchange process. The saturation indices demonstrate oversaturated condition with respect to iron containing minerals like $Fe(OH)_3$ and hematite and undersaturated with anhydrite, aragonite, calcite, dolomite, gypsum and manganite. Oversaturation of $Fe(OH)_3$ and hematite indicate the abundance of iron minerals in the study area aquifer. The study explains that the groundwater quality is controlled by anthropogenic activities and natural weathering processes.

Keywords: Correlation coefficient; groundwater quality assessment; hydrogeochemical facies; lower Kelantan basin; saturation indices.

1 INTRODUCTION

Groundwater has been proven to play an important role in the development of human civilization and economy growth of major developed countries in the world. Approximately one third of the world's population depend on groundwater for drinking purpose (Nickson et al., 2005). Groundwater overexploitation and other anthropogenic activities is a serious environmental issue nowadays. To protect the groundwater quality from degradation, geochemical assessment and monitoring are needed (Srinivas et al., 2015).

Coastal area particularly in Kelantan state, groundwater resource is abstracted from alluvial aquifers for drinking water, industrial and agricultural uses. Due to the increasing demand for water resources and pollution risks which pose a threat to human health, a deeper understanding of the availability and quality is necessary (Montcoudiol et al., 2015). Anthropogenic activity can affect the groundwater quality through agricultural, residential, industrial and municipal activities (Nas and Berktay, 2010). The poor water quality may also be attributed to the excessive content of ions and affect the soil fertility (Nishanthiny et al., 2010). Groundwater quality changes could be due to rock-water interaction and oxidation-reduction reactions during the water percolation through the aquifers (Krishnakumar et al., 2009).

Hydrogeochemical study is a useful tool in understanding and identifying the processes that are responsible for groundwater quality (Kumar et al., 2014). An understanding of the hydrogeochemical evolution, pollutant sources and regular water quality monitoring of groundwater is important for a sustainable development and effective management of water resources in any regions (Tiwari and Singh, 2014). Therefore, groundwater hydrogeochemistry assessment and sustainability consideration are of extremely importance especially in the Lower Kelantan Basin as almost 100% of urban and rural population still depend completely on treated and untreated groundwater resources. Moreover, very little study on assessing the groundwater hydrogeochemistry has been carried out in the study area. The aim of the study is to assess the groundwater hydrogeochemistry in shallow groundwater aquifer. Hydrogeochemical study could provide information that may be used for the utilisation of groundwater resources in a sustainable manner and can also help in the planning of water resources in the future.

2 MATERIALS AND METHODS

2.1 Study area

The study area is located in the most north-eastern part of Peninsular Malaysia which cover the Kota Bharu and Bachok districts. It lies between 5° 53' N and 6° 14' N and 102° 10' E and 102° 28' E covers an area of approximately 675 km^2. It is facing the South China Sea to the east and is bounded by the Kelantan River to the west. The study area is generally characterised by low lying coastal plain in the east and river plain in the west with surface elevations range a few meters to more than 150 m above mean sea level near the coastal area.

The study area is mainly drained by the three major rivers, namely; Pengkalan Datu, Kemasin and Semerak Rivers. Generally, all the rivers system flow northwest direction before discharging into the South China Sea. The land use is predominantly covered by agricultural followed by cleared land, built-up area, peat swamp and forest. The dominant agricultural land uses are paddy cultivation, mixed agricultural such as tobacco and vegetable, other crop (fruit), rubber and coconut. The study area has a hot and tropical climate with mean annual air temperature is 27°C and air temperatures are generally uniform throughout the year. Monthly mean of relative humidity is high and ranging from 80-87%. The average annual evapotranspiration and rainfall is about 1,510 mm 2,646 mm respectively (DID, 2011).

The geology of the study area is composed of marine Quaternary alluvium and fluviatile origin deposits (MacDonald, 1967). The Quaternary alluvium has the thickness of a few meters near the foot hills to more than 150 m in coastal area and forming the various layers of sand and gravels making up the productive aquifers (Ang and Ismail, 1996). The clay layer on the top can reach up to 8 m thick and disappear towards the coastal area. The alluvium is underlain by granitic bedrock and some small hills outcropping in south-eastern part of study area. The sedimentary or metasedimentary bedrock generally occur in south and western part consisting mainly of shale, sandstone, phyllite and slate (Abdul Rashid, 1989). The geological map of the study area is shown in Figure 1.

2.2 Sampling and analysis

Groundwater samples were collected 4 times from 2009-2014 from 37 wells utilized for domestic and agricultural purposes. The depth of sampling wells ranges from 3.0 to 12.0 m. The water samples were pumped out at least three well volumes to remove the stagnant water using a portable stainless steel submersible pump. The *in-situ* measurement was performed immediately after sampling on the samples pumped out from wells using YSI multiparameter instrument package with a built-in program and data-logging. Each portable meters were calibrated with standard solutions according to instrument manual. The parameters measured were temperature, pH, electrical conductivity (EC) and total dissolved solid (TDS).

The groundwater samples were filtered through 0.45 µm membrane filters and split into 2 polyethylene bottles, which contained the 250mL unpreserved water sample and another 250 mL was acidified with nitric acid (HNO_3^-) to a pH less than 2 to stops most bacterial growth, minimise adsorption of metals to container walls, oxidation reaction, and prevents adsorption or precipitation of cations (Appelo and Postma, 2005). The bottles were rinsed with distilled water before collecting the sample water. All groundwater samples were stored at a temperature of 4°C until the analysis were performed.

Total dissolved solids (TDS) were estimated by weighing the solid residue obtained by evaporation of a measured volume of water samples to dryness (Chopra and Kanvar, 1980). The calcium (Ca^{2+}), magnesium (Mg^{2+}), sodium (Na^+), potassium (K^+) were analysed using Inductively Coupled Plasma Mass Spectrometry (ICP-MS) NexION® 300 (PerkinElmer). Anion concentration were determined using Ion Chromatographs (IC) DX-500 (Dionex). Carbonate (CO_3^-) and bicarbonate (HCO_3) concentration were determined using acid titration method. Chloride (Cl^-) concentration was measured by $AgNO_3$ titration method; sulfate (SO_4^{2-}) was measured by SulfaVer 4 method (HACH) using a spectrophotometer.

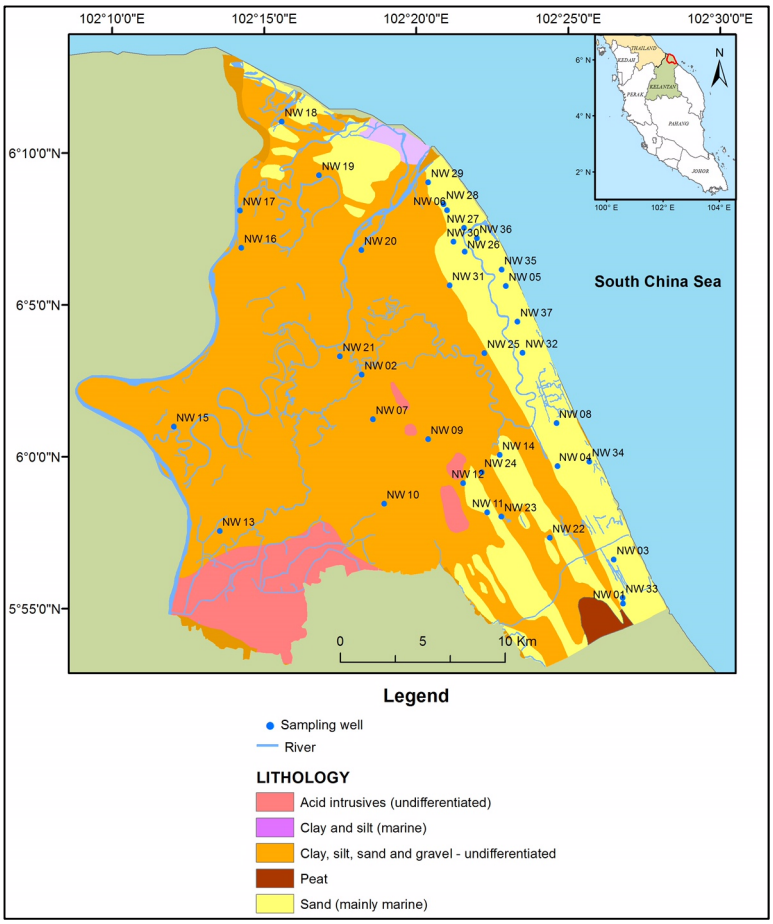

Figure 1. Sampling location and geology of the study area.

All the groundwater collection method and the water sample analysis followed APHA (2005). The concentrations were expressed in milligrams per litre (mg/L), except for pH and EC. Quality controls and quality assurance were applied to obtain reliable data by checking the blank samples and a calibration curve was constructed for the elements. The analytical precision for ions was checked again by the ionic balances calculated as (cations - anions)/ (cations + anions) x 100, which is generally within ±5% (Hem, 1985). The water types were determined using Aquachem 2014.2 software.

3 RESULTS AND DISCUSSIONS

3.1 General hydrogeochemistry

Groundwater chemistry is an important factor in determining water quality for domestic, agricultural and industrial purposes. The statistical summary of physicochemical parameters analyzed is presented in Table 1. The pH value ranges from 5.13-7.53 with an average of 6.63, reflecting slightly acidic to alkaline condition. The concentration of EC ranges from 46-1105 µS/cm, with an average value of 257 µS/cm. The higher EC is a result of ion exchange and influence of anthropogenic sources, such as domestic sewage and septic tanks (Sanchez-Perez and Tremolieres, 2003). The relative abundance of major cations and anions were ranked in the order $Ca^{2+} > Na^{+} > Mg^{2+} > K^{+} = HCO_3^{-} > Cl^{-} > CO_3^{2-} > SO_4^{2-}$ respectively.

HCO_3^{-} concentration varied in range of 1.74-296.00 mg/L with an average of 72.04 mg/L. The high concentration of HCO_3^{-} is an indication of carbonate weathering and organic matter decomposition (Avtar et al., 2013). The concentration of Cl^{-} ranges within 3.63 and 118.36 mg/L with an average of 22.18 mg/L. Most groundwater samples lie within the recommended a maximum permissible limit of 250 mg/L (WHO, 2004). The relatively higher concentration of Cl^{-} in some groundwater samples can be attributed from natural sources such as dissolution of Cl^{-} bearing minerals.

The concentration of SO_4^{2-} was found to range from 1.00-56.87 mg/L with an average 15.92 mg/L, the enrichment of groundwater from SO_4^{2-} could be due to the decaying of organic matter in soil layer. The concentration of NO_3^{-} varied from 0.18 to 86.45 mg/L with an average value of 11.81 mg/L. About 18% had nitrate concentration above the WHO and MOH drinking water guideline of 10 mg/L. High concentration of NO_3^{-} in groundwater is an indication of excessive use of fertilizers in agricultural and anthropogenic pollution

caused by lack of domestic sewage. High concentrations of NO_3^- can cause methemoglobinemia or blue baby syndrome in infants (Samatya et al., 2006).

Table 1. Comparison of hydrochemical parameters with WHO (2004) and Malaysian Ministry of Health national standard for drinking water quality (MOH, 2004).

Parameter	Unit	Shallow aquifer			WHO (2004)	MOH (2004)
		Range	Mean	SD		
pH	-	5.13-7.53	6.63	0.52	6.5-9.2	6.5-9.0
EC	µS/cm	46-1,105	257	215	1,500	NA
TDS	mg/l	39-696	180	139	1,000	1,000
Ca^{2+}	mg/l	1.94-88.85	22.77	22.41	200	NA
Mg^{2+}	mg/l	0.39-38.26	4.79	7.00	150	150
Na^+	mg/l	3.40-71.57	13.27	12.51	200	200
K^+	mg/l	1.16-16.02	5.93	3.47	200	NA
CO_3^{2-}	mg/l	0.50-6.38	1.07	1.31	NA	NA
HCO_3^-	mg/l	1.74-296.00	72.04	80.49	NA	NA
Cl^-	mg/l	3.63-118.36	22.18	23.49	250	250
SO_4^{2+}	mg/l	1.00-56.87	15.92	13.15	250	250
NO_3^-	mg/l	0.18-86.45	11.81	16.80	10	10
Fe^{2+}	mg/l	0.08-21.99	3.13	4.17	NA	0.30
Mn^{2+}	mg/l	0.03-0.83	0.19	0.21	0.4	0.1

Note: SD (standard deviation); NA (no available standard), DO (dissolved oxygen), EC (electrical conductivity), TDS (total dissolved solids)

3.2 Hydrogeochemical facies

Hydrogeochemical facies interpretation is a useful tool for evaluation of the geochemical processes and mechanisms in the aquifer system based on the dominant cation and anion (Piper, 1953). Based on the Piper trilinear plot (Figure 2), groundwater of study area was classified into four major water types, namely Ca-HCO_3, Na-Cl, Na-HCO_3 and Ca-Cl. The Ca-HCO_3 water type is the most common hydrogeochemical facies found in the study area. It represents 57% of all the groundwater sampled and suggest that calcite solution has played an important role in controlling the groundwater chemistry in the study area. Na-Cl water type generally close to the coastal area indicates a strong influence of ancient seawater (Pulido-Leboeuf, 2004). The Na-HCO_3 facies is a strong indicator of cation exchange process.

3.3 Saturation index (SI) and mineral equilibrium

The saturation index (SI) describes the deviation of water from equilibrium with respect to dissolved minerals quantitatively (Stumm and Morgan, 1981). Saturation index of minerals was calculated by the USGS geochemical PHREEQC Version 2.14.3 software (Charlton and Parkhurst, 2002) to evaluate the degree of equilibrium between water and the respective mineral. Mineral equilibrium calculations are useful in predicting the presence of reactive minerals in the groundwater system and estimating mineral reactivity. Saturation indices (SI) could be used to predict the reactive mineralogy of the subsurface from groundwater data without collecting the samples of the solid phase and analysing mineralogy (Deutsch, 1997). Saturation index (SI) is the logarithm of the ratio of ion activity product (IAP) to the solubility product of the mineral expressed as:

$$\text{Saturation index (SI)} = \log (IAP/K_{sat}) \quad [1]$$

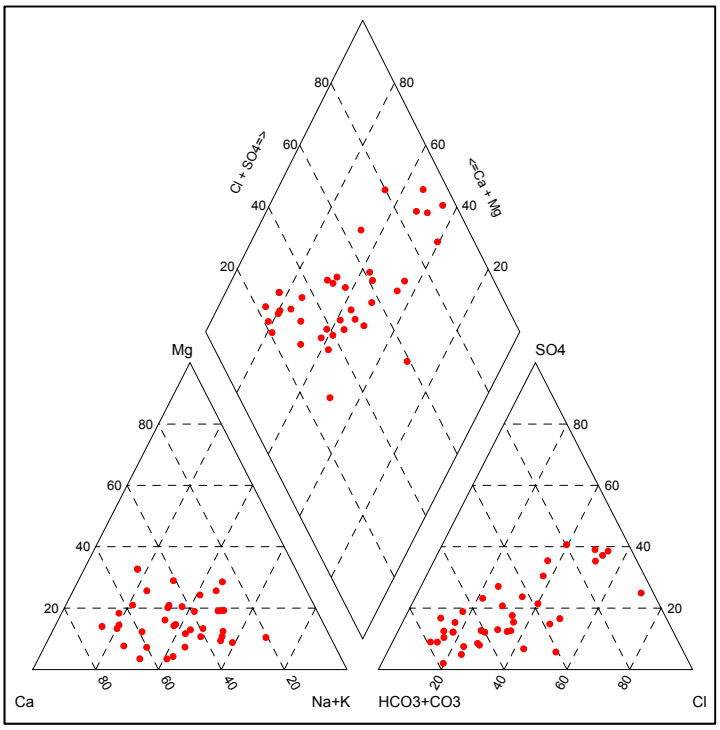

Figure 2. Piper diagram plot of chemical analysis of groundwater samples in the study area.

A negative saturation index (SI<0) indicates that the groundwater is undersaturated with respect to particular mineral and reflect insufficient amount of mineral for solution or short residence time. A positive saturation index (SI>0) indicates that the groundwater is oversaturated with respect to a particular mineral and therefore incapable of dissolving more of the mineral and under suitable physico-chemical condition, the mineral phase in equilibrium may precipitate. Such an index value reflects groundwater discharging from an aquifer containing ample amount of mineral with sufficient resident time to reach equilibrium. A neutral SI (SI=0) indicates the saturation in equilibrium state with the particular mineral phase.

The calculated saturation index values of minerals demonstrate that the groundwater in the area is oversaturated with iron containing minerals like $Fe(OH)_3$ and hematite. The groundwater is undersaturated with anhydrite, aragonite, calcite, dolomite, gypsum and manganite. Oversaturation of $Fe(OH)_3$ and hematite indicate the abundance of iron minerals in the aquifer. Sufficient residence time to be in contact with these minerals and their weathering has resulted in abundance of iron in the groundwater. The high concentration of calcium may be attributed to the dissolution of calcite and dolomite as carbonate weathering. Variation of the saturation index for minerals in different aquifer is shown in Table 2.

Table 2. Saturation indices for the minerals in shallow aquifer.

Parameter	Minimum	Maximum	Average	Standard Deviation
Anhydrite	-4.86	-2.11	-3.43	0.70
Aragonite	-3.57	-0.22	-1.77	0.99
Calcite	-3.43	-0.08	-1.63	0.99
Dolomite	-6.94	0.06	-3.58	1.93
$Fe(OH)_3$	1.08	3.31	2.26	0.59
Gypsum	-4.64	-1.89	-3.21	0.70
Hematite	15.93	20.41	18.31	1.19
Manganite	-6.46	-5.36	-6.09	0.33

3.4 Correlation coefficient

The correlation coefficient is commonly used to measure the relationship between two variables and illuminating the links between parameters and controlling factors (Wang and Jiao, 2012). A correlation coefficient of less than 0.5 exhibits poor correlation, 0.5 represents the good correlation, and greater than 0.5 show the excellent correlation (Vasanthavigar et al., 2013). The pH shows strong positive correlation with HCO_3^- ($r=0.67$). HCO_3^- in groundwater is mainly derived from the dissolution of carbonate minerals with CO_2 present in the atmosphere and in soil above the water table. Carbonate-rich material principally formed from

deposition of biogenic marine materials. High alkalinity and pH value relatively high on the coastal area are due to the presence of calcium carbonate. EC shows positive correlation with TDS (*r=0.78*), Ca^{2+} (*r=0.84*), Mg^{2+} (*r=0.829*), Na^{+} (*r=0.83*), HCO_3^- (*r=0.84*), Cl^- *(r=0.70*) and SO_4^{2-} (*r=0.70*). This indicates that the quality of groundwater is characterized by sea water influence of marine origin. The Fe^{2+} shows strong positive correlation with Mn^{2+} (r=0.68). The correlation coefficient of physicochemical parameters was tabulated in Table 3.

Table 3. Correlation coefficient of major cations and anions in shallow groundwater aquifer.

Parameters	pH	EC	TDS	Ca^{2+}	Mg^{2+}	Na^{+}	K^{+}	CO_3^{2-}	HCO_3^-	Cl^-	SO_4^{2-}	NO_3^-	Fe^{2+}	Mn^{2+}
pH	1													
EC	0.46	1												
TDS	0.20	**0.78**	1											
Ca^{2+}	0.60	**0.84**	0.65	1										
Mg^{2+}	0.48	**0.83**	**0.71**	**0.75**	1									
Na^{+}	0.29	**0.83**	**0.66**	**0.68**	**0.73**	1								
K^{+}	0.12	0.45	0.41	0.45	0.41	0.34	1							
CO_3^{2-}	0.29	0.32	0.21	0.18	0.31	0.07	0.08	1						
HCO_3^-	**0.67**	**0.84**	**0.64**	**0.88**	**0.73**	0.53	0.34	0.33	1					
Cl^-	0.16	**0.69**	0.56	0.50	0.59	**0.80**	0.32	0.06	0.37	1				
SO_4^{2+}	0.17	**0.69**	0.58	0.55	0.52	**0.76**	0.36	0.09	0.39	**0.80**	1			
NO_3^-	-0.27	0.19	0.12	0.04	-0.03	0.156	0.37	-0.03	-0.12	0.32	0.37	1		
Fe^{2+}	0.18	0.11	0.27	0.21	0.34	0.05	0.28	0.03	0.20	0.04	0.05	-0.06	1	
Mn^{2+}	0.25	0.09	0.12	0.17	0.27	0.01	0.17	0.03	0.21	0.02	-0.02	-0.09	**0.67**	1

4 CONCLUSIONS

The shallow groundwater aquifer in Lower Kelantan Basin is slightly acidic to alkaline in nature. The relative abundance of major cations and anions were categorized in the order $Ca^{2+} > Na^{+} > Mg^{2+} > K^{+} = HCO_3^- > Cl^- > CO_3^{2-} > SO_4^{2-}$ respectively. Ca-HCO_3 is the dominant hydrogeochemical facies that strongly reflects the calcite solution has played an important role in controlling the groundwater chemistry in the study area. The saturation indices of anhydrite, aragonite, calcite, dolomite, gypsum and manganite exhibit oversaturation condition signify the presence of calcareous material in the subsurface soil profile. The groundwater is oversaturated with iron containing minerals like $Fe(OH)_3$ and hematite indicate the abundance of iron minerals in the aquifer. The study reveals that the groundwater quality is controlled by the anthropogenic activities such as agricultural and lack of sanitation, and natural weathering process influences.

ACKNOWLEDGEMENTS

The authors would like to thank Ministry of Natural Resources and Environment (NRE) for providing research fund to this study under National Water Resources Council (P23101110117300).

REFERENCES

Abdul Rashid, B. (1989). *Groundwater Monitoring System in the Eastern Sungai Kelantan Delta, Kelantan.* Geological Survey of Malaysia.

American Public Health Association (APHA). (2005). *Standard Methods for the Examination of Waters and Wastewaters (21st Edition)*. Washington D.C: American Public Health Association.

Ang, N.K. & Ismail, C.M. (1996). *Groundwater Monitoring Report in Peninsular Malaysia 1995 (Kelantan)*. Geological Survey of Malaysia.

Appelo, C.A.J. & Postma, J. (2005). *Geochemistry, Groundwater and Pollution, 2nd Edition*. A.A. Balkema, Leiden.

Avtar, R., Kumar, P., Singh, C.K., Sahu, N., Verma, R.L., Thakur, J.K. & Mukherjee, S. (2013). Hydrogeochemical Assessment of Groundwater Quality of Bundelkhand, India using Statistical Approach. *Water Quality, Exposure and Health*, 5(3), 105-115.

Charlton, S.R. & Parkhurst, D.L. (2002). *PHREEQCI-A Graphical User Interface to the Geochemical Model PHREEQC* (No. 031-02).

Chopra, S.L. & Kanwar, J.S. (1980). *Analytical Agricultural Chemistry.* Kalyani Publishers. *Ludhiana, India*.

Department of Drainage and Irrigation Malaysia (DID), (2011). *Review of the National Water Resources Study (2000-2050) and Formulation of National Water Resources Policy, Volume 10*. Ministry of Natural Resources and Environment Malaysia, Kuala Lumpur.

Deutsch, W.J. & Siegel, R. (1997). *Groundwater Geochemistry: Fundamentals and Applications to Contamination*. CRC press.

Hem, J.D. (1985). *Study and Interpretation of the Chemical Characteristics of Natural Water* (Vol. 2254). Department of the Interior, US Geological Survey.

Kumar, P.S., Elango, L. & James, E.J. (2014). Assessment of Hydrochemistry and Groundwater Quality in the Coastal Area of South Chennai, India. *Arabian Journal of Geosciences*, 7(7), 2641-2653.

Kumar, S.K., Rammohan, V., Sahayam, J.D. & Jeevanandam, M. (2009). Assessment of Groundwater Quality and Hydrogeochemistry of Manimuktha River Basin, Tamil Nadu, India. *Environmental Monitoring and Assessment*, 159(1), 341-351.

MacDonald, S. (1967). *The Geology and Mineral Resources of North Kelantan and North Terengganu* (No. 10). Geological Survey of Malaysia.

Ministry of Health (MOH). (2004). *National Guidelines for Drinking Water Quality*. Ministry of Health, Kuala Lumpur.

Montcoudiol, N., Molson, J. & Lemieux, J.M. (2015). Groundwater Geochemistry of the Outaouais Region (Québec, Canada): A Regional-Scale Study. *Hydrogeology Journal*, 23(2), 377-396.

Nas, B. & Berktay, A. (2010). Groundwater Quality Mapping in Urban Groundwater Using GIS. *Environmental Monitoring and Assessment*, 160(1), 215-227.

Nickson, R.T., McArthur, J.M., Shrestha, B., Kyaw-Myint, T.O. & Lowry, D. (2005). Arsenic and Other Drinking Water Quality Issues, Muzaffargarh District, Pakistan. *Applied Geochemistry*, 20(1), 55-68.

Nishanthiny, S.C., Thushyanthy, M., Barathithasan, T. & Saravanan, S. (2010). Irrigation Water Quality Based on Hydro Chemical Analysis, Jaffna, Sri Lanka. *American-Eurasian Journal of Agricultural & Environmental Science*, 7(1), 100-102.

Piper, A.M. (1953). *A Graphical Procedure in the Geochemical Interpretation of Water Analysis.* Transaction American Geophysical Union, 25(6), 914-928.

Pulido-Leboeuf, P. (2004). Seawater Intrusion and Associated Processes in a Small Coastal Complex Aquifer (Castell De Ferro, Spain). *Applied Geochemistry*, 19(10), 1517-1527.

Samatya, S., Kabay, N., Yüksel, Ü., Arda, M. & Yüksel, M. (2006). Removal of Nitrate from Aqueous Solution by Nitrate Selective Ion Exchange Resins. *Reactive and Functional Polymers*, 66(11), 1206-1214.

Sanchez-Pérez, J.M. & Trémolières, M. (2003). Change in Groundwater Chemistry as a Consequence of Suppression of Floods: The Case of the Rhine Floodplain. *Journal of Hydrology*, 270(1), 89-104.

Srinivas, Y., Aghil, T.B., Oliver, D.H., Nair, C.N. & Chandrasekar, N. (2015). Hydrochemical Characteristics and Quality Assessment of Groundwater along the Manavalakurichi Coast, Tamil Nadu, India. *Applied Water Science*, 1-10.

Stumm, W. & Morgan, J.J. (1981). *Aquatic Chemistry: An Introduction Emphasizing Chemical Equilibria in Natural Waters.* Wiley-Interscience Publication, John Wiley and Sons, New York. 795.

Tiwari, A.K. & Singh, A.K. (2014). Hydrogeochemical Investigation and Groundwater Quality Assessment of Pratapgarh District, Uttar Pradesh. *Journal of the Geological Society of India*, 83(3), 329-343.

Vasanthavigar, M., Srinivasamoorthy, K. & Prasanna, M.V. (2013). Identification of Groundwater Contamination Zones and its Sources by Using Multivariate Statistical Approach in Thirumanimuthar Sub-Basin, Tamil Nadu, India. *Environmental Earth Sciences*, 68(6), 1783-1795.

Wang, Y. & Jiao, J.J. (2012). Origin of Groundwater Salinity and Hydrogeochemical Processes in the Confined Quaternary Aquifer of the Pearl River Delta, China. *Journal of Hydrology*, 438, 112-124.

World Health Organization (WHO). (2004). *Guidelines for Drinking-Water Quality. Vol. 1, Recommendations (3rd Edition).* WHO, Geneva.

Proceedings of the 37th IAHR World Congress
August 13 – 18, 2017, Kuala Lumpur, Malaysia

SEASONAL GROUNDWATER LEVEL FLUCTUATIONS IN SUKHUMA DISTRICT OF SOUTHERN LAOS

SINXAY VONGPHACHANH[(1)], WILLIAM MILNE-HOME[(2)], ASHIM DAS GUPTA[(3)] & JAMES E BALL[(4)]

[(1,2,3,4)]School of Civil and Environmental Engineering, Faculty of Engineering and Information Technology, University of Technology Sydney, Australia
Sinxay.Vongphachanh@student.uts.edu.au, William.Milne-Home@uts.edu.au, adasgupta.05@gmail.com, James.Ball@uts.edu.au

ABSTRACT

The objective of this study is to investigate the seasonal fluctuation of groundwater level in Sukhuma District by using observed data on groundwater, rainfall and streamflow from June 2015 to May 2016 and remote sensing data derived from the Gravity Recovery and Climate Experiment (GRACE) and the Global Land Data Assimilation System (GLDAS) for the period of June 2015 to March 2016. The results show that the groundwater level in Sukhuma District increased to the peak elevation during the late wet season (September – October) and it started declining from November until reached the lowest elevation during the late dry season (April – May). Rainfall was found at a significant ($P<0.01$) factor influencing the groundwater level fluctuation. The delay time between rainfall and groundwater level rise was also estimated at about 4 weeks. Moreover, the results also show that groundwater level during the study period in Sukhuma District was not yet depleted. However, the time-series for this analysis is very short to investigate the trend of groundwater level in Sukhuma District. The results of this research also showed good correlation between the soil moisture from GLDAS and groundwater level measurement in Sukhuma District ($R^2 = 0.91$) and also showed a good agreement between the soil moisture from GLDAS at a GRACE footprint and the equivalent water height (EWH) derived from GRACE at a GRACE footprint with an R^2 value of 0.72. Therefore, regarding the results of this study, a further investigation using these remote sensing data for groundwater study in this region will be carried out to support in groundwater study for Sukhuma and Southern Laos. The products from GRACE and GLDAS will provide pivotal data for the study of hydrogeology in the areas with limited field observation data.

Keywords: Sukhuma District; seasonal groundwater level fluctuation; correlation; GLDAS; GRACE.

1 INTRODUCTION

Groundwater is the main source of water supply for agricultural and domestic uses in many developing countries. The monitoring and analysis of groundwater levels fluctuations are necessary for developing an effective management plan for sustainable use of groundwater resources (Pavelic et al., 2014). In recent year, groundwater abstraction in Laos has been increasing to enhance the resilience to climate variability, such as in Southern Laos (Suhardiman et al., 2016; Vote et al., 2015; Wade et al., 2015). However, groundwater levels measurement data is sparse in Southern Laos (Vongphachanh et al., 2016). This is because groundwater levels measurement is generally expensive and requires well trained manpower (Anayah and Kaluarachchi, 2009). There is urgent need to have the groundwater levels monitoring systems along with good institutional support to acquire sufficient information for the long-term groundwater resource development in Laos (Pavelic et al., 2014).

Knowing and understanding of seasonal fluctuations of groundwater levels are crucial for sustainable surface water and groundwater resources management and development (Lutz et al., 2014). In Sukhuma, groundwater is the only source for domestic water supply. Khamouan River and its tributaries are usually dry during the dry season and water in the river is commonly unusable during the rainy season due to sediment content and contamination. In 2015, Sukhuma District Nam Sa-Ath (fresh water) Office reported that about 6,000 bores were drilled in Sukhuma District and this number will be increased in future. However, assessment of seasonal groundwater fluctuations is limited. Therefore, this study is aiming to assess these phenomena in Sukhuma by using very limited field data and remote sensing data.

2 METHODOLOGY

2.1 Study area

This study was conducted from June 2015 to May 2016 in Sukhuma District which is located on the floodplain of Champasak Province, Southern Laos. It lies between latitudes 14° 28′ 15″ N and 14° 49′ 16″ N and longitudes 105° 28′ 32″ E and 105° 52′ 20″ E. It covers an area of about 1,200 km^2. The lowest ground elevation is about 74 m amsl (above mean sea level) along the Mekong River and Khamouan River's mouth

and the highest is about 600 m amsl on the Western side (along the border with Thailand) (Figure 1). Sukhuma shares a border with Champasak District to the North, Mounlapamok District to the South, Khong District to the Southeast, Pathoumphone District to the East, and Thailand to the West.

Geologically, the topsoil layer of about 2 m depth consists of silty clay and sand. The underlying layer has an average thickness of about 25 m and mainly consists of fractured laterite, clay, sandy shale and mudstone, shale and sandstone. Generally, the groundwater aquifer in Sukhuma District is identified as a fractured sandstone aquifer and its actual depth is unknown. It is continuous with the groundwater aquifers of the Khorat Plateau in Thailand on the west of Sukhuma District. Vote et al. (2014) reported that the average value of transmissivity and hydraulic conductivity for the fractured sandstone aquifer in Sukhuma were about 98.9 m^2/day, 7.34 m/day, respectively. Moreover, Vongphachanh et al. (2016) indicated that an average value of specific yield for this aquifer was about 0.01.

Sukhuma is subject to a monsoonal climate which consists of wet and dry seasons. Commonly, the wet season is from May to October and the dry season from November to April. The average annual rainfall is about 2,052 mm (average from 1993-2015). The daily temperature usually ranges from 23 °C to 33°C with an average of about 27°C. The average annual evapotranspiration is estimated at about 1,660 mm. The main source of domestic water use comes from groundwater resources and it has been increasing.

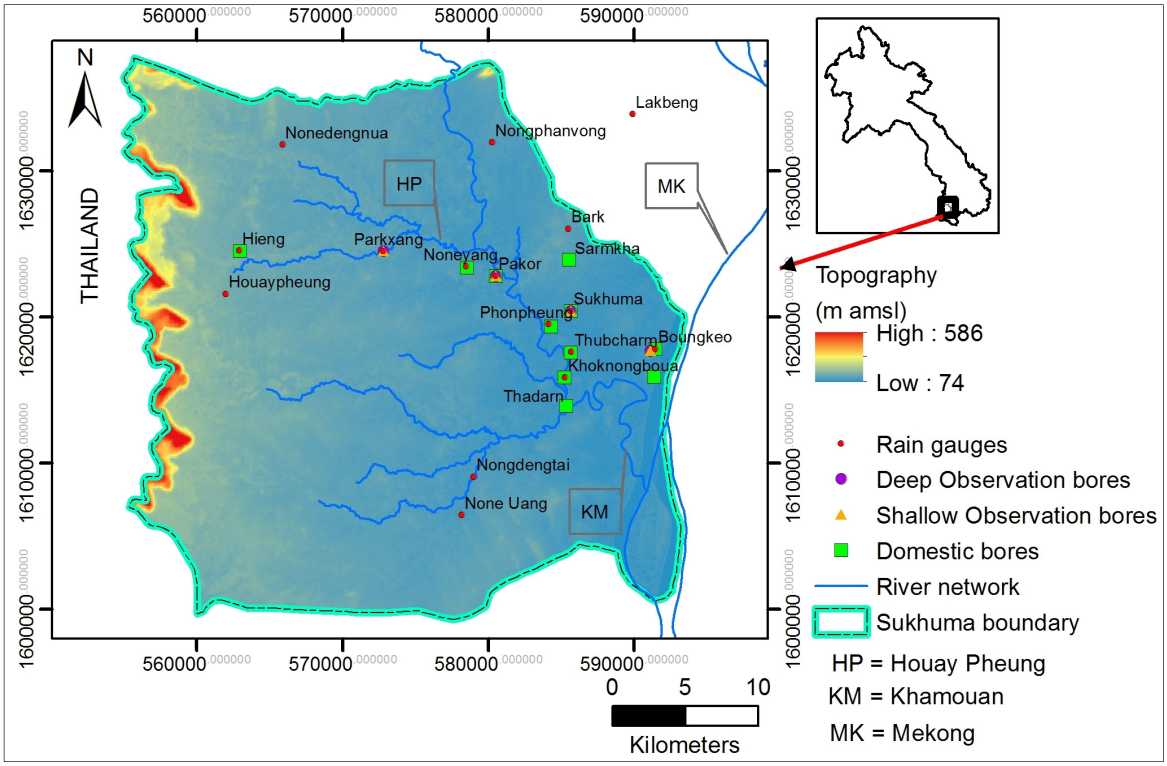

Figure 1. Location map of Sukhuma District, stream and rainfall gauges, topography and monitoring wells. KM is the Khamouan.

2.2 Data collection and analysis

The primary input data for this study include field observation data and remote sensing data. The field measurement data included the data of groundwater levels, rainfall and stream stage collected in Sukhuma District from the period of June 2015 to May 2016. The weekly groundwater levels data were measured manually at the eleven domestic wells and five paired shallow and deep observation wells. These data were converted into monthly average groundwater level at each observation well. The daily rainfall data were collected from the 16 rain gauges (Figure 1). The mean daily river flow was measured manually at the Khamouan River gauge. The daily rainfall and flow data were aggregated into monthly data at each observation point. The locations of monitoring wells are presented in Table 1.

Due to the limitation of field observation data (including hydrology, climate and geology) in Sukhuma District as well as Southern Laos, the feasibility of applying remotely sensed data derived from the Gravity Recovery and Climate Experiment (GRACE) (Tapley et al., 2004) and the Global Land Data Assimilation System (GLDAS) (Rodell et al., 2004) to the future study of hydrogeology in the region was investigated. Currently, the monthly total water storage anomalies (TWSA), expressed as equivalent water height (EWH) from GRACE, are available from August 2002 to March 2016 on the website of the European Gravity Service for Improved Emergency Management (EGSIEM) [http://plot.egsiem.eu/]. From this website, users can download EWH data at a spatial resolution of ~12,000 km^2 (Bourgogne, 2016). The GRACE-TWSA or

GRACE-EWH data consist of a combined total storage of groundwater, soil moisture and surface water (including lakes, reservoirs, and rivers) (Leblanc et al., 2009). For this research, the monthly EWH derived from the GRACE GFZ (GeoFoschungsZentrum Potsdam) RL05a on the EGSIEM website were downloaded for the period of June 2005 to March 2016 at a grid scale of GRACE that is located between latitude 14.5 to 15.5° N and longitude 105.5 to 106.5° E with a spatial resolution of ~12,000 km^2 (Figure 2). Figure 2 illustrates a comparison between the footprint scales of GRACE and GLDAS and Sukhuma District area. This figure also depicts the locations of monitoring wells, rainfall stations and stream gauges that are located in the study area.

Table 1. The code and location of monitoring wells.

No.	Well code	Locations	Well status	Latitude (m)	Longitude (m)	Elevation of measurement point (m amsl)
1	SKM_Dom	Sukhuma	Domestic	585663.00	1620405.00	98.00
2	Pkor_Dom	Parkor	Domestic	580519.15	1622802.21	107.00
3	NY_Dom	Nonyang	Domestic	578529.35	1623387.15	105.00
4	KNB_Dom	Khoknongboua	Domestic	585228.64	1615856.35	100.00
5	THC_Dom	Thubcharn	Domestic	585661.59	1617564.21	97.00
6	BK_Dom	BoungKeo	Domestic	591483.00	1617810.00	98.00
7	PPH_Dom	Phonphueng	Domestic	584290.88	1619336.13	105.00
8	SKH_Dom	Sarmkhar	Domestic	585526.79	1623896.54	111.00
9	DHB_Dom	Donghouabarn	Domestic	591383.00	1615913.00	102.00
10	THD_Dom	Thadarn	Domestic	585346.00	1613938.00	98.00
11	BK_DW	Boungkeo	Deep Observation	591103.94	1617673.77	101.00
12	SKM_DW	Sukhuma	Deep Observation	585663.00	1620395.00	98.00
13	Pkor_DW	Parkor	Deep Observation	580519.15	1622802.21	107.00
14	PKX_DW	Pakxang	Deep Observation	572798.00	1624489.00	111.00
15	BK_SW	Boungkeo	Shallow Observation	591103.94	1617673.77	101.00
16	SKM_SW	Sukhuma	Shallow Observation	585663.00	1620395.00	98.00
17	Pkor_SW	Parkor	Shallow Observation	580519.15	1622802.21	107.00
18	PKX_SW	Pakxang	Shallow Observation	572798.00	1624489.00	111.00
19	Hieng_Dom	Hieng	Domestic	562939.38	1624512.69	125.00

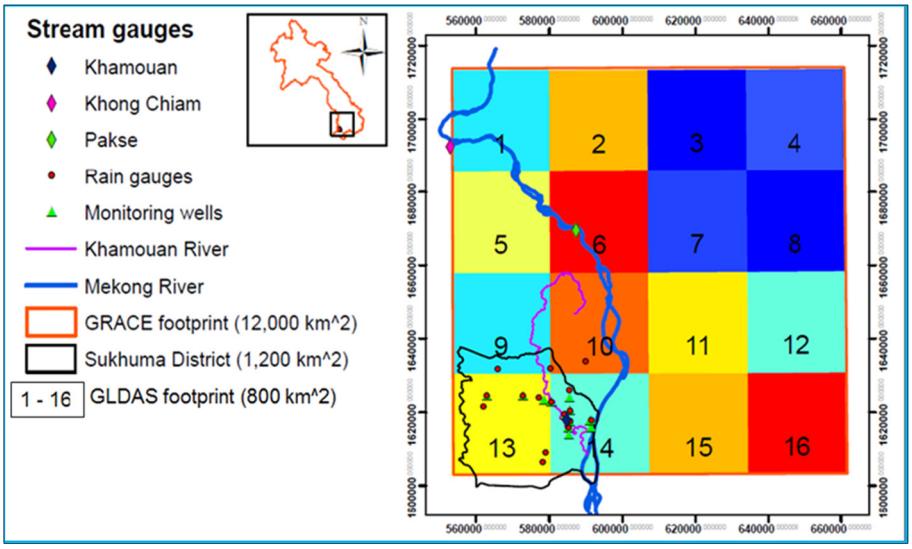

Figure 2. Locations of stream gauges and rainfall stations in the study area, and comparison between GRACE footprint scale, GLDAS footprint scale and Sukhuma District area.

Since field observations of soil moisture data are not available in Sukhuma District and in the districts nearby, reliance is placed on the remote sensing data from NASA's Earth Science Data System website [https://earthdata.nasa.gov/] with a spatial resolution of 0.25 degree x 0.25 degree (~800 km^2) (Figure 2) and a temporal resolution of 3-hourly and monthly (Rui and GES DISC, 2016). For this research, the soil moisture data from June 2005 to March 2016 at grid 13 of GLDAS and at a grid scale of GRACE, which cover a total of 16 grids of GLDAS (Figure 2), were downloaded from the National Centers for Environmental Prediction/Oregon State (Noah) land surface model (Ek et al., 2003) on the NASA's website. The Noah model provides soil moisture data for four soil depth layers ranging from 0 to 10, 10 to 40, 40 to 100, and 100 to 200 cm. The unit of soil moisture data is kg/m^2 or millimeter.

3 RESULTS AND DISCUSSION

3.1 Trend of water table fluctuation

Groundwater level fluctuation in Sukhuma District is different in magnitude at different locations depending on the groundwater pumping and recharge. The available data at the 19 wells from June 2015 to May 2016 are plotted as the well hydrographs of Sukhuma District (Figure 3). This figure illustrates that all hydrographs increased during the wet season (May – October), declined during the dry season (November – April) with the water table level reaching approximately the same elevation at the beginning of the wet season. In some locations, groundwater level rapidly increased during the wet season, such as at Pakor domestic, Pakor shallow and Donghouabarn domestic wells, while other areas had gentle rises. The location of these bores is presented in Figure 1. During the dry season, well hydrographs depicted smooth decline until the end of the season in May (Figure 3). Moreover, Figure 3 also illustrates that the highest rainfall intensity in Sukhuma District was concentrated in July and August for 2015. However, the groundwater level rises to its peak during September and October (Figure 3). This could also mean that rain water would take some time to infiltrate into the deep soil and refill the groundwater. More details of lags between rainfall and the start of rise in groundwater level are given in Section 3.3. From this study, it was observed that the trend of groundwater level in Sukhuma District remained the same from the end of dry season 2015 to the end of dry season 2016. However, the time-series data of groundwater level for this study are too short to provide the accurate result of the trend of groundwater level fluctuation. Therefore, longer time-series data should be employed for future study.

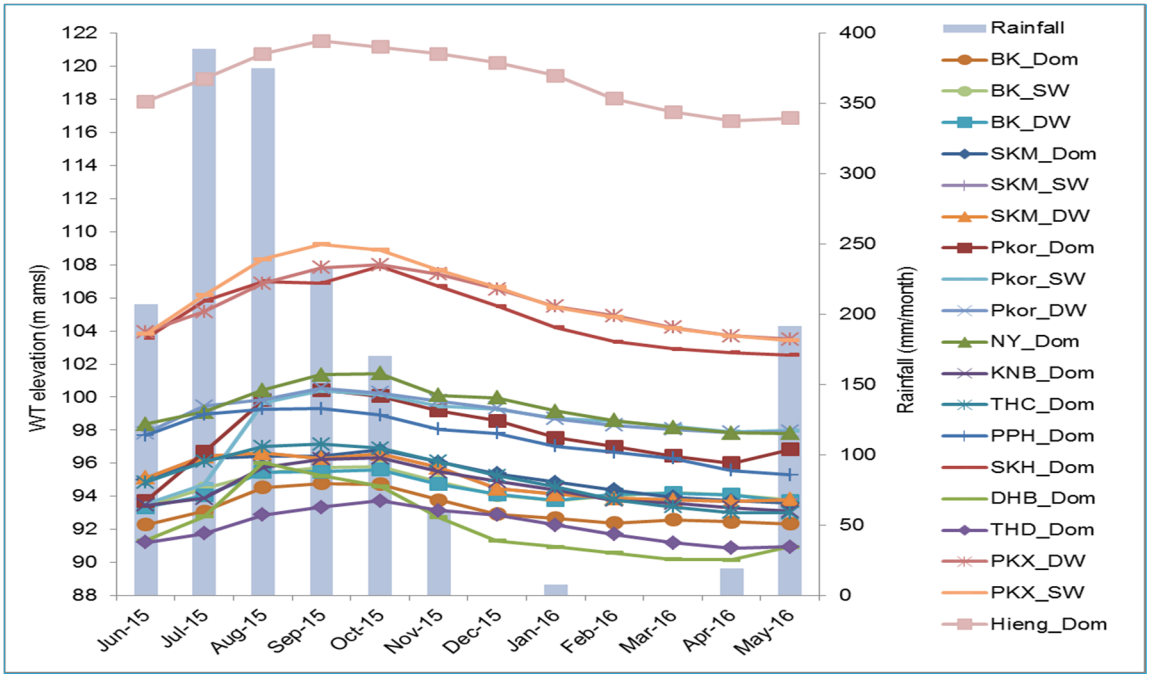

Figure 3. Well hydrograph of 19 monitoring wells and the area-averaged rainfall of 16 stations of Sukhuma District from June 2015 to May 2016.

3.2 Spatial and temporal variation of groundwater level

Due to limitation of data availability, a representative area encompassing all the observation points is selected, as shown in Figure 4, to assess the groundwater level fluctuation in the area. The spatial variations of groundwater level at two time scale, respectively for the end of wet season of October 2015 and for the late dry season of May 2016 are indicated in Figure 4 and Figure 5.

The elevation of groundwater level is comparatively high in the West and the North and low in the Southeastern area of the district. The western area shows the highest groundwater level because the density of population in this area is not as high compared to the southeastern area and that the groundwater abstraction is also low. The highest and lowest groundwater level elevations at Hieng domestic well were 123.54 m amsl in September 2015 and 118.70 m amsl in April 2016. The north area had always showed high groundwater level where Sarmkha (SKM) domestic well was monitored. Some reasons for this are many small surface water bodies (ponds) occuring there; a small forested upland area is located about 1.5 km north-west from the Sarmkha well and moreover, there is not many groundwater wells in this area. At Sarmkha well, the highest water table was observed at 108.89 m amsl in October 2015 and the lowest was 103.55 m amsl in May 2016.

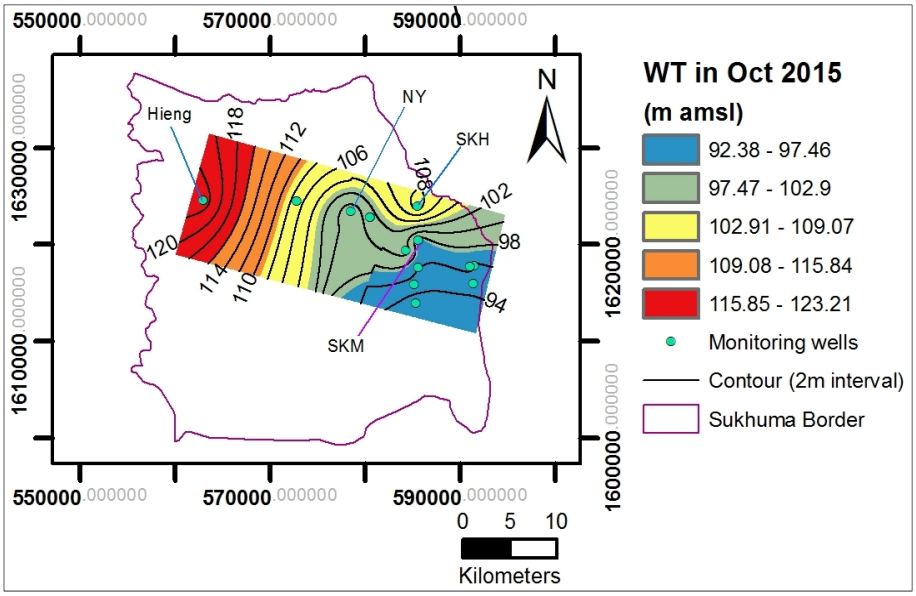

Figure 4. Groundwater contour maps of Sukhuma District during the late wet season (October 2015)

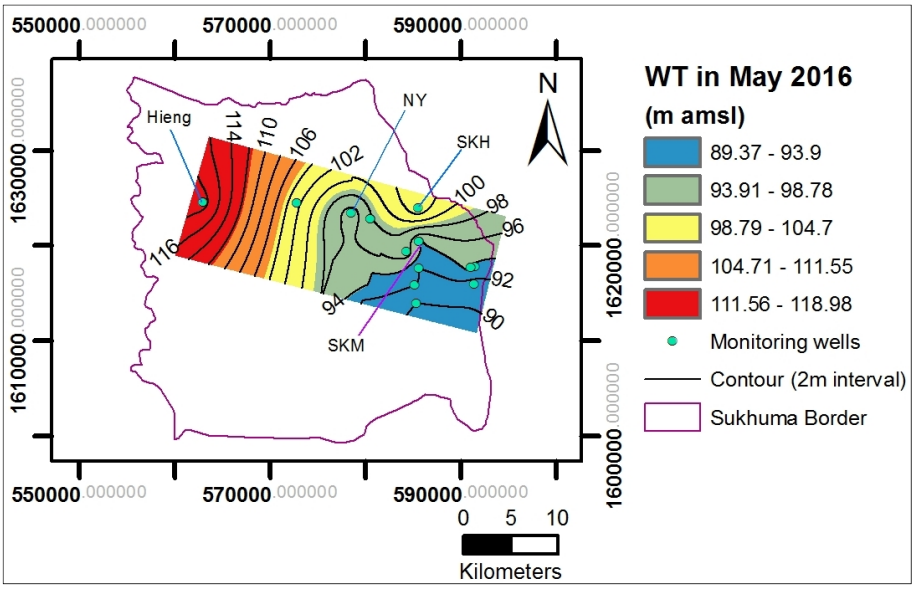

Figure 5. Groundwater contour maps of Sukhuma District during the late dry season (May 2016).

The groundwater level contours near the None Yang (NY) and Sukhuma monitoring wells show a groundwater sink for both wet and dry seasons (Figure 5). The main reason for this sink in the None Yang area is because a big bottled water factory has been set up close to it. However, for this study, we do not have information on the volume of groundwater pumped by this factory. In the case of the groundwater level sink in vicinity of the Sukhuma monitoring well, it is clearly found that this area is the city center of Sukhuma District. This area has a higher density of population than other areas. Also, many bottled water factories, guest houses and restaurants are located in this area. According to the data on bores recorded for 2015 at

Sukhuma District Nam Sa-Ath (Fresh Water) Office about 6,000 bores had been drilled. This number is more than half of the households in the district, which is about 9,000 households. The maximum water table recorded at the Sukhuma well was 96.81 m amsl in October 2015 and the minimum was 93.58 m amsl in May 2016. However, the groundwater level at the Phone Pheung well, located close to Sukhuma well, has always showed groundwater mounding (Figure 5) for wet and dry seasons. This is because a big reservoir (about 1 km x 1 km) is located about 500 m from this monitoring point. Therefore, groundwater levels in the Phone Pheung well could be affected by leaking from this reservoir. The connection between groundwater level fluctuation at this well and water level change in the reservoir should be taken into account for the future study of groundwater level fluctuation in Sukhuma District.

The groundwater flow directions and hydraulic gradients were determined by using an Excel spreadsheet method (Devlin, 2003). The results show that groundwater flows in Sukhuma District from north-west and north to south and southeast and finally, it drains to the Mekong River in the east. These results are similar to the previous studies by JICA (1995). Moreover, these results indicate a good connection between groundwater flow direction and topography in Sukhuma District. The hydraulic gradient of groundwater flow in this region for wet and dry seasons was estimated equivalent with an average value of 0.0013.

3.3 Statistical analysis

In this research, the time series of weekly rainfall and weekly groundwater levels at each monitoring well from Jun 2015 to May 2016 were used as the input and the output, respectively, for the cross-correlation analysis. Regarding the preliminary assessment of these time lags in some areas the domestic bores and shallow and deep bores were similar. For example, the monitoring wells in Sukhuma domestic, shallow and deep wells all showed similar lags of 4 to 5 weeks. This similarity could be caused by the way how the wells were constructed and geological structure. However, the results show that time lags between rainfall and rise in groundwater levels at all monitoring wells vary at different locations and range from two to six weeks with an average of four (4) weeks between the start of the rainy season and rise in water level. An example of a lag of four to five weeks found at the Boungkeo domestic bore is shown in Figure 6. The spatial variation in the delay between rainfall and water table rise depends on a number of factors, such as: spatial variation of surface soil types; land use and vegetation cover; and, spatio-temporal variation of rainfall. Lucas and Wendland (2016) indicated that land use and vegetation cover was a parameter influencing the groundwater recharge rate. However, the impacts of these parameters (land use and cover, soil type, etc.) on the rainfall recharge are out of the scope of this research.

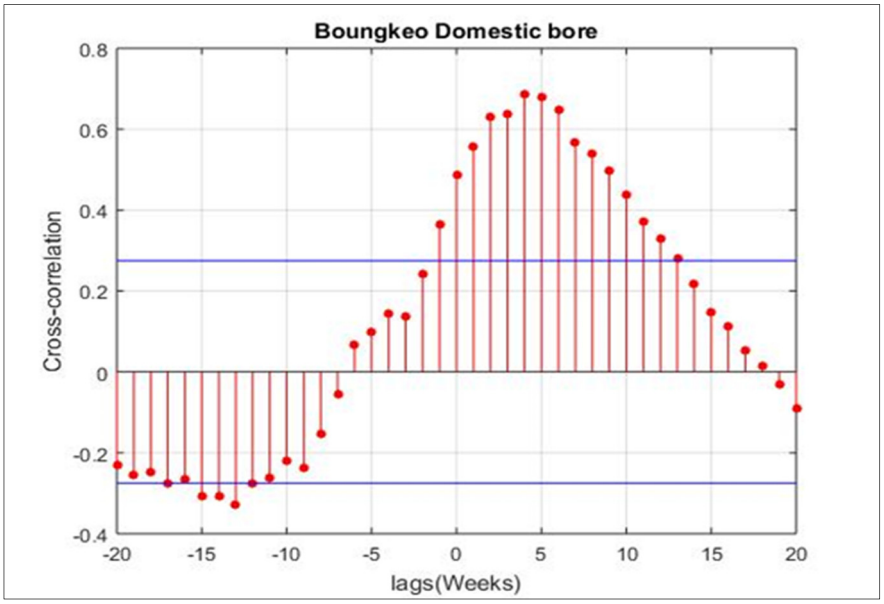

Figure 6. Cross-correlation between weekly rainfall and weekly water table fluctuations at Boungkeo Domestic well during June 2015 to May 2016.

Dependency of water table fluctuation with rainfall and streamflow is investigated through linear regression analysis. The monthly change in water table elevation is correlated with monthly rainfall data at Sukhuma District and with monthly streamflow data at Khamouan River gauge, as shown in Figure 7. The R^2 (coefficient of determination) values for correlation of change in water table elevation with rainfall and streamflow are 0.86 and 0.63, respectively. This implies that the groundwater table responses are much more dependent on rainfall rather than streamflow. However, it is to be pointed out that groundwater table

fluctuation observed close to the stream will have a higher correlation with streamflow because of hydraulic interconnection between stream and groundwater aquifer.

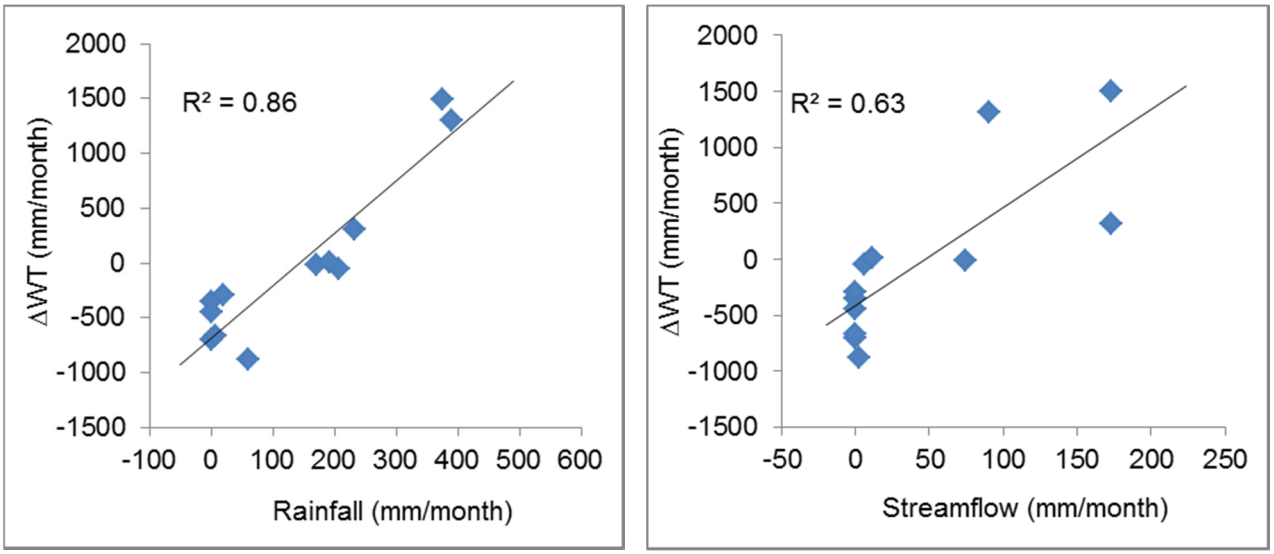

Figure 7. Correlation between rainfall, streamflow and change in water table (ΔWT) in Sukhuma District for the period of June 2015 to May 2016.

Soil moisture data derived from GLDAS at grid 13 are correlated with the area-averaged monthly change in water table of 19 monitoring wells in Sukhuma District (Figure 8). The result shows good correlation between two datasets with an R^2 value of 0.9. This result also provides a potential for taking the further investigation of using data derived from GLDAS to support the future study of seasonal groundwater level fluctuation in Sukhuma District. Moreover, GLDAS also provides data for the large scale area; therefore, these data can be used to estimate the groundwater fluctuation and availability in Southern Laos.

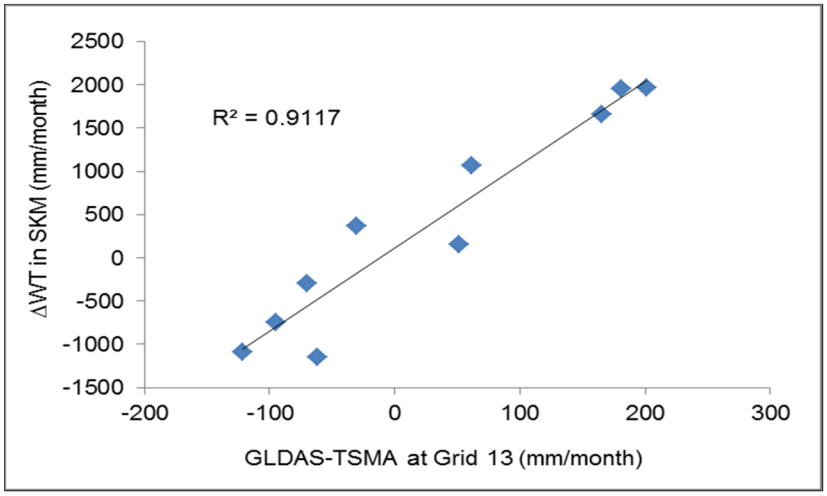

Figure 8. Correlation between the change in water table in Sukhuma District and the total soil moisture anomalies derived from GLDAS at the grid 13, which is covered by Sukhuma District boundary, for the period of June 2015 to March 2016.

In order to assess the possibility of utilizing the products from GLDAS for studying the groundwater in Sukhuma District and Southern Laos, the total soil moisture of 2 m depth derived from GLDAS at the GRACE footprint scale was correlated with the equivalent water height (EWH) or the total water storage (TWS) derived from GRACE at a GRACE footprint scale. This study found that soil moisture from GLDAS and GRACE-EWH correlates well with an R^2 value of 0.72 (Figure 9). Liesch and Ohmer (2016) also reported a strong correlation (R^2 = 0.74) between these two datasets for the Yarmouk basin in Jordan. GRACE satellite data has been widely utilized to determine the variations in groundwater storage in many countries, including the areas with limited field observation data (Shamsudduha et al., 2012). Therefore, the results of this preliminary assessment of using the products from GLDAS and GRACE show a great potential for conducting further of

using these remotely sensed data to determine the long-term groundwater storage fluctuation in Sukhuma District and Southern Laos.

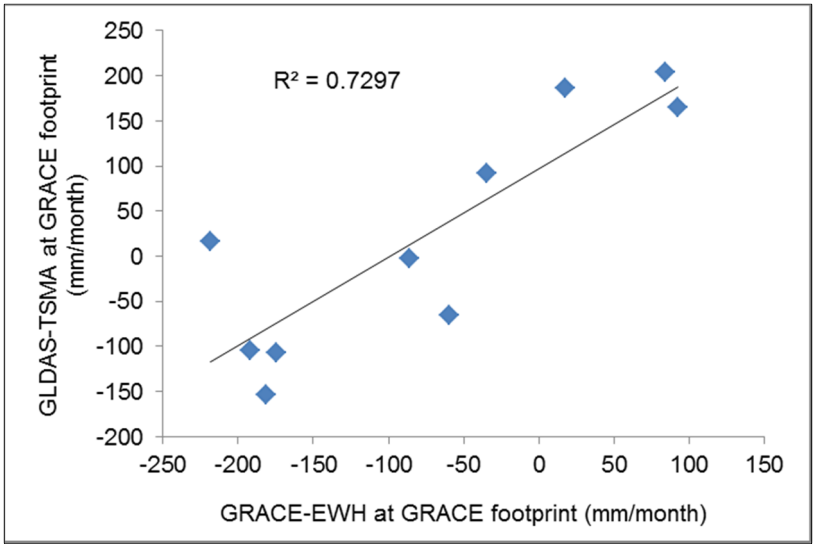

Figure 9. Correlation between the EWH derived from GRACE and the total soil moisture anomalies derived from GLDAS at the scale of GRACE footprint for the period of June 2015 to March 2016.

4 CONCLUSIONS

The observed trend of groundwater level in Sukhuma District during the period of June 2015 to May 2016 reflected not much overall decline as the groundwater levels in most of the observation wells at the end of May 2016 reach more or less the same levels as they were in June 2015. During the study period, the magnitudes of groundwater level fluctuation were different between west and north and south area of Sukhuma District. Moreover, this study also found that rainfall is a significant ($P < 0.01$) factor influencing the groundwater fluctuation in Sukhuma District. The delay between rainfall and groundwater level rise was estimated at about 4 week lags.

The soil moisture derived from GLDAS (grid 13) a grid of GLDAS (grid 13) has correlated with observed groundwater level in Sukhuma District with an R^2 value of 0.91 and also showed a good agreement between the soil moisture from a large area, which is the same as the GRACE footprint, and the GRACE-EWH with an R^2 value of 0.71. Further evaluation and study of GRACE and GLDAS data will be carried out to assist in groundwater study for this area.

Furthermore, for the future study of groundwater level fluctuation in Sukhuma District and Southern Laos, the data of groundwater abstraction should be collected, particularly from the bottled water factories. Also, the continued monitoring of groundwater levels and other hydrological variables in Sukhuma District is of great importance. This information will improve the accuracy of water balance analyses and will provide sufficient information for the long-term water resources management in the region.

ACKNOWLEDGEMENTS

The authors would like to thank staff of the Sukhuma District Agriculture and Forestry Office and the Sukhuma District Natural Resources and Environment Office for assistance with fieldwork and data collection. Special thanks to the Australian Centre for International Agricultural Research (ACIAR) Project LWR/2010/81 and the International Water Management Institute (IWMI) for supporting funds for fieldworks and data collection. We gratefully acknowledge the University of Technology Sydney (UTS) for funding the attendance of Sinxay Vongphachanh at this conference. We would also like to thank the reviewers for their helpful and constructive comments that really contributed to improving the final version of the paper.

REFERENCES

Anayah, F. & Kaluarachchi, J. J. 2009. Groundwater resources of northern Ghana: Initial assessment of data availability. *Utah State University, College of Engineering Report, Logan, USA*.

Bourgogne, S. 2016. *Plot GRACE time-series* [Online]. Available: http://plot.egsiem.eu/index.php?p=timeseries [Accessed 16 October 2016].

Devlin, J. 2003. A spreadsheet method of estimating best-fit hydraulic gradients using head data from multiple wells. *Ground Water,* 41**,** 316-320.

Ek, M., Mitchell, K., Lin, Y., Rogers, E., Grunmann, P., Koren, V., Gayno, G. & Tarpley, J. 2003. Implementation of Noah land surface model advances in the National Centers for Environmental Prediction operational mesoscale Eta model. *Journal of Geophysical Research: Atmospheres,* 108.

Leblanc, M. J., Tregoning, P., Ramillien, G., Tweed, S. O. & Fakes, A. 2009. Basin-scale, integrated observations of the early 21st century multiyear drought in southeast Australia. *Water Resources Research,* 45**,** 1-10.

Liesch, T. & Ohmer, M. 2016. Comparison of GRACE data and groundwater levels for the assessment of groundwater depletion in Jordan. *Hydrogeology Journal***,** 1-17.

Lucas, M. & Wendland, E. 2016. Recharge estimates for various land uses in the Guarani Aquifer System outcrop area. *Hydrological Sciences Journal***,** 1-10.

Lutz, A., Minyila, S., Saga, B., Diarra, S., Apambire, B. & Thomas, J. 2014. Fluctuation of Groundwater Levels and Recharge Patterns in Northern Ghana. *Climate,* 3**,** 1-15.

Pavelic, P., Xayviliya, O. & Ongkeo, O. 2014. Pathways for effective groundwater governance in the least-developed-country context of the Lao PDR. *Water International,* 39**,** 469-485.

Rodell, M., Houser, P., Jambor, U. E. A., Gottschalck, J., Mitchell, K., Meng, C., Arsenault, K., Cosgrove, B., Radakovich, J. & Bosilovich, M. 2004. The global land data assimilation system. *Bulletin of the American Meteorological Society,* 85**,** 381-394.

Rui, H. & Ges Disc. 2016. *Readme document for Global Land Data Assimilation System Version 1 (GLDAS-1) Products* [Online]. Available: http://hydro1.sci.gsfc.nasa.gov/data/s4pa/GLDAS_V1/README.GLDAS.pdf [Accessed 5 June 2016.

Shamsudduha, M., Taylor, R. & Longuevergne, L. 2012. Monitoring groundwater storage changes in the highly seasonal humid tropics: Validation of GRACE measurements in the Bengal Basin. *Water Resources Research,* 48.

Suhardiman, D., Giordano, M., Leebouapao, L. & Keovilignavong, O. 2016. Farmers' strategies as building block for rethinking sustainable intensification. *Agriculture and Human Values,* 33**,** 563-74.

Tapley, B. D., Bettadpur, S., Watkins, M. & Reigber, C. 2004. The gravity recovery and climate experiment: Mission overview and early results. *Geophysical Research Letters,* 31.

Vongphachanh, S., Milne-Home, W. & Ball, J. Groundwater Recharge Estimation in Sukhuma District, Champasak Province, Southern Laos: A Preliminary Assessment. Water Infrastructure and the Environment Conference, 28 Nov–2 Dec 2016, 2016.

Vote, C., Eberbach, P., Zeleke, K., Inthavong, T., Lampayan, R. & Vongthilath, S. 2014. The use of groundwater as an alternative water source for agricultural production in southern Lao PDR and the implications for policymakers. A policy dialogue on rice futures: rice-based farming systems research in the Mekong region, 2014 Phnom Penh, Cambodia, 7–9 May. ACIAR Proceedings No. 142. Australian Centre for International Agricultural Research, Canberra, 103-15.

Vote, C., Newby, J., Phouyyavong, K., Inthavong, T. & Eberbach, P. 2015. Trends and perceptions of rural household groundwater use and the implications for smallholder agriculture in rain-fed Southern Laos. *International Journal of Water Resources Development***,** 1-17.

Wade, L., Jackson, T., Locker, J. & Boothey, S. 2015. Developing Improved Farming and Marketing Systems in Rainfed Regions of Southern Lao PDR. Final Report FR2016-04, Proj. CSE/2009/004. Canberra.

EVALUATION OF GROUNDWATER SUSTAINABILITY IN A MULTILAYER AQUIFER

IMAN KARIMIRAD(1), KUMARS EBRAHIMI(2) & SHAHAB ARAGHINEJAD(3)

(1,2,3) Department of Irrigation & Reclamation Engineering, Faculty of Agricultural Engineering and Technology, College of Agriculture and Natural Resources, University of Tehran, Karaj, IRAN,
IKarimirad@ut.ac.ir; EbrahimiK@ut.ac.ir; shahab_araghinejad@yahoo.com

ABSTRACT

Sustainability of aquifers is a necessary term for the long-term utilization of groundwater resources. Groundwater sustainability indicators maintain the sustainable management of groundwater resources and help to analyze human impacts on groundwater systems. In this paper, the sustainability of phreatic and confined aquifers in multilayer groundwater system have been evaluated. Assessing sustainability in such groundwater systems can be complicated due to the different effects of recharge and discharge processes on each layer. For this purpose, some indicators were selected based on their feasibility in the study area because they proved to be the most reliable. The indices were applied to a 4700 km² alluvial aquifer located in Golestan province, northern Iran, which has semi-arid climate conditions. Results have proven that the region is facing water scarcity and the aquifer is undergoing intensive use. As a result, in spite of detecting no significant trend in the precipitation data, there were descending trends in the water table and piezometric level of phreatic and confined aquifers, respectively. According to the results aquifer sustainability index of phreatic and confined layers were 0.89 and 1.01, respectively that means both layers are unsustainable. Confined layer's condition is worse although the issue has been covered by non-renewable groundwater resources. Phreatic aquifer is also threatened by salty salt-water intrusion. Of course, both layers can be recovered soon. Altogether changing economic axis of the region from agriculture to less water demand sectors such as industry and services or at least cropping patterns is highly advised. Eventually, application of the methodology described here may be proved useful for the evaluation of similar systems in semi-arid climates.

Keywords: Confined aquifer; falkenmark indicator; golestan province; phreatic aquifer; water scarcity.

1 INTRODUCTION

Water has an important role in urban and rural development especially in arid and semi-arid countries. Population growth along with consumerism, development of agricultural and urban regions and limited surface water resources has led to excessive withdrawal of groundwater aquifers that can cause irreparable damages to these natural resources. Domestic water consumption per capita in the very high human development index[b] (HDI) countries, at 425 litres a day, is more than six times than that in the low HDI countries, where it averages 67 litres a day (Klugman, 2011). Nowadays, densely populated arid areas, Central and West Asia, and North Africa, with projected availabilities of less than 1000 m^3/capita/year strongly suffer from water scarcity (Rijsberman, 2006). It causes water withdrawals in developing countries to be 27% higher in 2025 than in 1995 (Watkins, 2006). Continued increase in domestic water withdrawals and demands led to the recognition of the importance of water for ecological sustainability (Sullivan, 2002; Vorosmarty et al., 2005; Chaves and Alipaz, 2007).

Groundwater, with a global withdrawal rate of 600–700 km^3/year (Zektser and Everett, 2004), is the world's most extracted raw material. The use of groundwater has increased significantly in recent decades due to its widespread occurrence, mostly good quality, high reliability during droughts and generally modest development costs. Groundwater is the main water supply source in several mega-cities (e.g. Mexico City, Sao Paulo and Bangkok) and provides nearly 70% of piped water supply in the European Union countries (Vrba et al., 2007). Poor protection and management in groundwater resources development plans has led to uncontrolled aquifer exploitation and contamination. Over-exploitation of groundwater may affect springs and streams base-flow and can lead to downfall in groundwater piezometric levels and land subsidence. Sustainable groundwater resources development and environmentally sound protection is a holistic process. The main objective of this process is to ensure quantity, quality, safety and sustainability of groundwater as an important component of the ecosystem and a strategic source for life (e.g. drinking and other sanitary purposes) and economic development (e.g. agriculture, industry) (Vrba et al., 2007).

Groundwater indicators provide summary information about the present state and trends in groundwater systems, help to analyze the extent of natural and anthropogenic impacts on groundwater system in space

[b] A composite index measuring average achievement in three basic dimensions of human development—a long and healthy life, knowledge and a decent standard of living [Klugman, J. (2011)].

and time and support sustainable management of groundwater resources (Vrba et al., 2007). In the past 20 years, many indices have been developed to quantitatively evaluate water resources vulnerability such as water scarcity or water stress indices (Brown and Matlock, 2011). Some indices are frequently used to evaluate water availability and sustainability, including Falkenmark indicator (FI), renewable groundwater resources per capita (RGPC), dependence to groundwater (DG), dependence of agriculture to groundwater (DAG), the role of groundwater in the supply of drinking (RGSD), aquifer sustainability (AS), sustainability of groundwater quality (SGQ), groundwater abstraction development (GAD), pressure on non-renewable resources of groundwater (PNRG), aquifer recovery potential (ARP) and groundwater decay rate (GDR). Among above mentioned indices, the first two indices (FI and RGPC), relates to water resources availability of the studied region, the next three indiceslook at multilayer aquifer as a unit water body and the other indices deal with each layer of the aquifer separately. The main functions of indicators are simplification, quantification, communication, ordering and allowing for comparison of different resources. They evaluate the effect of performed policy making actions and can help to develop new actions. Indicators also serve to forecast trends in groundwater quality, but only if they are repeatedly generated during a long period of time to be statistically significant (Vrba et al., 2007).

Combinations of several indicators are frequently used, because implementation of one single indicator can rarely satisfy the intended objectives. For example, Lamban et al. (2011) applied sustainability indicators such as AS and GAD to a small carbonate aquifer (26 km^2) situated in the province of Seville, southern Spain, with semi-arid climate. They concluded that the aquifer is undergoing intensive use and exploitation of its water resources is surpassing the threshold of sustainability when both the quantity and the quality of the groundwater are taken into consideration. Shrestha and Udmale (2014) studied groundwater resources of Dhubdhubhi watershed in Maharashtra state of India. They calculated that the FI, RGPC, DAG, AS and GAD equal to 537, 490, 87.5, 71.5 and 64.5, respectively and concluded that the whole watershed is at the stage of sustainable development; even though over exploitation are detected in some parts of the region. Also, Anbazhagan and Jothibasu (2016) used AS and GAD to evaluate sustainability of Uppar Odai sub-basin, India. The study demonstrates that only in 29 percent of the area groundwater development is possible.

Shiklomanov (2000) assessed world water resources per capita using FI. The results show that among the most water scarce regions in the world, FI of Western Asia that IRAN is located in it, is equal to 2110 m^3 per capita and is placed third after Northern Africa and Southern Asia. Golestan province is an agricultural hub with high water consumption in agriculture. Of course this province has a great talent for agricultural development if the water is supplied. On the other hand, groundwater resources are the main domestic water supply of many parts of the region. Almost maximum capacity of the aquifer is using for various tasks, therefore it is necessary to control water table drop based on studies on groundwater variations and performing management measures in order to prevent the major source of water to be faced with serious risks (Kuhestani et al., 2013). The groundwater system consists of a multilayer aquifer with both phreatic and confined layers. The confined aquifer is abstracting all over the plain but it is only recharging across its southern and south-eastern boundary, that confining layer does not exist. However, rainfall recharges the phreatic aquifer throughout the plain.

Worldwide researches on water resources sustainability and lack of such studies in the region besides importance of groundwater among water resources system of Golestan province, altogether lead to do evaluative works on current hydrological status and future development capability of this vital resource. After all, different porous media characteristics, recharge regime and accessibility create different geo-hydrological processes which should be investigated, separately, in order to efficiently integrate water resources management. Looking at this aquifer as a lump system can cause unsustainability of one layer while the total system is in sustainable state. In another research, Karimirad et al. (2016) investigated the effect of climatic variability on multilayer aquifer of Golestan province using groundwater resource index (GRI) and correlation analysis. They concluded that confined aquifer is more reliable and react to climate fluctuations (as a main driver) with more delay and recover more quickly. This paper aims to evaluate phreatic and confined aquifers in the multilayer groundwater system in terms of sustainability through index-based approach.

2 MATERIALS AND METHODS

Golestan is one of the 30 provinces of IRAN, located in the northeastern part of the country, south-east of the Caspian Sea. Golestan is situated between 36° 44' and 38° 05' north latitude and 53° 51' and 56° east longitude. The region's climate classified as semi-arid in the north and semi-humid in the south and southwest according to De-Martonne method (Mostafazadeh and Sheikh, 2012). There is an alluvial multilayer aquifer in this province that has about 4720 square kilometers area. The location of Golestan province and the multilayer aquifer in Iran is illustrated in Figure 1. This groundwater system includes both phreatic and confined aquifers. The confined aquifer beneath the phreatic one (multi-layer aquifer in Figure 1); it spread across the phreatic one except about 400 square kilometers in southern part (single-layer aquifer in Figure 1). The aquifer is extended from the Caspian Sea in the west to the city of Kalale in the East for about 130 kilometers and from the southern mountains to the Great Wall of Gorgan in the north for about 35 kilometers.

The multilayer aquifer supply almost all demands for drinking water and about 65 percent of agricultural needs (Kankash-Omran, 2009).

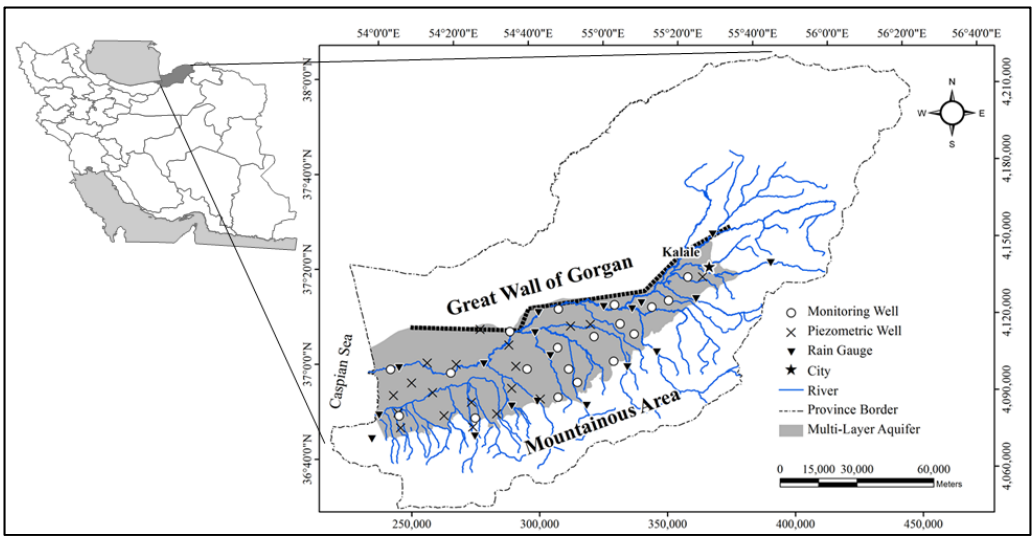

Figure 1. Location of alluvial multilayer aquifer in Golestan province of IRAN

In the present paper, the long-term monthly precipitation data of 19 gauges in time period of 1976 to 2013 which have a good distribution over the studied area was used. Also, recorded data of 19 observational wells drilled in the phreatic aquifer with the time period of 38 years (the same as the precipitation data) and 19 piezometric wells in the confined aquifer with 14-year time period (2000-2013) were used. This data were measured and recorded by the Golestan regional water authority. Consumption of each water resource in drinking and agricultural sectors and share of each exploitation method in total abstraction of Golestan aquifer are shown in Figure 2. Also, geo-hydrological characteristics of Golestan aquifer are presented in Table 1 (Kankash-Omran, 2013).

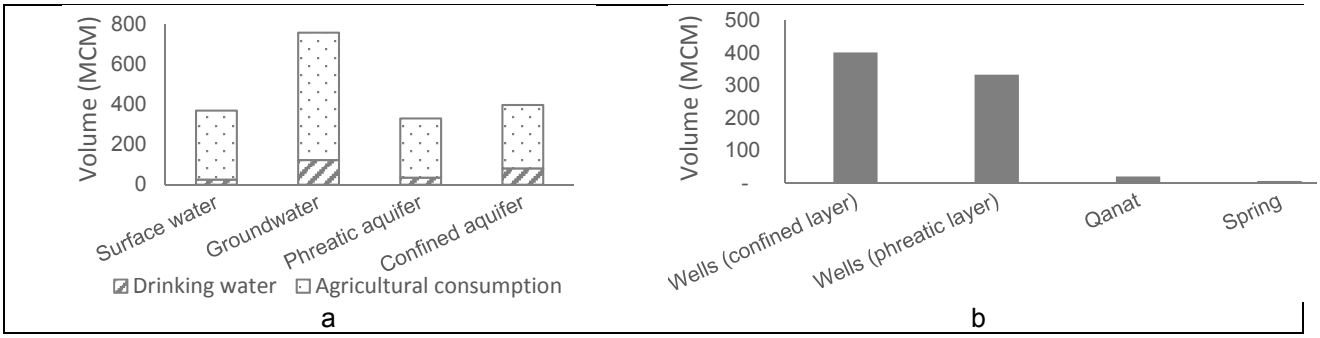

Figure 2. a. Consumption of each water resource in drinking and agricultural sectors, b. Share of each exploitation method in total abstraction of the aquifer (Kankash-Omran, 2013)

Table 1. Geo-hydrological characteristics of each layer in Golestan aquifer (Kankash-Omran, 2013)

Characteristic	Phreatic layer	Confined layer
Static volume (non-renewable water) (MCM/year)	1533	1121
Dynamic volume (renewable water) (MCM/year)*	513	397
Recharge (MCM/year)	852	398
Underground discharge (MCM/year)	399	2
Discharge into the sea (MCM/year)	2	2
Total abstraction (MCM/year)	358	401
Abstraction from non-renewable water (MCM/year)	0	3
Average thickness (m)	15	150
Average drop in last 10 years (m)	0.047	0.726
Aquifer area (Km^2)	4393	4050
Saline water area (Km^2)	1402	0

*Calculated according to instruction of FAO[1] (2003)

[1] Food and Agriculture Organization (United Nations)

Eleven proposed groundwater indicators were selected based on available data in the region. They provide information about groundwater quantity and quality and are focused on social (groundwater accessibility, exploitability and use), economic (groundwater abstraction and protection) and environmental (groundwater depletion and pollution) aspects of groundwater resource. These indices are described as below.

2.1 Falkenmark indicator (FI)

The Falkenmark indicator is perhaps the most widely used measure of water stress (Eq. [1]). Based on the per capita usage, the water conditions in an area can be categorized as in Table 2. The index thresholds 1,700 m^3 and 1000 m^3 per capita per year were used as the thresholds between water stressed and scarce areas, respectively (Falkenmark, 1989). In the context of this indicator, particular drivers were population growth and climate change, which can dramatically affect groundwater resource availability. However, FI do not consider important variations in demand among countries due to culture, lifestyle and others. Moreover, the water availability per person was calculated as an average without considering both the temporal and the spatial scale and thereby neglects water shortages in dry seasons or in certain regions within the region.

$$\text{FI } (m^3 \text{ per capita per year}) = \frac{\text{Renewable freshwater resources (MCM)}}{\text{Population}} \quad [1]$$

Table 2. Water resources conditions according to FI (Falkenmark, 1989)

FI (m^3 per capita per year)	Condition
>1,700	No stress
1,000-1,700	Under stress
500-1,000	Scarcity
<500	Absolute Scarcity

2.2 Renewable groundwater resources per capita (RGPC)

The state of this index annually in the study area gives an indication of the availability of groundwater (Shrestha and Udmale, 2014).

$$\text{RGPC } (\%) = \frac{\text{Renewable groundwater resources (MCM)}}{\text{Population}} \quad [2]$$

where, the numerator is total renewable groundwater resources, without considering groundwater quality but excluding brackish and saline waters. Renewable groundwater resources calculation is explained by FAO (2003).

2.3 Dependence to groundwater (DG)

This index demonstrate groundwater share in total water consumption in different sectors of the region (Eq. [3]). Different grades of groundwater dependency given in Table 3 (Beiki-khoshk, 2011).

$$\text{DG } (\%) = \frac{\text{Total groundwater abstraction (MCM)}}{\text{Total water consumption (MCM)}} \quad [3]$$

where, total groundwater abstraction is the total withdrawal of water from a given aquifer by means of wells, qanats, springs and other ways for the purpose of public water supply or agricultural, industrial and other usage.

Table 3. Grades of Groundwater dependency using DG index (Beiki-khoshk, 2011)

Range	Groundwater dependency
G < 25 %	High
25 % < G < 50 %	Moderate
G > 50 %	Low

2.4 Dependence of agriculture to groundwater (DAG)

Regarding the importance of groundwater to supply agricultural needs, this index is defined as follows (Beiki-khoshk, 2011):

$$\text{DAG } (\%) = \frac{\text{Groundwater used in agriculture (MCM)}}{\text{Total water used in agriculture (MCM)}} \quad [4]$$

2.5 The role of groundwater in the supply of drinking (RGSD)

RGSD can be used to represent the amount of dependence on groundwater to supply drinking water compared with surface water. This indicator is of particular social importance since it highlights the importance of groundwater for drinking purposes on a national basis, i.e. the population dependency on groundwater and therefore, it is the key role in public and domestic water supply. Ideally, at a later stage, the indicator could be applied separately for urban and rural areas (Vrba and Lipponen, 2007).

$$\text{RGSD (\%)} = \frac{\text{Groundwater used for drinking (MCM)}}{\text{Total drinking water (MCM)}} \quad [5]$$

2.6 Aquifer sustainability (AS)

AS index present groundwater abstraction as a portion of aquifer recharge (Vrba and Lipponen, 2007):

$$\text{AS} = \frac{\text{Total groundwater abstraction (MCM)}}{\text{Aquifer recharge (MCM)}} \quad [6]$$

The main sources of recharge are rainfall, surface water bodies, irrigation losses and seepage from urban water supply distribution and waste water collection systems. For the indicator, two possible scenarios are conceivable: (1) sustainable use of the groundwater with respect to quantity (total output < recharge) and (2) non-sustainable use of the groundwater (groundwater mining) with respect to the amount (total output > recharge). This indicates, in a preliminary manner, the degree of sustainability with regard to the use of groundwater, although aspects related to quality and/or affections to groundwater-fed ecosystems are not considered. The meaning of different values of AS are given in Table 4.

Table 4. Aquifer sustainability on basis of AS index (Vrba and Lipponen, 2007)

Range	Aquifer sustainability
AS > 1	Critical
1 > AS > 0.8	Highly unsustainable
0.8 > AS > 0.6	Unsustainable
0.6 > AS > 0.4	Little sustainable
0.4 > AS	Sustainable

2.7 Sustainability of groundwater quality (SGQ)

Groundwater quality indicators can inform about the present status and trends in groundwater quality and help to deal with groundwater quality problems in space and time. One of the parameters that determine the quality of groundwater is groundwater salinity that SGQ index accordingly defined and is expressed as follows (Beiki-khoshk, 2011):

$$\text{SGQ (\%)} = \frac{\text{Saline zone of aquifer (KM}^3\text{)}}{\text{Total area of aquifer (KM}^3\text{)}} \quad [7]$$

2.8 Groundwater abstraction development (GAD)

In many countries there is an intention to quantify GAD as an index to specify usable groundwater reserves. Accordingly, aquifer's ability to develop is concluded according to table 5. (Vrba and Lipponen, 2007).

$$\text{GAD (\%)} = \frac{\text{Total groundwater abstraction (MCM)}}{\text{Exploitable groundwater resources (MCM)}} \quad [8]$$

where, total exploitable non-renewable groundwater resource means that the total amount of water that can be abstracted from a given aquifer under prevailing economic, technological and institutional constraints as well as ecological conditions (GIWG, 2004).

Table 5. GAD index values and development capability of aquifer (Vrba and Lipponen, 2007)

Range	Development capability
GD < 25 %	Capable
25 % < GD < 40 %	Limited
40 % < GD	No development

2.9 Pressure on non-renewable resources of groundwater (PNRG)

Non-renewable groundwater is a finite water resource to which no or very little recharge takes place and has accumulated over geologic time, and therefore is not replenished over human timescales. Its depletion can cause irreparable damage to the aquifer (e.g. land subsidence) and should be maintained. Through PNRG index (Eq. 9) the situation of non-renewable part of aquifer can be disclosed somewhat (Vrba and Lipponen, 2007).

$$\text{PNRG (year)} = \frac{\text{Total exploitable non-renewable groundwater resources (MCM)}}{\text{Annual abstraction of non-renewable groundwater resources (MCM/year)}} \quad [9]$$

2.10 Aquifer recovery potential (ARP)

This index (Eq. 10) show the ability of aquifer to recover or return to normal state (Vrba and Lipponen, 2007):

$$\text{ARP} = \frac{\text{Static volume of aquifer (MCM)}}{\text{Recharge of aquifer (MCM)}} \quad [10]$$

where, static volume is part of aquifer contains non-renewable groundwater. The potential of aquifer to be recovered can be determined according to table 6.

Table 6. Aquifer recovery potential classification (Vrba and Lipponen, 2007)

Range	Aquifer recovery potential
ARP < 10	High
10 < ARP < 30	Fair
30 < ARP < 50	Low
50 < ARP	No recovery

2.11 Groundwater decay rate (GDR)

Beiki-khoshk (2011) developed groundwater decay rate index to estimate the number of years that an aquifer is reliable as follows:

$$\text{GDR (year)} = \frac{\text{Average thickness of aquifer (m)}}{\text{Average decline in groundwater table or piezometric level in last 10 years (m)}} \times \frac{2}{3} \quad [11]$$

3 RESULTS AND DISCUSSION

Monthly time series of precipitation, water table of the phreatic aquifer and piezometric level of confined aquifer, are shown in Figure 3. Each chart illustrates average of 19 rain gauges and respective wells. Stationarity checked at 95 percent confidence level using Hurst exponent method and accordingly all three used time series are stationary. Mann-Kendall test results at 95 percent confidence level show no significant trend in precipitation data but water level of phreatic aquifer and Piezometric level of confined aquifer declining at the rate of 1 and 12 mm per month, respectively. It is worth mentioning during the same period with the confined aquifer data (last 14 years), the water level of the phreatic aquifer has no trend.

FI and RGPC for Golestan province is equal to 855 and 512 M^3 per capita per year, respectively, which means that the region is facing water scarcity. Other indices were calculated and demonstrated in Table 7.

Accordingly, calculated FI is far less than which has been estimated by Shiklomanov (2000) as an average amount for Western Asia. Sustainability of the studied aquifer looks alike which has been evaluated by Lamban et al. (2011). Index-based evaluation show better water availability (pay attention to FI and RGPC) compared to the case of Shrestha and Udmale (2014) but more dependency of agriculture to groundwater (pay attention to DAG) that caused over-exploitation of both layers specially confined one (pay attention to AS). It suggests change in cropping patterns or shifting economic axis of the region from agriculture to sectors with lower water demand such as industry and services. Of course non-renewable groundwater covered mentioned problem, currently (pay attention to GAD) and maybe it is the reason that Karimirad et al. (2016) evaluated the confined aquifer more reliable.

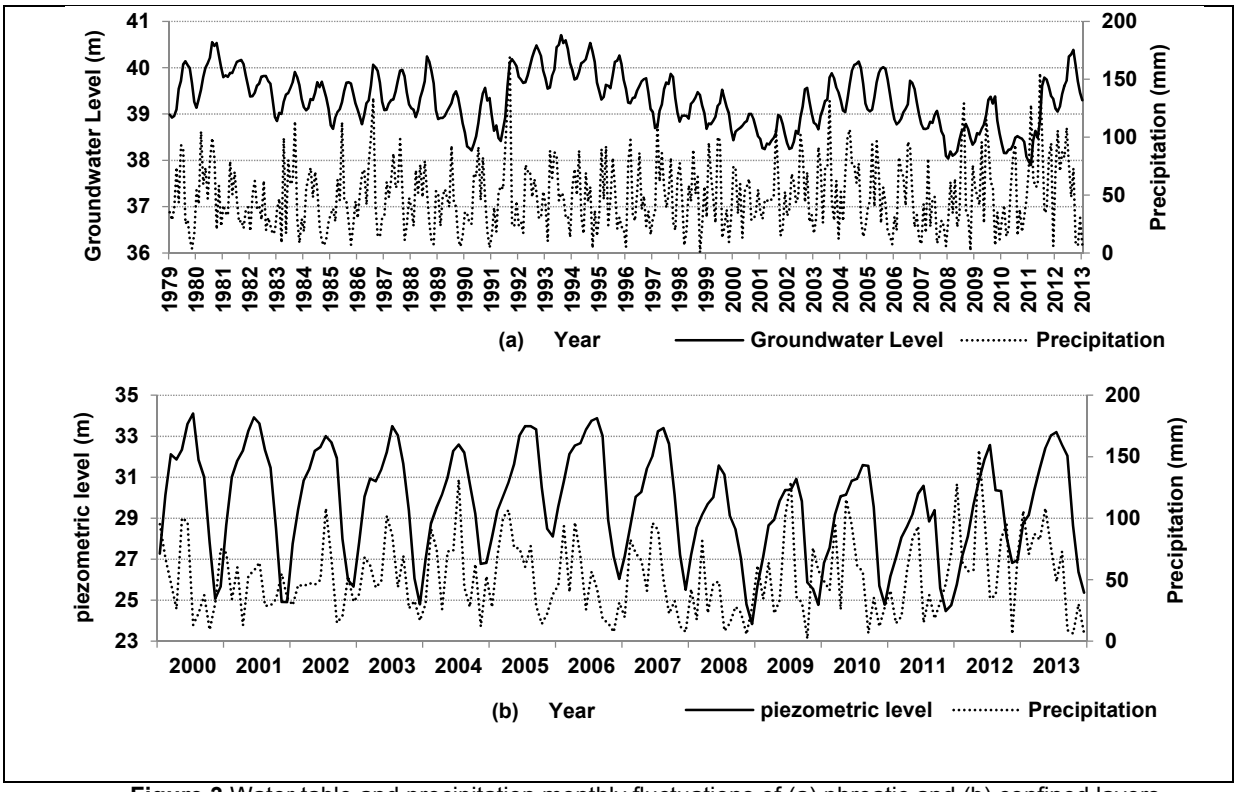

Figure 3 Water table and precipitation monthly fluctuations of (a) phreatic and (b) confined layers (Karimirad et al., 2016)

Table 7. Calculated indices of status and sustainability for whole aquifer and its layers separately

No	Index (Unit)	Multilayer aquifer		Interpretation
		Phreatic layer	Confined layer	
1	DG (%)	63.37		Dependency to groundwater is higher than surface water
2	DAG (%)	64.88		Agriculture is more dependent to groundwater
3	RGSD (%)	77.94		Drinking water is more dependent to groundwater
4	AS	0.89	1.01	Phreatic layer is highly unsustainable and Confined one is worse and critical
5	SGQ (%)	0.32	0	Nearly one third of phreatic aquifer area become saline
6	GAD (%)	0.32	0.26	Limitations must be considered to develop both phreatic and confined layers
7	PNRG (year)	0	332	Confined aquifer will be entirely depleted and irreversibly exterminated after 3 centuries
8	ARP	1.8	2.82	Both layers will be recovered soon
9	GDR (year)	213	138	If current trends continue, phreatic aquifer will be depleted 75 years after confined one

4 CONCLUSIONS

It can be concluded that the index-based investigation of groundwater resources in multilayer aquifer of Golestan province, IRAN revealed some valuable information about its current status, sustainability and future perspective. First of all, the region is facing water scarcity that is a limitation to economic development and human health and well-being. Studied society is depending on groundwater more than surface water resources and the situation prevailing in both main sectors of drinking and agriculture. First five indices clarified the current status of the region in terms of water resources in general and importance of implementing water management measures. Six other indices have gone more to the details and investigate quantitative and qualitative aspects of sustainability in each layer of aquifer, separately. Accordingly, both phreatic and confined layers are unsustainable and confined layer's condition is worse although it has been covered by non-renewable groundwater until now. However, in terms of quality situation, it is vice versa and phreatic aquifer is threatened by salt-water intrusion.

According to GAD implementation of water resources development plans is allowed with considering some limitations in terms of water quantity and quality. Some restorative measures are advisable to improve sustainability including: expanding watershed management actions especially in the confined aquifer recharge area, more control on abstraction of the aquifer using smart water meters, enforcement of the law through incentives and penalties such as agricultural subsidies, reduce on-farm water loss by changing traditional irrigation, covering canals and repairing distribution networks. However, changing economic axis of the region from agriculture to sectors with lower water demand such as industry and services or at least shifting cropping patterns is highly advised.

Despite all, fortunately, both layers can be recovered soon if driver factors change toward providing sustainable conditions. As an estimation GDR and PNRG predict one and three centuries, respectively, for confined aquifer depletion which anyway is negligible compared with the time it formed during geological periods. It is necessary to note that aquifer depletion and subsequent land subsidence can cause severe impact on human settlements in the region such as lack of water in dry season, sinkholes and others. Altogether, confined aquifer is more endangered quantitatively while quality degradation threatens phreatic aquifer. Overall, the proposed groundwater indicators are scientifically robust and policy relevant, based on available data, provide information about the present status, trends and impacts on groundwater system and support socially and economically sustainable management and environmentally sound protection of groundwater resources.

ACKNOWLEDGEMENTS

The authors would like to acknowledge University of Tehran, IRAN and Golestan province regional water authority, IRAN, for supporting this research.

REFERENCES

Anbazhagan, S. & Jothibasu, A. (2016). Groundwater Sustainability Indicators in Parts of Tiruppur and Coimbatore Districts, Tamil Nadu. *Journal of the Geological Society of India*, 87 (2), 161-168.

Beiki-khoshk, A. (2011). Groundwater management with sustainable development approach. *MSc Thesis*, University of Tehran, 75-93.

Brown, A. & Matlock, M.D. (2011). A Review of Water Scarcity Indices and Methodologies. *White Paper*, 106, 19.

Chaves, H.M.L. & Alipaz, S. (2007). An Integrated Indicator Based on Basin Hydrology, Environment, Life, and Policy: The Watershed Sustainability Index. *Water Resource Management*, 21(5), 883-895.

Falkenmark, M. (1989). The Massive Water Scarcity Threatening Africa: Why isn't it being Addressed?. *Ambio*, 18 (2), 112-118.

Food and Agriculture Organization (2003). Review of World Water Resources by Country. *Water Reports*, 23.

Groundwater Indicators Working Group (2004). *Development of groundwater indicators for second edition of the World Water Resources*. United Nations Environmental, Scientific and Cultural Organization, Paris

Kankash-Omran Consulting Engineers Co. (2009). *Updating report on combination the water resources studies of gharesoo and gorganrood rivers drainage basin*. (In Persian).

Kankash-Omran Consulting Engineers Co. (2013). *Updating report on water balance of gharesoo and gorganrood rivers drainage basin*. (In Persian).

Karimirad, I., Ebrahimi, K., & Araghinejad, S. (2016). Investigation of effect of climate variability on multilayer aquifers (case study: Gorgan plain). *Water management and irrigation*, 5 (2), 261-275. (In Persian).

Klugman, J. (2011). Human Development Report 2011. Sustainability and Equity: A better future for all.

Koohestani, N., Meftah, H.M. & Dehghani, A. (2013). Numerical Simulation of Groundwater Level Using MODFLOW Software (A Case Study: Narmab Watershed, Golestan Province). *International Journal of Advanced Biological and Biomedical Research*, 1(8), 858-873.

Lambán, L.J., Martos, S., Rodríguez-Rodríguez, M. & Rubio, J.C. (2011). Application of Groundwater Sustainability Indicators to the Carbonate Aquifer of the Sierra De Becerrero (Southern Spain). *Environmental Earth Sciences*, 64 (7), 1835-1848.

Mostafazadeh, R. & Sheikh, V. (2012). Rain-Gauge Density Assessment in Golestan Province Using Spatial Correlation Technique. *Watershed Research*, 24(4), 79-87. (In Persian)

Rijsberman, F.R. (2006). Water Scarcity: Fact or Fiction?. *Agricultural Water Management*, 80 (1), 5-22.

Shiklomanov, A. (2000). Appraisal and Assessment of World Water Resources, *Water International*, 25(1), 11-32.

Shrestha, S. & Udmale, P. (2014). Evaluation of Sustainability of Groundwater Resources in a Semi-Arid Region of the Maharashtra State of India. *International Journal of Water Resources and Environmental Engineering*, 6 (7), 203-211.

Sullivan, C. (2002). Calculating a Water Poverty Index. *World Development*, 30 (7), 1195-1210.

Vorosmarty, C.J., Douglas, E.M., Green, P.A. & Revenga, C. (2005). Geospatial Indicators of Emerging Water Stress: An Application to Africa. *Ambio*, 34 (3), 230-236.

Vrba, J., Hirata, R., Girman, J., Haie, N., Lipponen, A., Shah, T. & Wallin, B. (2007). *Groundwater Resources Sustainability Indicators*. United Nations Environmental, Scientific and Cultural Organization, Paris.

Watkins, K. (2006). Human Development Report 2006. Beyond scarcity: power, poverty and the global water crisis. *Human Development Reports*, United Nations Development Programme- Human Development Report Office.

Zektser, I.S. & Everet, L.G. (2004). Groundwater resources of the world and their use. *Groundwater (No. 6)*, International Hydrological Programme series, United Nations Environmental, Scientific and Cultural Organization, Paris.

Proceedings of the 37th IAHR World Congress
August 13 – 18, 2017, Kuala Lumpur, Malaysia

DELINEATION OF SULPHATE AND NITRATE SOURCE IN KUWAIT GROUNDWATER USING ENVIRONMENTAL ISOTOPES

HARISH BHANDARY[1] & MOHAMED AL-SENAFY[2]

[1,2] Water Research Center, Kuwait Institute for Scientific Research, Kuwait
hkaup@kisr.edu.kw; msenafy@kisr.edu.kw

ABSTRACT

A study is conducted to delineate the sources of nitrate and sulphate concentrations in the groundwater of Kuwait using environmental isotopes. Groundwater sampling campaigns are carried out to collect water samples from the two main aquifers of Kuwait, namely, the Kuwait Group and Dammam formation aquifers throughout Kuwait. The samples are analyzed for environmental isotopes, i.e, $^{2/1}H$, $^{18/16}O$, $^{34/32}S$ and $^{18/16}O$ (SO_4^{2-}), $^{15/14}N$ and $^{18/16}O$ (NO_3^{2-}), ^{3}H, and ^{14}C. The δ^2H vs $\delta^{18}O$ results show that most of the groundwater samples fall below the Global Meteoric Water Line (GMWL) suggesting evaporation prior to recharge and the recharge has taken place during a different climatic condition than exists today (paleo water). Most of the groundwater samples measured ^{3}H values less than that of the rainwater indicating that they are not modern but old water. The $\delta^{34}S(SO_4^{2-})$, $\delta^{18}O(SO_4^{2-})$ and SO_4^{2-} values of groundwater samples of Kuwait Group of Aquifers has revealed that most of the groundwater samples (SO_4^{2-}: 100 to 4600 mg/L), $\delta^{34}S(SO_4^{2-})$: +3 to +24‰, $\delta^{18}O(SO_4^{2-})$: +10 to +15‰) have evaporatic origin. The $\delta^{15}N(NO_3^{2-})$, $\delta^{18}O$ (NO_3^{2-}) and NO_3^{2-}values of the groundwater samples of Kuwait Group Aquifer has indicated that the majority of the groundwater samples (NO_3^{2-}: 3 -100 mg/L, $\delta^{15}N(NO_3^{2-})$: +4 to +21‰, $\delta^{18}O$: +1 to +38‰) are either desert nitrate or nitrate in precipitation. Similarly, the $\delta^{15}N(NO_3^{2-})$, $\delta^{18}O$ (NO_3^{2-}) and NO_3^{2-} values of the groundwater samples of Dammam Formation Aquifer has indicated that they are characteristic of desert nitrates. It is concluded that the major source of high sulphate and nitrate concentration of Kuwait groundwater is geogenic in nature due to the dissolution of evaporites and desert nitrates during the flow course of groundwater.

Keywords: Pollutants; aquifer; Kuwait group; Dammam formation; evaporates; geogenic.

1 INTRODUCTION

Groundwater is a very important element of the limited available water resources in Kuwait. Groundwater contamination is an ever present menace in Kuwait where urban and industrial development occurs at a rapid pace. A study was conducted to delineate the sources of nitrate and sulphate concentrations in the groundwater of Kuwait using environmental isotopes. Nitrate and sulphate concentrations in usable groundwater frequently exceed the normal standards that range between 4 and 110 mg/l and 100 and 2600 mg/l respectively (Akber et al., 2006). The importance of this study stems from the fact that the groundwater is the only natural water resource of the country; consumption of these high constituents in water may have adverse health effects. The isotopic composition of the groundwater often points towards the source of the pollutants affecting the groundwater and hence, leads to the formulation of better protection measures from these pollutant sources (Fritz and Fontes., 1980; Fukuda et al., 2003). In Kuwait, extraction of groundwater is from two main aquifers, namely, the Kuwait Group of aquifers and the Dammam Formation aquifer. The total dissolved solids of the Kuwait Group aquifer groundwater increase generally from about 3,000 mg/l in the southwest to about 130,000 mg/l in the northeast over a distance of about 150 km. Fresh groundwater is only encountered in the north, where the unique geomorphology and lithology are responsible for the formation of freshwater lenses floating over the main saline water body.

2 METHODOLOGY

2.1 Groundwater Sampling

Twenty groundwater samples were collected for deuterium, oxygen 18, tritium, nitrogen 15, sulphur 34, Carbon 13 and Carbon 14 isotopic parameters from two main aquifers namely, Kuwait group and Dammam Formation aquifer. These groundwater samples were collected from all over Kuwait and the locations of sampling are presented in Figure 1. The samples were collected from the existing monitoring and production wells to cover the different aquifer zones of interest following the established sampling protocol. The groundwater samples were collected by introducing an electric submersible pump into the well, 1 to 2 m below the water table. The other end of the submersible pump was connected to a flow-through cell in which a number of portable field measurement instruments were installed to measure pH, temperature, electrical conductivity (EC), dissolved oxygen (DO), and oxidation reduction potential (Eh) on site. The purpose of

measuring these parameters on site is to ensure that purging would remove sufficient quantity of water to enable the collection of the representative groundwater sample. International Atomic Energy Agency's (IAEA) sampling protocols were followed for a sample collection of both stable and radioactive isotopes (IAEA, 2010).

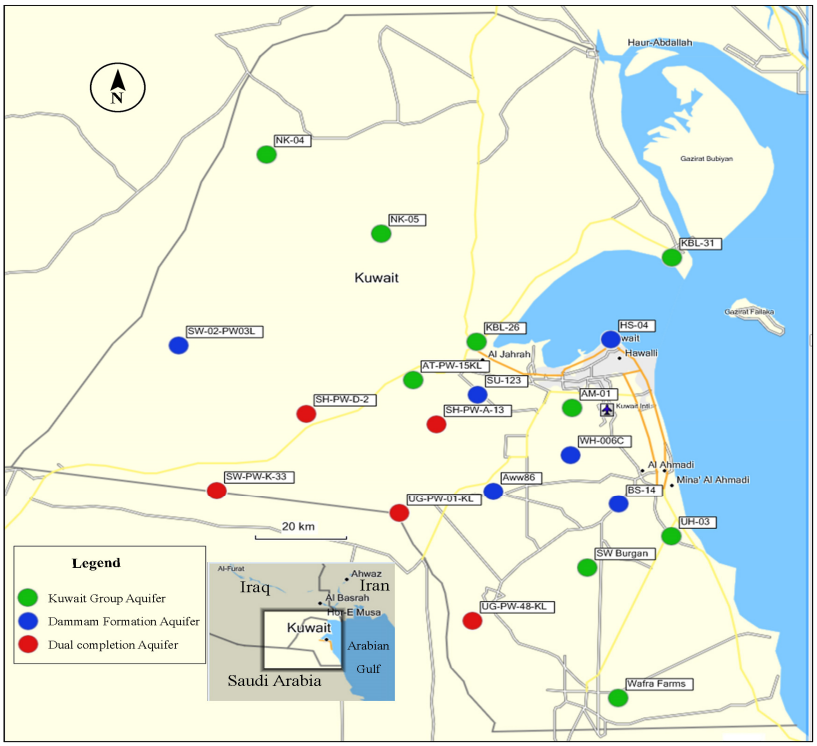

Figure 1. Groundwater sampling locations.

2.2 Laboratory Analyses.

The samples were analyzed for environmental isotopes, i.e., $^{2/1}H$, $^{18/16}O$, $^{34/32}S$ and $^{18/16}O$ (SO_4^{2-}), $^{15/14}N$ and $^{18/16}O$ (NO_3^{2-}), ^{3}H, ^{13}C, 14C and major ions. Analyses of stable isotopes ^{18}O and ^{2}H carried out in the Water Research Center laboratory of Kuwait Institute for Scientific Research using an off-axis integrated cavity output spectroscopy (OA-ICOS) water isotope analyzer (Los Gatos model 908-0008). The tritium was measured by the liquid scintillation counter after electrolytic enrichment in Seibersdorf laboratories in Austria. $\delta^{15}N(NO_3^-)$ and $\delta^{34}S(SO_4^{2-})$ were measured using an isotope ratio mass spectrometer (IRMS) in Helmholtz Center for Environmental Research, Germany, with respect to atmospheric air and Vienna-Canyon-Diablo Troilite (VCDT). Sulfur isotopic compositions were measured after conversion of $BaSO_4$ to SO_2 using an elemental analyzer (continuous flow flash combustion technique) coupled with an isotope ratio mass spectrometer (delta S, ThermoFinnigan, Bremen, Germany). Sulfur isotope results are reported in delta notation ($\delta^{34}S$) as part per thousand (‰) deviation relative to the Vienna Cañon Diablo Troilite (VCDT) standard. Sulfur isotope measurements of the prepared $BaSO_4$ were performed with an analytical error of the measurement of better than ± 0.4‰. Oxygen isotope analysis on barium sulfate samples was carried out by high temperature pyrolysis at 1450 °C in a TC/EA connected to a delta plus XL mass spectrometer (ThermoFinnigan, Bremen, Germany) with an analytical error of better than ±0.5‰. Results of oxygen isotope measurements are expressed in delta notation ($\delta^{18}O$) as part per thousand (‰) deviation relative to Vienna Standard Mean Ocean Water (V-SMOW). For normalizing the $\delta^{34}S$ data, the IAEA-distributed reference materials NBS 127 ($BaSO_4$) and IAEA-S1 (Ag_2S) were used. The assigned values were +20.3‰ (VCDT) for NBS 127 and 0.3‰ (VCDT) for IAEA-S1. The normalization of oxygen isotope data of sulfate was carried out using the reference material NBS 127 with an assigned $\delta^{18}O$ value of +8.6‰ (V-SMOW) (Knoller and Schubert, 2010).

The nitrogen and oxygen isotopic composition of nitrate, expressed in δ notation relative to the standards AIR and VSMOW, respectively, was measured by the denitrifier method using a GasbenchII/delta V plus combination (Thermo). $\delta^{15}N$ and $\delta^{18}O$ were determined in the measuring gas N_2O, produced by controlled reduction of sample nitrate performed with the Pseudomonas chloroaphis supsp. auerofaciens (ATCC 13895) (Casciotti et al., 2002; Sigman, 2001). For the calibration of nitrogen and oxygen isotope values, the reference nitrates IAEA-N3 ($\delta^{15}N$: +4.7 ‰ AIR, $\delta^{18}O$: +25.6 ‰ VSMOW), USGS32 ($\delta^{15}N$: +180 ‰ AIR, $\delta^{18}O$: +25.7 ‰ VSMOW), USGS 34 ($\delta^{15}N$: -1.8 ‰ AIR, $\delta^{18}O$: -27.9 ‰ VSMOW), and USGS 35 ($\delta^{15}N$: +2.7 ‰ AIR, $\delta^{18}O$: +57.5 ‰ VSMOW) were used. The analytical precision of the denitrifier method for $\delta^{15}N$ and $\delta^{18}O$ was ±0.4‰ and ±1.6‰ respectively.

The ^{14}C activity and ^{13}C were analyzed for groundwater samples in Center for Isotope Research laboratory in the Netherlands. ^{14}C activity was measured using accelerator mass spectrometry (AMS) and expressed as percentage modern carbon (pmc), and ^{13}C was measured using an isotope ratio mass spectrometer (IRMS) in the form of CO_2 gas and expressed as permil (‰). The standard used was Pee Dee Belemnite (PDB). The precision of measurement was ±0.5‰.

3 RESULTS AND DISCUSSION

The laboratory analyses results of the groundwater samples for isotopic parameters are presented in Table 1.

Table 1. Laboratory Analysis Results of Environmental Isotopes.

Sample ID	C13 ‰	C14%	N15 (‰) (air)	^{18}O (NO_3) VSMOW	S34(‰) (VCDT)	$^{18}O(SO_4)$ VSMOW	Tritium TU	^{2}H ‰	^{18}O ‰
T2A	-10.19	22.95	4.6	18.9	15.2	12.9	<0.3	-15.58	-2.08
NK-10	-13.35	29.61	20.8	23.8	12.1	12.7	<0.3	-18.04	-2.05
P -02	-12.25	93.15	4.3	0.9	14.7	12.4	<0.2	-14.51	-3.57
SB-01	-7.71	6.79	3.8	19.4	14.3	13.9	<0.3	-10.59	-0.98
NK-08	-8.79	11.95	12.6	37.8	13	13.2	-	-23.02	-2.77
NK-03	-9.33	12.09	6.5	34.3	3.1	12.1	<0.3	-32.96	-4.04
KBL-17	-7.65	23.43	5.2	23.1	12.1	12.6	-	-29.35	-3.49
HS-17	-9.34	15.19	-	-	23.6	14.6	-	-29.43	-3.17
BN-01	-7.35	4.31	-	-	16.7	13.9	-	-26.97	-3.34
LF-05	-11.11	69.27	6.6	9.7	13.3	12.4	0.3±0.2	-0.06	0.55
QR-02	-11.28	49.77	8.7	24.3	11.5	12.1	-	-15.97	-1.89
Liyah	-8.42	12.24	4.5	33.2	11.4	10.4	-	-30.48	-3.62
KN-MAB-W-19	-10.44	61.07	7.8	37.7	13.4	11.2	-	-8.26	-0.49
AT-PW15K	-9.04	8.22	4.2	20.8	13.6	13.3	-	-28.48	-3.51
Dammam Formation Aquifer									
Kabd	-9.58	1.31	-	-	15.2	9.6	-	-31.04	-3.98
SH-PW-C-12	-6.54	1.69	9.1	18.8	13	12.4	<0.3	-38.51	-5.07
SL-01	-7.75	2.69	5.7	26.6	14.4	13.4	<0.3	-27.85	-3.89
T1-F	-18.55	55.49	-	-	18.6	13.5	<0.3	-19.15	-2.48
QR-01	15.74	-	-	-	30	15.9	-	-39.47	-3.41
Dual completion Aquifer									
UG-PW-43	-7.26	16.02	5	27	14.9	13.7	<0.3	-24.87	-2.98

3.1 ^{2}H and ^{18}O

The $\delta^{2}H$ vs $\delta^{18}O$ plot of groundwater samples is shown in Figure 2. Most of the groundwater samples fall below the Global Meteoric Water Line (GMWL), indicating that the groundwater samples have undergone evaporation prior to recharge at the recharge area or near the surface during recharge. Also, the groundwater recharge has taken place during a different climatic condition than what exists today (paleo water).

3.2 ^{3}H and ^{14}C

The environmental ^{3}H analyses of the groundwater samples collected from various locations indicated that most of the groundwater had very low values suggesting not recently recharged rainwaters. Hence, ^{14}C analyses of the groundwater were carried to estimate the groundwater ages. Various empirical models were used to correct the ^{14}C ages of the groundwater samples. The corrected ^{14}C ages of the groundwater samples of Kuwait Group of aquifers range from 1,500 to 15,000 a B.P and that of the Dammam formation aquifer, from 20,000 to 30,000 a B.P.

3.3 Sulphur-34/32

The $\delta^{34}S$ concentration of the Kuwait Group of aquifers ranges from 3.1 to 23.6 ‰ and that of the Dammam Formation aquifer, from 13 to 30 ‰. The depth wise distribution of SO_4^{2-}, $\delta^{34}S(SO_4^{2-})$ and $\delta^{18}O(SO_4^{2-})$ concentration in the groundwater samples show any clear trend. In the Kuwait Group of aquifers, depth wise variation, of SO_4^{2-} concentration is rather quite complex with large variations up to 60 m depth and thereafter, decreasing with depth. This probably indicates the different groundwater flow lines and the associated hydrogeochemical interactions with various sources of sulphate. In the Dammam Formation aquifer, the distribution shows a decreasing trend with depth.

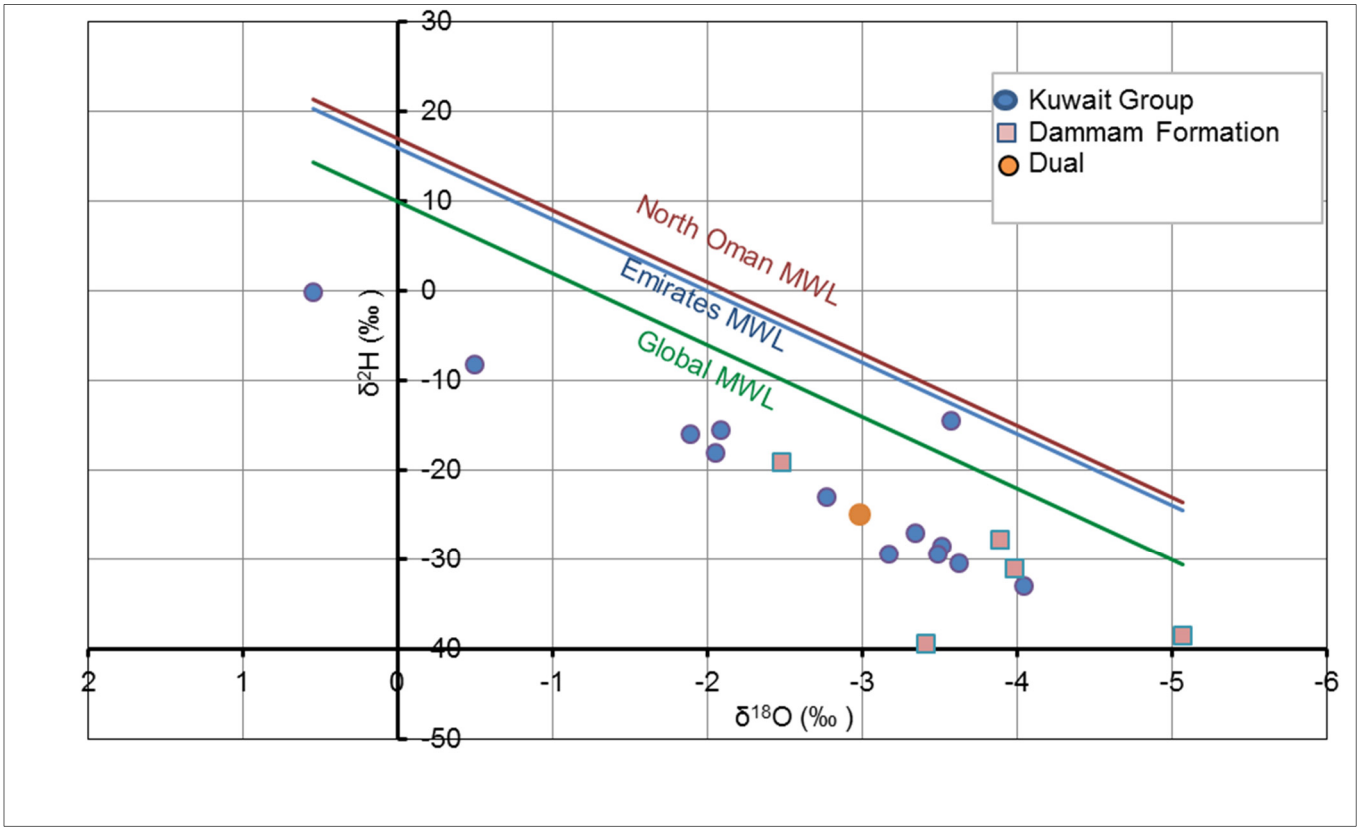

Figure 2. Plot of $\delta^{2}H$ and $\delta^{18}O$ of groundwater samples.

A plot of $\delta^{34}S(SO_4^{2-})$ vs. SO_4^{2-} (Figure 3) and $\delta^{34}S(SO_4^{2-})$ vs $\delta^{18}O(SO_4^{2-})$ of groundwater samples of Kuwait Group of aquifers show two groups; First Group samples have very low SO_4^{2-} and highly depleted $\delta^{34}S$ (2 to 4‰) and relatively lesser $\delta^{18}O$ (~11‰) values, and the remaining samples fall under a second group with wide range of SO_4^{2-} (0 to 3000 mg/L) and highly enriched $\delta^{34}S$ (13 to 15‰) and relatively higher $\delta^{18}O$ (12-18‰).

The figures which reveal that most of the groundwater samples of Kuwait Group of aquifers (Group 2) have evaporitic origin. The large variations in sulphate concentrations, with negligible $\delta^{34}S$ values, indicate dissolution of sulphates (and not bacterial reduction of sulphate) subsequently during their flow. In addition to evaporatic origin of groundwater samples, there is an evidence of precipitational origin (acid rain containing high sulphate) (Group 1).

A plot of $\delta^{34}S(SO_4^{2-})$ vs. $\delta^{18}O$ (SO_4^{2-}) and $\delta^{34}S(SO_4^{2-})$ vs. SO_4^{2-} (Figure 4) of groundwater samples of Dammam Formation aquifer indicates two types of groundwater: Group 2: dissolution of anhydride or gypsum and Group 1: dissolution of secondary sulphates, which originate from the oxidation of metallic sulphides (as pyrites). The large variations in sulphate and $\delta^{34}S(SO_4^{2-})$ seen in Group 1 suggest various local geological conditions and diagenetic history. The $\delta^{34}S(SO_4^{2-})$ values of Group 2 indicate the dissolution of sulphates subsequently during the flow.

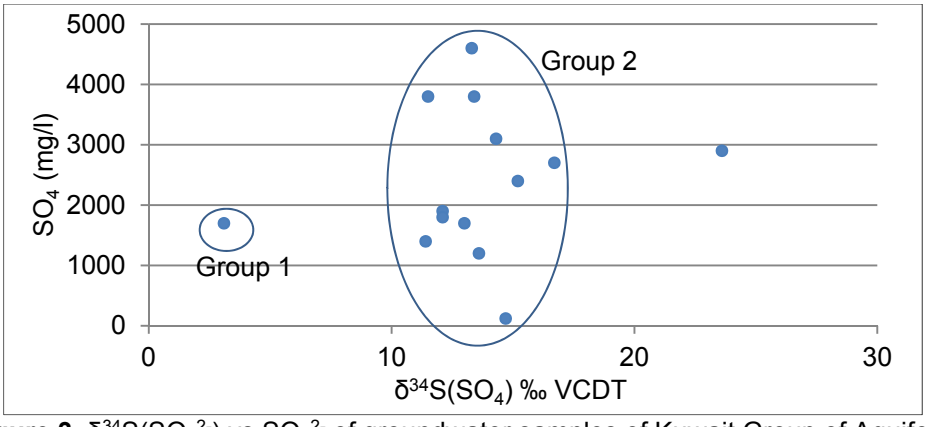

Figure 3. $\delta^{34}S(SO_4^{2-})$ vs SO_4^{2-} of groundwater samples of Kuwait Group of Aquifers.

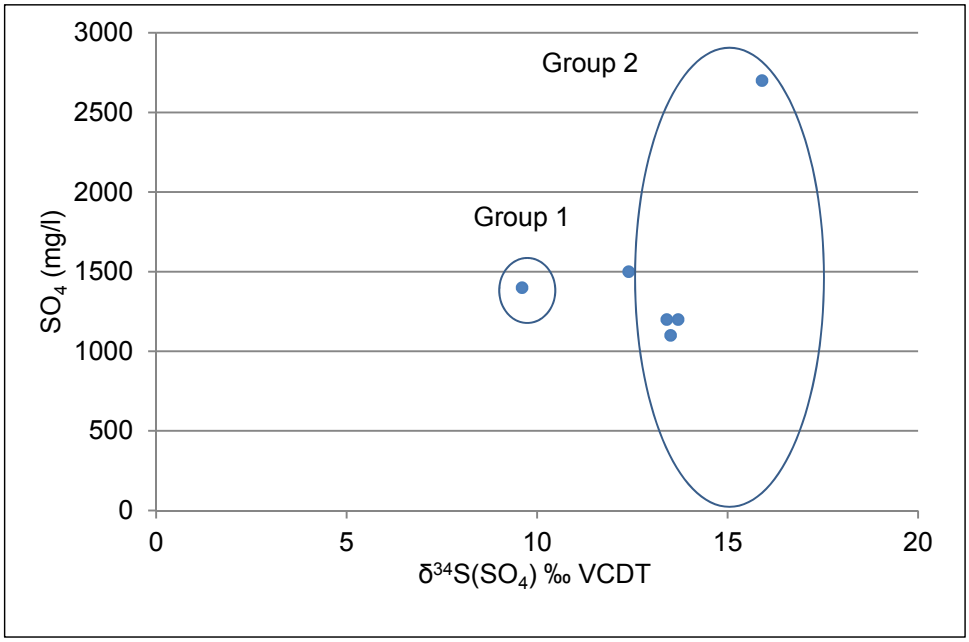

Figure 4. $\delta^{34}S(SO_4^{2-})$ vs SO_4^{2-} of groundwater samples of Dammam Formation Aquifers.

3.4 Nitrogen-15/14

The $\delta^{15}N(NO_3^{2-})$ values range from +2‰ to +37‰ and $\delta^{18}O$ (NO_3^{2-}) values range from +6 to +35‰. The wide ranges of values are possibly indicative of the varying sources of nitrate and the geochemical processes undergoing in the subsurface medium. The depth wise distribution of nitrate indicates that in the Kuwait Group of aquifers there is no unique trend. In the Dammam Formation aquifer, the nitrate concentration decreases with depth. The depth distribution of $\delta^{15}N$ does not show any clear trend in the Kuwait Group of aquifers but a fairly decreasing trend is observed in the Dammam Formation aquifer as well with relatively enriched $\delta^{15}N(NO_3^{2-})$ values at higher depths (>300 m). A similar observation is seen with the depthwise distribution of $\delta^{18}O(NO_3^{2-})$.

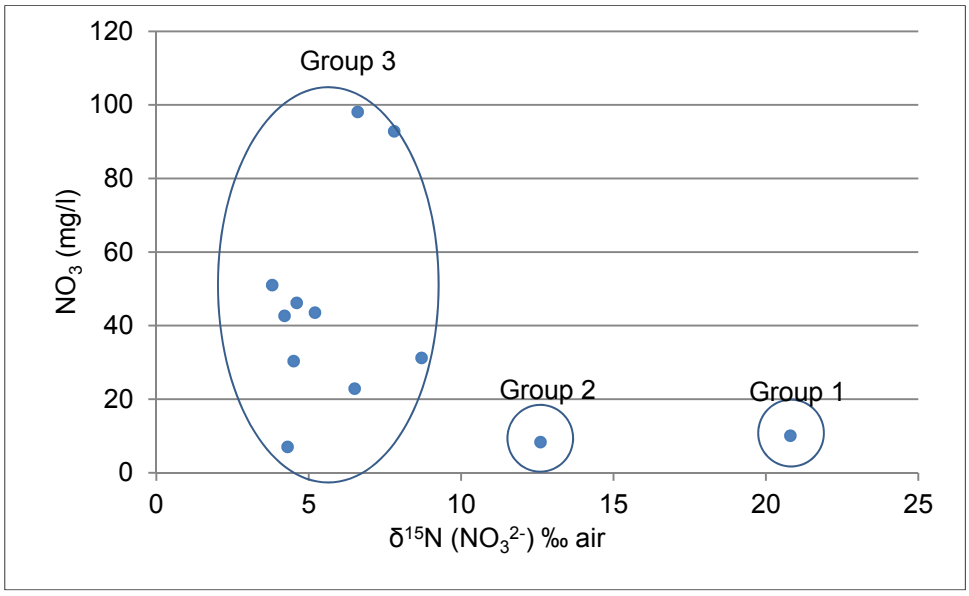

Figure 5. A plot of $\delta^{15}N(NO_3^{2-})$ vs NO_3^{2-} of groundwater samples of Kuwait Group aquifer.

A plot of $\delta^{15}N(NO_3^{2-})$ vs. $\delta^{18}O$ (NO_3^{2-}) and $\delta^{15}N(NO_3^{2-})$ vs. NO_3^{2-} (Figure 5) of the Kuwait Group of aquifer indicate three groups; Group 1 samples with very low NO_3^{2-} (~2 mg/L) and highly enriched $\delta^{15}N$ (~+37‰) and $\delta^{18}O$ (+35‰) values; Group 2 samples with lesser NO_3^{2-} (22 to 24 mg/L), intermediate $\delta^{15}N$ (+22 to +24‰) and relatively enriched $\delta^{18}O$ (+16 to +20‰) values and Group 3 with a wide range of NO_3^{2-} (2-100 mg/L), highly depleted $\delta^{15}N$ (+2 to +9‰) and a wide range of $\delta^{18}O$ (+6 to +26‰).

As seen from Figure 5, majority of the groundwater samples fall under Group 3 with their isotopic values indicating that the source of NO_3^{2-} in groundwater is either desert nitrate or nitrate in precipitation. Desert nitrates are nitrate-rich salt deposits seen in hyperarid deserts, formed due to long-term accumulations of atmospheric deposition in the relative absence of soil leaching or biologic cycling. The lower values of $\delta^{15}N$ of Group 3 suggest no septic tank releases/animal waste nor fertilizers ($\delta^{15}N$=0). However, $\delta^{15}N$ of the Group 2 samples show some evidence of septic tank releases/animal waste but not fertilizers, which are localized in nature.

The $\delta^{15}N(NO_3^{2-})$ of groundwater samples of the Dammam Formation aquifer also show the values that are characteristic of desert nitrates, and these samples have lesser NO_3^{2-} values compared to the overlying Kuwait Group of aquifers.

4 CONCLUSIONS

The δ^2H vs $\delta^{18}O$ results show that most of the groundwater samples fall below the GMWL suggesting evaporation prior to recharge, and the recharge has taken place during a different climatic condition than exists today (paleo water). Most of the groundwater samples measured ^3H values less than that of the rainwater indicating that they are not modern but old water (Corrected 14C ages: Kuwait Group Aquifers-1,500 to 15,000 a B.P. and Dammam Formation aquifer 20,000 to 30,000 a B.P.).

In the Kuwait Group of aquifer, depthwise variation of SO_4^{2-} concentration is quite complex with large variations up to 60 m deep and decreasing with depth. In the Dammam Formation aquifer, the distribution shows decreasing trend with depth. The $\delta^{34}S(SO_4^{2-})$, $\delta^{18}O(SO_4^{2-})$ and SO_4^{2-} values of groundwater samples of Kuwait Group of aquifers reveal that most of the groundwater samples (SO_4^{2-}: 100 to 4600 mg/L), $\delta^{34}S(SO_4^{2-})$: +3 to +24‰, $\delta^{18}O(SO_4^{2-})$: +10 to +15‰) have evaporatic origin.

The depthwise distribution of NO_3^{2-} $\delta^{15}N(NO_3^{2-})$ and $\delta^{18}O(NO_3^{2}-)$ indicates that in the Kuwait Group aquifer, there is no unique trend, whereas in the Dammam Formation aquifer the nitrate concentration decreases with depth. The $\delta^{15}N(NO_3^{2-})$, $\delta^{18}O$ (NO_3^{2-}) and NO_3^{2-} values of the groundwater samples of Kuwait Group Aquifer indicate that the majority of the groundwater samples (NO_3^{2-}: 3 -100 mg/L, $\delta^{15}N(NO_3^{2-})$: +4 to +21‰, $\delta^{18}O$: +1 to +38‰) are either desert nitrate or nitrate in precipitation. Similarly, the $\delta^{15}N(NO_3^{2-})$, $\delta^{18}O$ (NO_3^{2-}) and NO_3^{2-} values of the groundwater samples of Dammam Formation aquifer indicate that they are characteristic of desert nitrates.

It is concluded that the major source of high sulphate and nitrate concentration of Kuwait groundwater is geogenic in nature due to the dissolution of evaporites and desert nitrates during the flow course of groundwater.

ACKNOWLEDGEMENTS

The authors would like to express their gratitude to the International Atomic Energy Agency (IAEA) for their in-kind contribution for the project. The constant support and encouragement of the Kuwait Institute for Scientific Research's (KISR's) management are gratefully acknowledged.

REFERENCES

Akber, A.A., Mukhopadhyay, E., Al-Awadi, H., Al-Qallaf, A., Al-Haddad, E.A. & H. Bhandary. (2006). *Investigation on the Distribution of Nitrogen Compounds in the Groundwater of Kuwait*. Kuwait Institute for Scientific Research, Report No. KISR8165, Kuwait.

Casciotti, K.L., Sigman, D.M., Hastings, M.G., Bohlke, J. K. & Hilkert A. (2002). Measurement of the Oxygen Isotopic Composition of Nitrate in Seawater and Freshwater using the Denitrifier Method. *Analytical Chemistry,* 74(19), 4905 – 4912.

Fritz, P. & J. Ch. Fontes. (1980). *Handbook of Environmental Isotope Geochemistry. Vol. 1 - The Terrestrial Environment: Amsterdam* -A, Elsevier.

Fukuda, T., K.M. Hiscock, Dennis, P.F. & Grischek, T. (2003). A Dual Isotope Approach to Identify Denitrification in Groundwater at a Riverbank Infiltration Site. *Water Research Center*, 37(13), 3070-3078.

IAEA. (2010). *Sampling Procedures for Isotope Hydrology*. Kuwait: International Atomic Energy agency and Kuwait Institute for Scientific Research.

Knoller, K. & Schubert, M. (2010). Interaction of Dissolved and Sedimentary Sulfur Compounds in Contaminated Aquifers. *Chemical Geology*. 276(3–4), 284–293.

Sigman, D. M. (2001). A Bacterial Method for the Nitrogen Isotopic Analysis of Nitrate in Seawater and Freshwater. *Analytical Chemistry* 73(17), 4145 – 4153.

